Structure control of La/B multilayer systems by partial nitridation

Graduation Committee

Chair: Prof. dr. ir. J.W.M. Hilgenkamp

Secretary: Prof. dr. ir. J.W.M. Hilgenkamp

Supervisor: Prof. dr. F. Bijkerk

Co-supervisor: Dr. A.E. Yakshin

Members: Prof. dr. ir. W.M.M. Kessels
Prof. dr. D. Depla
Prof. dr. ir. L. Abelmann
Dr. ir. M.P de Jong
Dr. ir. H. Wormeester

STRUCTURE CONTROL OF LA/B MULTILAYER SYSTEMS BY PARTIAL NITRIDATION

PROEFSCHRIFT

**ter verkrijging van de graad van doctor
aan de Universiteit Twente, op gezag
van de rector magnificus, prof. dr. T.T.M. Palstra,
volgens besluit van het College voor Promoties
in het openbaar te verdedigen op
8 november 2018 om 16:45 uur**

door

**Dmitry Sergeyevich Kuznetsov
geboren op 28 juni 1990
te Moskou, Rusland**

Dit proefschrift is goedgekeurd door de promotor:

Prof. dr. F. Bijkerk

en de assistent-promotor:

Dr. A.E. Yakshin

ISBN: 978-90-365-4654-6
DOI: 10.3990/1.9789036546546
© Dmitry Sergeyevich Kuznetsov, 2018

This thesis is based on the following publications:

D.S. Kuznetsov, A.E. Yakshin, J.M. Sturm, R.W.E. van de Kruijs, E. Louis, and F. Bijkerk "High-reflectance La/B-based multilayer mirror for 6.x nm wavelength", Optics Letters, Vol. **40**, No. 16, 3778 (2015)

D.S. Kuznetsov, A.E. Yakshin, J.M. Sturm, R.W.E. van de Kruijs, and F. Bijkerk "Structure of high-reflectance La/B-based mirrors for with partial La nitridation", AIP Advances **6**, 115117 (2016)

D.S. Kuznetsov, A.E. Yakshin, J.M. Sturm, and F. Bijkerk, "Thermal stability of high-reflectance La/B-based multilayers for 6.x nm wavelength", Journal of Applied Physics **122**, 125302 (2017)

D.S. Kuznetsov, A.E. Yakshin, J.M. Sturm, and F. Bijkerk, "Grazing-incidence La/B-based mirrors with "La surface nitridation" for 6.x nm wavelength", Journal of Nanoscience and Nanotechnology, Vol. **19**, 1-8 (2019)

B. Krause, D.S. Kuznetsov, A.E. Yakshin, S. Ibrahimkutty, T. Baumbach, and F. Bijkerk "In situ and real-time monitoring of structure formation during non-reactive sputter deposition of lanthanum and reactive sputter deposition of lanthanum nitride", Journal of Applied Crystallography **51**, 1013-1020 (2018)

Patents:

D.S. Kuznetsov, A.E. Yakshin, H. Enkisch, V.V. Medvedev, and F. Bijkerk, (submitted)

Contents

Chapter 1: Introduction

1.1 Background……9
1.2 Single layers and multilayers
1.2.1 Single layers: principal limitations……10
1.2.2 Multilayers: working principle……10
1.3 The applications of XUV multilayers for wavelength above 6.6 nm
1.3.1 Aerospace research……10
1.3.2 XRF……11
1.3.3 FEL……12
1.4 Multilayers for wavelengths above 6.6 nm
1.4.1 The properties and interactions of materials……13
1.4.2 The current status……14
1.4.3 The generic challenge……14
References……15

Chapter 2: Experimental

2.1 Requirements
2.1.1 Quality of interfaces……17
2.1.2 Reproducibility……19
2.1.3 Uniformity……20
2.2 Deposition……20
2.3 Analysis
2.3.1 X-ray photoelectron spectroscopy (XPS) ……21
2.3.2 High-resolution Rutherford backscattering (HR-RBS) ……22
2.3.3 Grazing-incidence X-ray reflectivity (GIXR, GIXRR) ……22
2.3.4 Reflectivity above 6.6 nm……24
2.3.5 X-ray diffraction (XRD) ……24
2.3.6 Optical microscopy……24
2.3.7 Atomic force microscopy (AFM) ……24
2.3.8 Reflection high-energy electron diffraction (RHEED) ……25
References……25

Chapter 3: High-reflectance La/B-based multilayer mirror for 6.x nm wavelength..28
Acknowledgements……33
References……33

Chapter 4: Structure of high-reflectance La/B-based multilayer mirrors with partial nitridation……35
4.1 Introduction……35
4.2 Experimental ……35
4.3 Synthesis of fully-passivated LaN……36
4.4 BN formation……38

4.5 Special scheme of La nitridation ("partial" or "delayed" nitridation)........40
4.6 Summary........44
References........45
Acknowledgments........45

Chapter 5. Thermal stability of high-reflectance La/B-based multilayers for 6.x nm wavelength........47
5.1 Introduction........47
5.2 Experimental........48
5.3 Period expansion........50
5.4 6.x nm reflectivity (PTB)........50
5.5 Non-destructive XPS spectra........52
5.6 XPS depth-profiles........54
5.7 Non-destructive HR-RBS........54
5.8 Dedicated studies of B-on-LaN and LaN-on-La-on-B interfaces........55
5.9 Discussion........57
5.10 Summary and conclusions........58
Acknowledgments........58
References........59

Chapter 6: Grazing-incidence La/B-based multilayer mirrors for 6.x nm wavelength........61
6.1 Introduction........61
6.2 Experimental........62
6.3 LaN/B multilayers........63
6.4 B protective properties........64
6.5 La surface nitridation in single films........66
6.6 La surface nitridation in multilayers........68
6.7 Stability of La/B multilayers with La surface nitridation........70
6.8 Summary........71
Acknowledgments........72
References........72

Chapter 7: In situ and real-time monitoring of structure formation during non-reactive sputter deposition of lanthanum and reactive sputter deposition of lanthanum nitride........74
7.1 Introduction........74
7.2 Experimental
7.2.1 Thin-film deposition........75
7.3 Results
7.3.1 Surface analysis........77
7.3.2. Crystalline phases........79
7.3.3 Structure formation during reactive and non-reactive........82

7.3.4 Nitridation of an already deposited La film 86
7.4 Summary and conclusions 88
Acknowledgments 89
Note on Chapter 7..91
References 91

Summary 92
Samenvatting 94
Valorisation 96
Acknowledgements 98
Short CV 100

Chapter 1: Introduction

1.1 Background

Modern materials engineering is of fundamental importance to fields such as electronics, micromechanics, and optics. One particularly highly advanced area involves the synthesis of layered structures with thicknesses in the nanometre (nm) and sub-nm ranges. It is possible to fine-tune the properties of each individual layer, through the precise control of interface processes. Given the large number of processes involved, and the complexity of their interactions, this is quite a challenge. To identify some of these factors in modern advanced coatings, it is necessary to explore ways of controlling the chemical interactions between materials, ballistic intermixing and the growth mode. One recurrent topic within the thesis is extreme ultraviolet (XUV) multilayer optics, which is a particularly challenging technique. Its range of applications includes optical microscopy, X-ray fluorescence analysis, synchrotrons, free-electron lasers, aerospace research, and complex optical systems involving multiple optical elements. In addition to the above-mentioned processes, XUV multilayers require precise control of layer growth. Given that the layers are only a few nm thick, this imposes stringent requirements on the quality of the interfaces between layers. This, in turn, requires advanced control at the atomic scale and the use of cutting-edge analysis techniques.

A Mo/Si stack is one example of an XUV multilayer. The fabrication details for multilayer stacks of this kind were first published in 1985 [1]. Since then, over 20 years of research has led to the synthesis of stacks capable of significantly improved performance in experimental setups. For instance, an XUV reflectivity of 70.15% (±0.1%) has already been achieved – at an operating wavelength of 13.5 nm and an angle of incidence (AOI) of 1.5° off-normal [2].

The present study involves La/B-based multilayers for wavelengths above 6.6 nm (in this thesis referred to as “6 nm” or “6.x nm” multilayers), which are particularly relevant to the above-mentioned applications. The stacks used at these wavelengths have bilayers that are about half the thickness of those in Mo/Si-based multilayer stacks. The layers in La/B-based stacks are about 2.0 nm and 1.5 nm thick, so neither of them consists of more than 10 atomic layers. This means that the synthesis processes for 6 nm stacks have to meet significantly stricter requirements. Computer modelling has demonstrated that the interfaces between layers just 0.3 nm thick can result in a significant loss of performance. The use of 6 nm stacks requires far more accurate control of interaction and growth. Moreover, for any given compound (such as BN [3]), the formation of even a single monolayer can reduce reflectivity to a level that is totally inacceptable for practical applications.

1.2 Single layers and multilayers

1.2.1 Single layers: principal limitations

Over the past few decades, multilayer mirrors designed specifically for light in the XUV/hard X-ray region of the spectrum have become increasingly important. They are now being used in numerous practical applications. The need for reflective multilayers is due to the fact that light from this region of the spectrum is highly absorbed by most materials, giving reflectivity of just a few percent. An exception to this is the total reflection range (the angular range below the critical angle). With regard to real-world applications, however, there is a pressing need for optics with high reflectance at a non-glancing AOI. This is especially true of multicomponent optical systems, which have complex optical paths. The only way to achieve acceptably high reflectivity at a range of AOIs is to use multilayer optics.

1.2.2 Multilayers: working principle

Multilayers achieve high reflectivity by the constructive interference of light reflected from the interfaces of stacked layers of different optical contrasts. At any given wavelength, materials with a high δ and a low β act as reflective layers (the refractive index is equal to $1 - \delta + i\beta$). Those with a low δ and a low β serve as spacer layers. A sequence of layers with high and low δ (interspersed reflectors and spacers in a stack) provides optical contrast. Both the reflector and spacer layers require a low β, to minimize any loss of light by absorption. For instance, at a wavelength of above 6.6 nm, the properties of La enable this element to act as a reflector. At the same wavelength [4], B acts as a spacer. If the Bragg condition [5] is to be satisfied, both the thickness of a bilayer (also referred to as the multilayer period) and its reflector:period thickness-ratio (referred to as the gamma-ratio, or simply 'gamma') should be optimized for the wavelength and AOI in question. Reflection from the facets of natural crystals serves as a convenient illustration of the working principle involved here [6].

1.3 The applications of XUV multilayers for wavelengths above 6.6 nm

1.3.1 Aerospace research

In recent decades, XUV multilayers have become increasingly important in aerospace research. This particularly applies to multilayers that are used to convert multispectral light originating from objects of interest (e.g. the sun) into monochromatic light. The first reported use of XUV multilayers involved a W/C coating for telescope mirrors in studies of solar activity (1985) [7]. The study of multiple emission lines in the light emitted by objects provides information about a range of dynamic processes. For instance, studies of the interface between the sun's photosphere and its corona were key to understanding the relationship between solar activity and space weather [8].

The research into various zones (such as the plasmasphere) in the region of space around the Earth also involves the use of multilayer mirrors, as light-guiding optical elements and as filters. The aim is to select light with wavelengths corresponding to the emission lines of the chemical elements under investigation.

Studies of the plasmasphere [9], for example, used an Al/Y_2O_3 coating optimized for a wavelength of 30.4 nm (He^+ emission line) plus an Al/C multilayer as a 30.4 nm filter. In aerospace research, paired materials like these are selected based on a range of criteria. The most important of these criteria are briefly outlined, by means of an example [9]. The first consideration is that the synthesized multilayer must be highly reflective at the wavelength (or wavelengths) of interest, to deliver high-intensity images within the timescale involved. Secondly, the ratio between the ion of interest (He^+) and its corresponding neutral element (He) should be as high as possible, to achieve high-contrast images (wavelength selectivity). Accordingly, for the purposes of observing He^+ emission lines, Al/Y_2O_3 rather than Mo/Si was selected. Thirdly, the mirrors involved must be stable over time when exposed to atmosphere and elevated temperatures. This requirement excluded the use of Mg/SiC in the work cited above [9].

Aerospace research requires high reflectance, wavelength-selective multilayer coatings (for wavelengths above 6.6 nm) which are stable over time when exposed to atmosphere and elevated temperatures. Multilayers of this kind could be used to study newly discovered emission lines originating from processes in important celestial objects (such as the Sun and the Earth).

1.3.2 XRF

X-ray fluorescence (XRF) spectrometry is used to determine the elemental composition of a sample [10]. One variant of this technique, known as total reflection X-ray fluorescence (TXRF) [11], can be used to detect nanoparticles deposited on a flat surface, for example, or to trace the positions of heavy ions in organic monolayers or thick Langmuir-Blodgett films [12-16]. The multilayer coatings used in monochromators are essential in the analysis of low intensity emittance, in the case of light elements such as Li, Be, B, C, N [10]. The latter elements have a relatively low fluorescence yield. This factor, coupled with strong absorption in the sample itself, greatly reduces the intensity of the measured signal. Accordingly, the detection of light elements with XRF is difficult without multilayer coatings. Compared to single layers, the multilayers used in energy-dispersive techniques have a higher integrated reflectivity (over the Bragg peak), which makes it possible to detect light elements. These materials make the fine-tuning of reflectivity, of the position, of the reflection-peak wavelength and of the angle of incidence a matter of routine. For the purpose of detecting B (K emission line) at angles of incidence close to 45°, for example, La/B_4C and Mo/B_4C multilayers were used [17]. One XRF-based application (grazing-incidence X-ray reflectivity) involves the angular-dependent measurement of samples to give depth-profiles of selected elements and details of the density of individual layers [18]. With this technique, unlike secondary ion mass spectrometry (SIMS), XPS depth-profiling, Rutherford backscattering spectroscopy (RBS) and other methods that involve sample sputtering, the sample is not damaged by incident X-rays. It also means that the XRF yield (including angular-dependent information) can be measured in-house (using a standard lab reflectometer with an X-ray tube), thus avoiding the need for restricted and expensive access to equipment at ion centres, synchrotrons, etc. The

Dutch-English company Malvern Panalytical (Almelo) manufactures analytical equipment of this kind, which can be used for XRF yield-based measurements and analysis. To summarize, XRF-based methods can be used to non-destructively determine a sample's chemical composition at varying depths, including special cases covered by TXRF. Thus, in practical terms, there is great interest in developing multilayer coatings for a range of chemical elements, including B. The most critical properties in this regard are high reflectance, thermal stability and stability over time (which coincide with the requirements imposed on multilayers for use in aerospace research).

1.3.3 FEL

Another major application of multilayer optics is in free electron lasers (FELs), or fourth generation light sources. The wavelength range above 6.6 nm is particularly important in this regard, as FELs could potentially be used as high-intensity sources in multicomponent systems such as XUV lithography scanners. One current source, the Linac Coherent Light Source (LCLS) – which emits wavelengths in the hard X-ray region of the spectrum (0.12-1.5 nm) – delivers 10^{11} to 10^{13} coherent photons per pulse [19]. This characteristically yields peak and average spectral brightness values that are several orders of magnitude higher than those produced by standard undulator-based sources [20]. Indeed, the peak spectral brightness is up to 10 orders of magnitude higher. In addition, when LCLS and similar FELs are used, the pulses used to probe samples can be as short as 1 fs, which is on the atomic time scale. Thus, high-intensity FELs are ideal for observing dynamic behaviour in contexts such as chemical reactions [21], biomolecular systems (e.g. proteins) and other complex non-crystalline substances.

High-intensity FELs in the XUV and soft X-ray ranges are also available. These include FLASH at DESY, Fermi@Elettra in Trieste, and SLAC.

One advantage of FELs is that the energy of the emitted radiation (the wavelength) can be tuned to suit the needs of a particular experiment or application. Moreover, FELs could potentially be scaled down to create table-top light sources [22]. This would enable laboratories to routinely carry out research, in-house, that currently requires the use of large, highly expensive synchrotrons. In this connection, a laser-generated electron beam, passed through a one-metre-long undulator, was found to yield narrow-bandwidth output light [21]. In-house FELs are moving out of the realm of science fiction and into the real world.

FELs may use multilayer optics as beam-splitters (to generate numerous experimental lines from a single FEL), monochromators (to select the wavelength of interest) and radiation-focusing mirrors. The latter serve to create the highest possible intensity at a focal point [6]. The use of multilayers that are highly efficient at reflecting and refracting light at selected wavelengths makes it possible to achieve a high degree of reflection (thus high output intensity) at those wavelengths. The system can be fine-tuned to the precise wavelength and angle of incidence required simply by modifying the multilayer period and the gamma. As stated in the "Single layers" section, multilayer optics span the full range of AOI including normal (and near normal) angles.

Single layers – regardless of the materials used – are fundamentally unable to create high levels of XUV reflection (i.e. high output intensity). In addition to high reflectance and stability over time (as previously mentioned), the multilayer optics used in FELs must have a long service life under the thermal load of high-intensity radiation.

1.4 Multilayers for wavelengths above 6.6 nm

1.4.1 The properties and interactions of materials

Based on their optical properties (high contrast and low absorption of 6 nm light), La and B were selected [4]. However, LaB_6 – which is thermodynamically favourable (enthalpy of formation ΔH = -160 kJ/mol [23]) – is formed in La/B multilayers [24, 25]. Chemical interactions between La and B result in the formation of interface zones between the layers in a stack, which reduces optical contrast and, as a result, reflectivity [26]. One way to limit compound formation in La/B multilayers is to intentionally deposit (or pre-deposit) the compound, instead of one (or both) of the layers.

One requirement is that this compound should be thermodynamically stable, so that it will not dissolve if it interacts with the other layers in a stack. However, this can result in the formation of superfluous amounts of compound in the interface zones, which impairs optical contrast. The enthalpy of formation can be used to assess a compound's tendency to dissolve into its constituent elements upon interaction with another material. If this parameter has a negative value, then compound formation (with a release of energy) is favoured. Therefore, if they are to be stable in such situations, compounds should have an enthalpy of formation with the highest possible absolute value and a negative sign.

In La/B-based multilayers, a well-known solution is to deposit the compound LaN, rather than elemental La. The synthesis method involves the magnetron sputter deposition of LaN in a nitrogen atmosphere (with N_2 gas being introduced into the chamber) [26]. The enthalpy of formation (ΔH) for LaN = -303 kJ/mol, versus ΔH = -160 kJ/mol for LaB_6 and ΔH = -253 kJ/mol for BN [23]. Therefore, based on these compounds' thermodynamic properties, the interaction of LaN with B is not expected to result in the formation of LaB_6 (LaB_x) or BN. No account has been taken of complex compounds such as $La_xB_yN_z$, because, to the best of our knowledge, they do not occur in these situations. Furthermore, as previously demonstrated [4], if the La in B-based multilayers is replaced by LaN, this has no impact on the system's theoretical reflectivity (about 82%). In practice, LaN/B produced a significantly higher optical contrast than La/B (confirmed by comparing reconstructed profiles against optical constants) [26]. The previously cited value of R=57.3% for 6.7 nm near-normal (1.5° off-normal) incidence (a record, to the best of our knowledge) was achieved using a LaN/B stack [26].

1.4.2 The current status

Yet, the above-mentioned value of 57.3% would result in a substantial loss of intensity in all of the above-mentioned applications. This meant that further work was needed to boost reflectivity. In addition, the thermal stability of multilayers with enhanced reflectivity required further study. The same applied to the performance of multilayers for wavelengths (λ) of 6.6 nm and above, at grazing incidence (GI). With regard to GI, a reflectivity of 66.5% was demonstrated for a 7.3 nm-period La/B stack, at λ≈6.7 nm and an AOI of 61.3° off-normal [26]. At an AOI of 45°, a 4.8 nm-period La/B_4C multilayer demonstrated a reflectivity of 54.4% at λ≈6.7 nm [27, 28]. These experimental values still fall quite a long way short of the theoretical limit for GI La/B-based stacks (about 79.5%) [29] at the stated AOI.

Based on general principles, at a given wavelength, GI stacks have a thicker period than NI stacks. Therefore, assuming that both multilayers have the same interface zones, there should be a smaller reduction of reflectivity with GI than with NI systems. This seems to suggest that research should focus purely on NI stacks, and that a simple increase in the period would yield the GI parameters. However, in the section of this thesis dealing with GI, it will be shown that – in this particular case – the use of thicker layers (even if these are still in the nm range) is associated with various problems. The nature of these problems was explored in a separate series of studies (see the section on the in-situ growth of La vs LaN).

For instance, at AOIs of 45° and 65° off-normal, an La/B multilayer's maximum theoretical peak reflectivity at 6.66 nm is about 14% higher (in absolute terms) than the corresponding value for a La/B_4C multilayer. This is due to the fact that absorption in B_4C is much higher than in B [29]. For this reason, the thesis focuses on B-based stacks. The record for NI (which was set in 2013) involved reactive sputter deposition of La (producing the compound LaN) to reduce any chemical interaction between La and B [26]. For this reason, the thesis research focuses on LaN/B-based stacks. Introductions to research in areas such as thermal stability, GI, etc. are given in the relevant sections.

1.4.3 The generic challenge

The thesis focuses on the cutting-edge synthesis of La/B-based multilayers that has been developed over the past few years. It includes studies of the structure of multilayers, of their performance at elevated temperatures, the synthesis of stacks for various angles of incidence, and the results of research into the growth of La and LaN. The complex scientific and engineering issues involved posed a real challenge. Efforts to minimize the interface zones between layers required an unprecedented level of control at the atomic level, in terms of layer growth, intermixing, and compound formation.

References

1. Jr.T.W. Barbee, S. Mrowka, M.C. Hettrick, Applied Optics 24(6) (1985)
2. A.E. Yakshin, R.W.E. van de Kruijs, I. Nedelsu, E. Louis, F. Bijkerk, H. Enkisch, and S. Müllender, Proceedings of SPIE, Vol. 6517 (2007)
3. D.S. Kuznetsov, A.E. Yakshin, J.M. Sturm, R.W.E. van de Kruijs, E. Louis, and F. Bijkerk, Optics Letters 40(16) (2015)
4. I.A. Makhotkin, E. Zoethout, E. Louis, A.M. Yakunin, S. Müllender, and F. Bijkerk, Optics Express, Vol. 20, No. 11 (2012)
5. C. Kittel, “Introduction to Solid State Physics”, John Wiley & Sons (1971)
6. E. Louis, “Physics and technology development of multilayer EUV reflective optics”, PhD thesis, ISBN: 978-90-9027163-7 (2012)
7. J.H. Underwood, M.E. Bruner, B.M. Haisch, W.A. Brown, L.W. Acton, Science, 238 (1987)
8. D. Martinez-Galarce, P. Boerner, R. Soufli, J. Harvey, M. Bruner, J. Lemen, E. Gullikson, B. De Pontieu, N. Choi, M. Fernandez-Perea, N. Katz, S. Baker, E. Prast, S. Khatri, and J. Kong, “Recent advances in EUV optics for use in solar physics”, 2nd International Conference on Space Technology, pp. 1-4 (2011)
9. K. Uji, I. Yoshikawa, K. Yoshioka, G. Murakami, and A. Yamazaki, Proceedings of SPIE, Vol. 8528 (2012)
10. P.Y. Tu, “Multilayer monochromators for EUV and X-ray optics and the interface characterization”, PhD thesis, Universiť e Pierre et Marie Curie, Paris (2015)
11. M.K. Tiwaria, K.J.S. Sawhneya, and G.S. Lodhab, Spectrochimica Acta Part B: Atomic Spectroscopy, Vol. 65, Issue 6 (2010)
12. M.J. Bedzyk, D.H. Bilderback, G.M. Bommarito, M. Caffrey, and J.S. Schildkraut, Science 241 (4874) (1988)
13. H.D. Abruña, G.M. Bommarito, and D. Acevedo, Science 250 (4977) (1990)
14. N.N. Novikova, S.I. Zheludeva, N.D. Stepina, A.L. Tolstikhina, R.V. Gaynutdinov, W. Haase, A.I. Erko, A.A. Knyazev, and Y.G. Galyametdinov, Applied Physics A 94 (2009)
15. S.I. Zheludeva, M.V. Kovalchuk, N.N. Novikova, A.N. Sosphenov, V.E. Erochin, and L.A. Feigin, Journal of Applied Physics 26 (1993)
16. M.K. Tiwari, G.M. Bhalerao, M. Babu, A.K. Sinha, and C. Mukherjee, Journal of Applied Physics 103 (2008)
17. C. Hombourger, P. Jonnard, J.-M. AndréJ, and. J.-P. Chauvineau, X-Ray Spectrometry 28(3) (1999)
18. I.A. Makhotkin, E. Louis, R.W.E. van de Kruijs, A.E. Yakshin, E. Zoethout, A.Yu. Seregin, E.Yu. Tereschenko, S.N. Yakunin, and F. Bijkerk, Physica Status Solidi A 208, No. 11 (2011)
19. P. Emma, R. Akre, J. Arthur, R. Bionta, C. Bostedt, J. Bozek, A. Brachmann, P. Bucksbaum, R. Coffee, F.-J. Decker, Y. Ding, D. Dowell, S. Edstrom, A. Fisher, J. Frisch, S. Gilevich, J. Hastings, G. Hays, Ph. Hering, Z. Huang, R. Iverson, H. Loos, M. Messerschmidt, A. Miahnahri, S. Moeller, H.-D. Nuhn, G. Pile, D. Ratner, J. Rzepiela, D. Schultz, T. Smith, P. Stefan, H. Tompkins, J. Turner, J. Welch, W. White, J. Wu, G. Yocky, and J. Galayda, Nature Photonics, Vol. 4 (2010)

20. C. Pellegrini, "Making X-Rays: bright times ahead of FELs", IOP CERNCOURIER (2010) http://cerncourier.com/cws/article/cern/44357
21. H.-P. Schlenvoigt, K. Haupt, A. Debus, F. Budde, O. Jäckel, S. Pfotenhauer, H. Schwoerer, E. Rohwer, J. G. Gallacher, E. Brunetti, R.P. Shanks, S.M. Wiggins, and D.A. Jaroszynski, Nature Physics 4 (2008)
22. K. Nakajima, Nature Physics 4 (2008)
23. A.I. Efimov, "Properties of inorganic compounds," Handbook, Khimiya, Leningrad (1983)
24. T. Tsarfati, R.W.E. van de Kruijs, E. Zoethout, E. Louis, and F. Bijkerk, Thin Solid Films 518(5) (2009)
25. T. Tsarfati, R.W.E. van de Kruijs, E. Zoethout, E. Louis, and F. Bijkerk, Thin Solid Films 518(24) (2010)
26. I.A. Makhotkin, E. Zoethout, R.W.E. van de Kruijs, S.N. Yakunin, E. Louis, A.M. Yakunin, V. Banine, S. Müllender, and F. Bijkerk, Optics Express, Vol. 21, No. 24 (2013)
27. P. Naujok, S. Yulin, A. Bianco, N. Mahne, N. Kaiser, and A. Tünnermann, Optics Express, Vol. 23, No. 4 (2015)
28. N. Kaiser, H.K. Pulker, "Optical Interference Coatings", chapter "Multilayer Coatings for EUV/Soft X-ray Mirrors", Springer-Verlag (2003)
29. D.S. Kuznetsov, A.E. Yakshin, J.M. Sturm, and F. Bijkerk, Journal of Nanoscience and Nanotechnology, Vol. 19, 1-8 (2019)

Chapter 2: Experimental

2.1 Requirements

2.1.1 Quality of interfaces

This section deals with one of the most critical requirements imposed on synthesized multilayers. For synthesized multilayers to be highly reflective, the interfaces between individual layers must be as sharp as possible. At a wavelength above 6.6 nm multilayers have a period that is roughly half the thickness of 13.5 nm Mo/Si-based multilayers, for example. On general principles, the absolute loss of optical contrast (and, therefore, reflectance) should be significantly higher for wavelength above 6.6 nm (which involves thinner layers), assuming that both types of stack have identical interface zones. Calculations were performed in IMD software [1] to obtain the specific values. Here, to achieve saturation of reflectivity, 220 periods were selected for the 6.7 nm coating model, and 50 periods for the 13.5 nm model. The structural design (gamma-ratio and period value) was optimized for maximum reflectance at AOI=1.5° off-normal, using the optical constants for materials from the CXRO database [2].

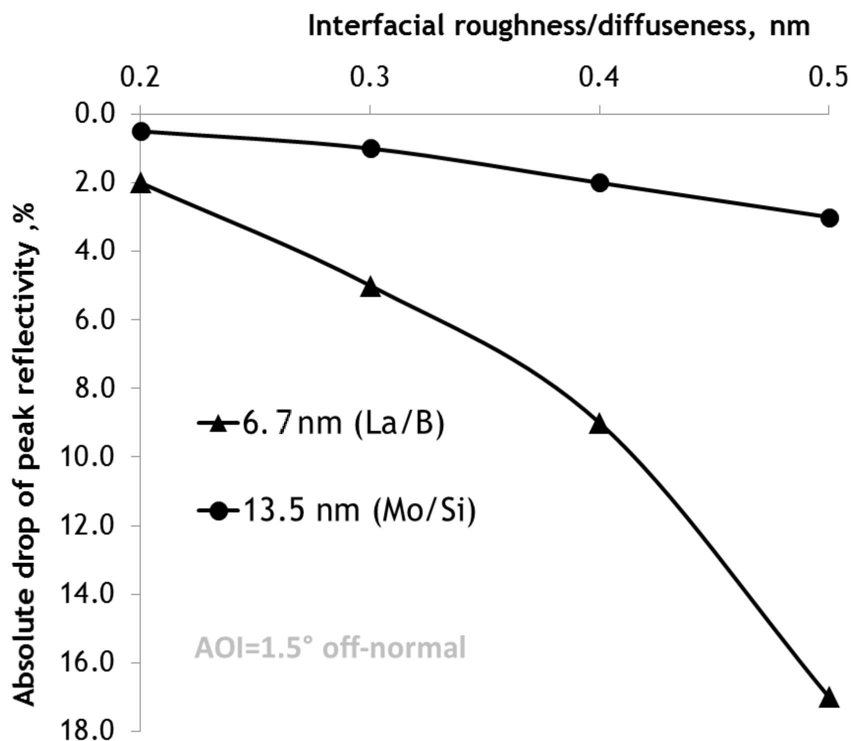

Fig. 1. Calculations of absolute peak reflectivity loss for 6.7 nm (La/B) and 13.5 nm (Mo/Si) multilayers for NI, in relation to effective interface width.

Both interfaces (for 6.7 nm, these were B-on-La and La-on-B) were assumed to have equal interface zones. This was represented mathematically by the use of error function-profiles, an approach known as “roughness/diffuseness” [1]. Fig. 1 illustrates

the absolute value of peak reflectivity loss in relation to interface width. As previously stated, the interface sharpness for 6.7 nm stacks is subject to highly challenging requirements. For instance, while 0.4 nm Mo/Si interfaces lose just 2% in absolute terms, the corresponding loss for La/B is about 9%. The calculated maximum peak reflectance for an ideal stack (NI La/B) is about 80% (the precise value depends on the set of optical constants selected, based on CXRO data [2]; the maximum modelled value is 79.4% @ λ=6.66 nm), while a level of about 70% is considered to be adequate. Therefore, the effective interface width should not exceed 0.4 nm at either interface. In summary, the interface zones that form in NI multilayers for above 6.6 nm are of crucial importance in terms of the synthesis (deposition) of these stacks.

Based on general principles, interface formation is known to be influenced by factors such as the growth of the layers (morphology). The latter includes aspects such as porosity, which results from a deficient energy input per deposited atom. This energy might be brought by (neutralized) ions, which expose a growing film to their "momentum flux". On the other hand, a different level of energy input might induce enhanced interdiffusion, resulting in the formation of wide interface zones and, probably, of compounds too. Roughness itself, and the way it evolves during layer growth, are complex phenomena. For instance, in a deposited layer just a few nm thick, roughness could result from crystallization. Moreover, it is highly dependent on interactions with the substrate-layer and on the type of growth mode involved. The latter depends on a wide range of conditions, including energy input per deposited atom [3], and (more importantly) the momentum flux [4], the shadowing effect, the diffusion mode of deposited atoms [5], etc.

Another factor in the formation of interface zones involves the growth of one layer on top of another (for instance, La on B and B on La). The process by which a layer is grown on top of a substrate-layer is commonly referred to as overlayer growth. One aspect of this process is ballistic intermixing, which occurs when the energy of the deposited atoms exceeds the displacement threshold [6] and/or due to other momentum flux [4]. The energy distribution of sputtered atoms may feature a high-energy tail (>20 eV) [7]. As a result, the possibility cannot be excluded that such ballistic intermixing could occur during magnetron sputter deposition. During growth on a substrate-layer, another process that contributes to ballistic intermixing is the reflection of neutralized ions (reflected neutrals) from the target material [8]. In the case of reactive sputtering (using a nitrogen gas supply, for instance), the reflection of reactive gas species might also contribute to intermixing [9]. It has been calculated [10] that the energy of reflected neutrals could be up to ~100-200 eV, dependant on the mass of the impinging ion and the mass of the target material's atoms. Since none of the materials involved has a bulk displacement threshold (i.e. through a monolayer) in excess of about 50 eV [11], there would clearly be substantial intermixing between reflected neutrals and the material's atoms in question during overlayer growth. Based on general principles, chemical reactions between materials during that growth process could also result in the formation of interface zones. This would lead to interdiffusion and subsequent compound formation, without the involvement of a relatively high energy input. For instance, the thermodynamically favourable

compound LaB_6 (enthalpy of formation ΔH = -160 kJ/mol [12]) tends to form in La/B multilayers [13-15]. As a result, these structures have a very much lower optical contrast than LaN/B multilayers. In the latter, any interactions are prevented by the intentional deposition of the thermodynamically stable compound LaN (ΔH = -303 kJ/mol) [16]. Another effect that might be seen when growing a material on top of a substrate-layer, is surface segregation [17], which has been observed and modelled in Ni/Cu systems [18-21]. Dedicated overlayer growth studies would require a separate, full-scale research effort (as in [22-23], for example).

2.1.2 Reproducibility

Another important factor, which is related to the parameters of a deposition setup requirement, is the reproducibility of the deposited stacks. The aimed-for thicknesses of the layers must be consistently reproduced over time, from one coating to another. NI multilayers for above 6.6 nm have a period of about 3.5 nm (B layer ≈2.0 nm, La-based layer ≈1.5 nm). Thus, even layer thickness errors in the sub-Ångström range would have a substantial impact on peak reflectance. Moreover, the Bragg reflectivity peak could be shifted out of the peak wavelength targeted by the multilayer's design. Calculations using modelling software [1] demonstrated that, for a 220-period stack (the number of periods required to achieve saturation of reflectivity for NI and above), random layer-thickness errors of just 0.03 nm would result in an absolute loss of peak reflectivity of up to 3%. The extent of the reflectivity loss depends on the distribution of thickness errors throughout the entire depth of a stack. Accordingly, the value of 3% obtained by numerous modelling iterations is considered to be the upper-boundary. In an optical system containing five mirrors, for example, a drop in R from 70.0% to 67.0% would produce a relative loss of total (output) intensity of about 25%.

Deposition rates (plus related parameters such as discharge current and voltage, pressure, etc.) should be monitored over time, to detect any layer thickness errors. In stacks, these values (and their trends over time) must be compared layer by layer, and from one deposition run to another. One well-known method for monitoring deposition rates in situ involves the use of quartz crystal microbalances (QCM). In the case of e-beam evaporation, for example, the bulk values employed in the analysis of QCM data have to be balanced against variations in temperature, particle plume instabilities, and uncertainty concerning the densities of growing layers. Due to the latter issues, the accuracy of QCM measurements (of the thickness of deposited material) is no better than 0.03 nm [24]. However, as calculations have shown, layer thickness errors of about 0.03 nm would result in unacceptably poor reflectivity-peak-value reproducibility (and wavelength-position) in 6 nm stacks. Therefore, neither QCM nor e-beam evaporation, relying on estimation of deposition rates by QCM, could be acceptable in our work.

Sputter-deposition techniques, such as magnetron sputtering, allow deposition rates to be calibrated to an accuracy of a few picometers, prior to coating. This involves the analysis of grazing-incidence X-ray reflectivity (GIXR) measurements, performed on specially synthesized calibration stacks. The use of these special stacks was outlined in our publication [25].

2.1.3 Uniformity

A secondary requirement (but one that is nonetheless important for the implementation of practical applications) concerns coating uniformity. The thickness of the deposited coating (the period of a multilayer) must be uniform over the entire surface of the mirror. If this is not the case, the period values will deviate from those targeted by the multilayer's design and the Bragg condition will not be satisfied [26], resulting in a loss of reflectivity. The modelling [1] of 220-period NI (AOI=1.5° off-normal) multilayers for wavelength ~6.7 nm with a period of 3.40 nm (Bragg peak at 6.77 nm) shows that an increase in the period of just 0.01 nm (Bragg peak at 6.79 nm) would result in an absolute loss of peak reflectivity of about 4.5%. In this case, a significantly greater loss is of the integrated intensity. The extent of such integrated intensity losses is highly dependent on the spectral width (FWHM) of the incident light at the peak wavelength of interest. Clearly, the uniform thickness requirement – which prohibits deviations from the design target thickness of more than a few picometers – must be met.

2.2 Deposition

Based on the requirements outlined above, magnetron sputter deposition was selected for the synthesis of multilayers for wavelengths above 6.6 nm. Methods such as heteroepitaxial growth, which is capable of atomic layer deposition [27], are theoretically capable of producing the sharpest interfaces. However, to the best of our knowledge, this method is not yet developed for the deposition of B, La, and LaN [28]. The research described in this thesis was carried out using an Advanced Development Coater (ADC) in the Industrial Focus XUV Optics Group at the University of Twente. This Ultra-High Vacuum (UHV) equipment can reach a vacuum of 10^{-9} mbar, prior to deposition. This minimizes the influence of any contaminants on growth and on the composition of the layers. The oxidation of La-based layers is very favourable, and expected, as ΔH = -1795 kJ/mol [12], and this is also a documented property of La in practice [29]. Accordingly, mass spectrometry is used to monitor the level of the vacuum before each deposition run, as well the composition of any residual contamination. This method is based on a determination of the mass-to-charge (m/q) ratio of ionized particles. A short outline is given in [30]. In theory, a certain level of oxygen pressure can be beneficial in some cases. For instance, in the case of Co/Cu spin valves, oxygen appeared to act as a surfactant, reducing the level of defects in films [31]. In the case of La-based multilayers, however, lanthanum oxide is known to exacerbate imperfections, which reduce 'at-wavelength' reflectivity [32]. The authors concluded that this was due to the growth of morphologically rough lanthanum oxide layers. Thus, the objective was to minimize the level of residual contaminants in the vacuum chamber and to control reproducibility from one coating to another.

A brief outline description of the ADC setup has already been given [28]. Ar is used as the sputter gas, and the magnetrons are operated in DC mode. Target composition is checked by pre-sputtering all new targets to a steady-state, and then depositing a single test layer. A steady-state is then assessed by operating the magnetron power source in the fixed current-mode and monitoring voltage and

current in situ. At a given fixed current, the voltage is dependent on the chemical composition of the target at and near the surface. While the target is pre-sputtered (surface and near-surface contaminants are being removed), the voltage changes (the secondary electron emission coefficient (SEEC) approaches that of the pure target material [17]). Once this value has stabilized and the intended current has been achieved, then the zone at or near the target's surface can be said to be in a steady state, free of contaminants, which were present in the near-surface region of a new target. In addition to its other applications, the ADC system has been specially designed to produce nm-period multilayers and other structures with layers of nanoscale thickness. In this connection, a thermalized particle deposition (TPD) technique has also been developed [33]. This technique is based on the interaction of two factors inside the deposition chamber – the relatively large target to substrate distance (about 27 cm) and the pressure of the sputter gas. TPD enabled synthesis of NI Mo/Si-based multilayers with high 'at-wavelength' reflectivity (R=70.5% at 13.3 nm, AOI=1.5° off-normal) [33].

Some of the special test samples for in situ growth studies and other purposes were produced in other deposition setups (i.e. not in the ADC). Descriptions of these samples are included in the relevant sections of the thesis, together with further details of the deposition parameters used in those experiments.

2.3 Analysis

2.3.1 X-ray photoelectron spectroscopy (XPS)

An analysis of the chemical composition of deposited structures is important for engineering purposes (such as contamination control from one coating to another), as well as for scientific studies. XPS is critically important in multilayer production, as it can detect compounds formed at the interfaces. In service lifetime studies, the technique can be used to measure the composition of a multilayer's upper zone. Here, the measured volume is limited by the probing depth, which typically ranges from 5 to 7 nm [34]. The probing depth is defined in our work commonly, as 3 times the electron mean free path. In addition, a series of XPS measurements can be carried out, to monitor the evolution of a sample's composition over time. In thermal stability studies (at elevated temperatures), XPS provides information on the evolution of 'as-deposited' structures and on the formation of new compounds at multilayer interfaces. This information is enormously important in terms of real-world applications, given the thermal loads to which optical systems are subjected. The physical, operational and analytical principles of XPS have been outlined in a series of monographs [34]. It should be noted that XPS is a non-destructive technique, as the samples are probed using X-rays. We have found that – potentially – XPS is sufficiently sensitive to detect even a single monolayer of a compound formed in La and/or B-based multilayers [35, 36].

Moreover, special angular-resolved XPS measurements (AR-XPS) can be used to study interfaces in layered structures. As it approaches a normal angle of incidence relative to the sample's surface, the X-ray beam penetrates ever further, collecting data on deeper layers. At a grazing incident angle, the probe is mainly limited to the

sample's near-surface zone. In this way, AR-XPS could be used to determine which compounds are formed in a multilayer, and at which interface.

Another option is to combine XPS with ion beam sputtering. XPS measurements could then be made after each etching step, at the same spot. This analysis would produce a depth profile of all the chemical elements in a sample. However, it is important to note that this approach does have certain limitations. For instance, ion beams (Ar^+, energy 0.5 keV) induce intermixing between stack layers that are just a few nm thick and, as mentioned above, XPS is limited to a probing depth of about 5-7 nm [34]. Thus, the smooth, broad element-content profiles that are typically observed are partly a result of the experimental conditions in question, and do not accurately represent the 'as-deposited' structure. The level of intermixing could be minimized by reducing the energy of the ions. However, this would inevitably involve a drop in the ion current, lengthening the duration of the experiment. More importantly, the energy required for sputtering will always induce a degree of intermixing. Accordingly, intermixing is an inevitable consequence of depth profiling. Nevertheless, XPS depth profiling can be used for relative comparisons. For instance, it could be used to compare a stack's 'as-deposited' state with its post-annealing state, to assess interface evolution at elevated temperatures.

The XPS equipment used in the thesis was a Thermo Scientific Theta Probe, with monochromatic Al-Kα radiation. The XPS binding energies were calibrated using Ag 3d 5/2 peak, measured on a sputter cleaned e-beam evaporated Ag film.

2.3.2 High-resolution Rutherford backscattering (HR-RBS)

RBS is, to some extent, a non-destructive technique, provided that the ion dose delivered to a measurement spot is limited. It is based on the elastic scattering of charged particles (usually ions) from nuclei in the target material. Details of the physical principles involved, plus analytical descriptions and numerous measurement data have been published previously [37]. Conventional RBS is restricted to a resolution of ~5-50 nm. Thus, HR-RBS [38] is the only backscattering technique that can be used to obtain useful information about multilayers with individual layers that are just a few nm thick. The HR-RBS work was performed at the Helmholtz-Zentrum Dresden-Rossendorf's Ion Beam Centre (IBC). Further details of these experiments can be found in the relevant section of the thesis. The IBC's equipment provides a resolution of less than 1 nm in the near-surface zone. C^{2+} ions were used, to obtain enhanced scattering from La (relatively high-Z element versus C) and minimal scattering from B. The Z-number for C is slightly higher than for B. This means that any C ions that collide with B atoms will generally experience a reduction in energy rather than elastic scattering. The aim was to study B-on-LaN and LaN-on-La-on-B interfaces separately from each other, in the 'as-deposited' and annealed states. Further details are given in the relevant section of the thesis.

2.3.3 Grazing-incidence X-ray reflectivity (GIXR, GIXRR)

GIXR was used for the in-house analysis of deposited structures. The measurements were made using a PANalytical (the company is now known as Malvern Panalytical)

Empyrean X-ray diffractometer (Cu-Kα radiation, 0.154 nm). GIXR is used to obtain information on interface thickness, density and roughness [28]. Here, the term 'roughness' does not necessarily refer to the morphological roughness of deposited layers. Various ways of representing interfaces were developed [1]. Details of the geometric experimental approach have been outlined [24]. Numerous examples of GIXR curves have been published [24]. The ability of GIXR to measure multilayer periods to an accuracy of just a few picometers is essential for the precise calibration of deposition rates, and for measuring period values and periodicities from one multilayer to another.

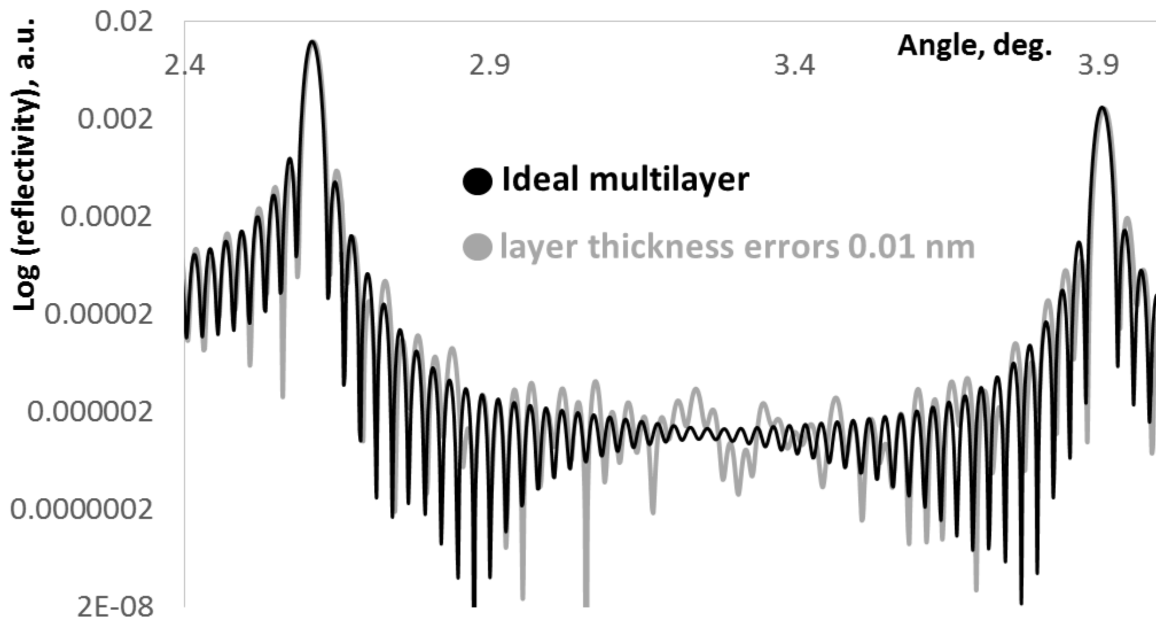

Fig. 2. Zoomed view (at angles of 2.4° – 3.9°) of a GIXR curve (calculated using a software package [1]) for an ideal multilayer and for the same multilayer but with random layer thickness errors of 0.01 nm.

Fig. 2 shows a plot of the GIXR curves calculated [1] for an ideal multilayer and for the same multilayer with layer thickness errors of 0.01 nm. The model parameters were 50 periods, a period of 3.40 nm, G=0.40, optical constants from the CXRO database [2], and a wavelength of 0.154 nm (Cu-k). Fig. 2 shows that layer thickness errors as small as 0.01 nm can be detected experimentally. The densities reported in the section of the thesis on La and LaN in situ growth (which was measured using a synchrotron rather than the in-house diffractometer) made it possible to assess the porosity of individual layers. Details of the analysis of interface zones in La/B-based multilayers using GIXR have been published elsewhere [39]. The use of a synchrotron for GIXR in situ measurement is outlined in the relevant section. GIXR has previously been used in thermal stability studies. This involved making in situ measurements of a multilayer being heated under a special annealing dome on a PANalytical Empyrean X-ray diffractometer. This makes it possible to track the evolution of structural changes at

elevated temperatures, over time. A detailed description can be found in the relevant section of the thesis.

2.3.4 Reflectivity above 6.6 nm

XUVR, or 'at-wavelength' reflectivity measurements, were used to directly obtain a value of the multilayer's Bragg peak reflectivity. In the context of this work, NI was always used at a fixed AOI of 1.5° off-normal. The specific measurement methods used for GI are outlined in the relevant section of the thesis. XUVR is more sensitive than GIXR to the chemical composition of layers and interfaces [28]. Further research, using more advanced approaches, is needed to obtain a more detailed analysis and a reconstruction of multilayer structure. For instance, when XUVR is combined with GIXR, the resultant reconstructed layer models are twice as accurate as those obtained by analysis of XUVR only [40]. 'At-wavelength' measurements were performed at the Physikalisch-Technische Bundesanstalt (PTB, Berlin) [41, 42], using synchrotron radiation from BESSY-II. At PTB, measurements of a mirror with an Mo/Si-based multilayer coating demonstrated a total uncertainty of peak reflectivity of just 0.10%. At the same time, the shift in peak wavelength observed at PTB was less than 1 pm [43].

2.3.5 X-ray diffraction (XRD)

XRD is a technique that is traditionally associated with crystallography. This thesis describes in situ two-dimensional (2D) XRD carried out at the ANKA synchrotron facility [44]. The aim was to study the formation and evolution of crystal structures during the growth of La and LaN. The purpose and details of those experiments are described in the relevant section of the thesis. Details of the physics and various geometries involved, together with analyses and numerous examples of XRD, have been published as monographs [45].

2.3.6 Optical microscopy

In our optical (visible light) microscopy studies of GI 6 nm stacks, we used a Nikon Eclipse ME600 microscope in a computer-controlled setup, using NIS-Elements imaging software (version D 3.10). The visual monitoring of sample surfaces over time enabled us to record the early stages of visible degradation, and to monitor the evolution of this process. The use of a computer-controlled microscope made it possible to program high frequency measurements of the same spot on a sample's surface, to observe its evolution over time. The information obtained in this way made it possible to directly compare different structures.

2.3.7 Atomic force microscopy (AFM)

The reflectivity of 6 nm multilayer mirrors depends on the characteristics of the top layer, such as roughness. As shown in the relevant section, the performance of GI 6 nm stacks is particularly sensitive to the properties of this top layer. A Bruker Dimension EdgeTM Atomic Force Microscope (AFM) was used to measure surface roughness. A

special high-resolution probe – Hi'Res-C14/Cr-Au by MikroMasch with a spike radius of about 1 nm – was used for this purpose. The use of a computer-controlled microscope made it possible to measure the same spot at set intervals, to monitor the evolution of surface roughness over time. In the case of GI multilayers, the information obtained using optical microscopy – in combination with AFM measurements – was used to develop an initial hypothesis concerning the nature of the ongoing processes involved.

2.3.8 Reflection high-energy electron diffraction (RHEED)

In the context of this thesis, RHEED was used – in addition to in situ 2D XRD studies – to explore the crystal structure of La and LaN single films. RHEED was measured after the composition of these films had been determined by XPS. In this way, it was possible to definitively exclude the possibility that any La_2O_3 structures had formed. RHEED also revealed aspects of the structure of LaN that were not fully understood. This was later resolved not by conventional techniques but through the use of high-intensity 2D XRD at the ANKA synchrotron facility [46].

References

1. D. L. Windt, Computers in Physics 12, 360 (1998)
2. B.L. Henke, E.M. Gullikson, and J.C. Davis, Atomic Data and Nuclear Data Tables, Vol. 54, No.2 (1993)
3. I. Petrov, F. Adibi, and J.E. Greene, Applied Physics Letters 63, 36 (1993)
4. S. Mahieu, D. Depla, Surface & Coatings Technology 204 (2010)
5. M. Pelliccione, Toh-Ming Lu, "Evolution of thin-film morphology", Springer series in Material Science 108, ISBN 978-0-387-75108-5 (2008)
6. D.K. Brice, J.Y. Tsao, S.T. Picraux, Nuclear Instruments and Methods in Physics Research Section B: Beam Interactions with Materials and Atoms 44 (1989)
7. D. Depla, "Magnetrons, reactive gases and sputtering", ISBN 978-1-304-34781-7 (2015)
8. B. Window, Journal of Vacuum Science & Technology A 11 (1993)
9. K. Sarakinos, J. Alami, P. M. Karimi, D. Severin and M. Wuttig, Journal of Physics D: Applied Physics 40 (2007)
10. www.srim.org
11. H.H. Andersen, Applied Physics 18 (1979)
12. A. I. Efimov "Properties of inorganic compounds," Handbook, Khimiya, Leningrad, (1983)
13. I.A. Makhotkin, E. Zoethout, E. Louis, A.M. Yakunin, S. Müllender, and F. Bijkerk, Optics Express 20(11) (2012)
14. T. Tsarfati, R.W.E. van de Kruijs, E. Zoethout, E. Louis, and F. Bijkerk, Thin Solid Films 518(5) (2009)
15. T. Tsarfati, R.W.E. van de Kruijs, E. Zoethout, E. Louis, and F. Bijkerk, Thin Solid Films 518(24) (2010)
16. I.A. Makhotkin, E. Zoethout, R.W.E. van de Kruijs, S.N. Yakunin, E. Louis, A.M. Yakunin, V. Banine, S. Müllender, and F. Bijkerk, Optics Express, Vol. 21, Issue 24 (2013)

17. D. Depla, S. Mahieu, “Reactive sputter deposition”, Springer Series in Material Science 108, ISSN 0933-033X (2008)
18. S.M. Foiles, Physical Review B 32 (1985)
19. Y.S. Ng, T.T. Tsong, and S.B. McLane Jr., Physical Review Letters 42 (1979)
20. P.R. Webber, C.E. Rojas, P.J. Dobson, and D. Chadwick, Surface Science 105 (1981)
21. D.G. Swartzfager, S.B. Ziemecki, and M.J. Kelley, Journal of Vacuum Science Technology 19 (1981)
22. R. Coloma Ribera, R.W.E. van de Kruijs, J. M. Sturm, A. E. Yakshin, and F. Bijkerk, Journal of Applied Physics 120 (6) (2016)
23. R. Coloma Ribera, R.W.E. van de Kruijs, J. M. Sturm, A. E. Yakshin, and F. Bijkerk, Journal of Applied Physics 121 (2017)
24. S.L. Nyabero, “Thermally induced diffusion phenomena and compound interlayer structural changes in EUV multilayers”, PhD thesis, ISBN: 978-94-6259-070-0 (2014)
25. D.S. Kuznetsov, A.E. Yakshin, J.M. Sturm, R.W.E. van de Kruijs, and F. Bijkerk, AIP Advances 6 (2016)
26. C. Kittel, “Introduction to Solid State Physics”, John Wiley & Sons (1971)
27. W. Wulfhekel, I. Beckmann, N.N. Lipkin, G. Rosenfeld, B. Poelsema, and G. Comsa, Applied Physics Letters 69(23) (1996)
28. I.A. Makhotkin, “Structural and reflective characteristics of multilayers for 6.x nm wavelength”, PhD thesis, ISBN: 978-94-6191-912-0 (2013)
29. N.N. Greenwood, A. Earnshaw, “Chemistry of the elements”, ISBN 978-0750633659, Second Edition, Elsevier (1997)
30. T. Tsarfati, “Surface and interface dynamics in multilayered systems”, PhD thesis, ISBN 978-90-5335-197-0 (2009)
31. W.F. Egelhoff Jr., P.J. Chen, C. J. Powell, M.D. Stiles, R.D. McMichael, J.H. Judy, K. Takano, and A.E. Berkowitz, Journal of Applied Physics 82 (1997)
32. Yu. Platonov, J. Rodriguez, M. Kriese, E. Gullikson, T. Harada, T. Watanabe, and H. Kinoshita, Proceedings of SPIE, Vol. 8076, EUV and X-Ray Optics: Synergy between Laboratory and Space II (2011)
33. A.E. Yakshin, R.W.E. van de Kruijs, I. Nedelcu, E. Zoethout, E. Louis, and F. Bijkerk, Proceedings of SPIE, Vol. 6517 (2007)
34. S. Hüfner, “Photoelectron Spectroscopy”, 3 edition, ISBN 3-540-41802-4, Springer (2003)
35. E. Zoethout, “Lanthanum nitride: creation at room temperature”, presented in FOM Institute Differ - Dutch Institute for Fundamental Energy Research, Nieuwegein, The Netherlands (2013)
36. E. Zoethout, “Lanthanum boron: growth at room temperature”, presented in FOM Institute Differ - Dutch Institute for Fundamental Energy Research, Nieuwegein, The Netherlands (2012, 2013)
37. H.R. Verma, “Atomic and Nuclear Analytical Methods”, Springer (2007)
38. M. Vieluf, F. Munnik, C. Neelmeijer, M. Kosmata, and S. Seichert, Thin Solid Films 520 (2012)
39. A. Zameshin, I.A. Makhotkin, S.N. Yakunin, R.W.E. van de Kruijs, A.E. Yakshin, and F. Bijkerk, Journal of Applied Crystallography, 49 (2016)

40. S.N. Yakunin, I.A. Makhotkin, K.V. Nikolaev, R.W.E. van de Kruijs, M.A. Chuev, and F. Bijkerk, Optics Express, Vol. 22, No. 17 (2014)
41. F. Scholze, C. Laubis, C. Buchholz, A. Fischer, S. Ploeger, H. Wagner, and G. Ulm, Proceedings of SPIE, Vol. 5751 (2005)
42. C. Laubis, A. Barboutis, M. Biel, C. Buchholz, B. Dubrau, A. Fischer, A. Hesse, J. Puls, C. Stadelhoff, V. Soltwisch, and F. Scholze, Proceedings of SPIE, Vol. 8679 (2013)
43. C. Laubis, A. Kampe, C. Buchholz, A. Fischer, J. Puls, C. Stadelhoff, and F. Scholze, Proceedings of SPIE, Vol. 7636 (2010)
44. A. Stierle, A. Steinhäuser, A. Rühm, F. U. Renner, R. Weigel, N. Kasper, and H. Dosch, Review of Scientific Instruments 75(12) (2004)
45. Bob B. He, "Two-dimensional X-ray Diffraction", Wiley, (2009) ISBN-13: 978-0470227220
46. B. Krause, D.S. Kuznetsov, A.E. Yakshin, S. Ibrahimkutty, T. Baumbach, and F. Bijkerk, Journal of Applied Crystallography 51 (2018)

Chapter 3: High-reflectance La/B-based multilayer mirror for 6.x nm wavelength

We report a hybrid thin film deposition procedure to significantly enhance the reflectivity of La/B based multilayer structures. This is of relevance for applications of multilayer optics at 6.7 nm wavelength and beyond. Such multilayers showed a reflectance of 64.1% @ 6.65 nm measured at 1.5 degrees off-normal incidence at PTB (BESSY-II). This was achieved by a special scheme of La passivation. The La layer was nitridated to avoid formation of the optically unfavorable LaBx compound at the B-on-La interface. To avoid the also undesired BN formation at the La-on-B interface, a time-dosed nitridation at the initial stage was applied. This research revealed a good potential for further increase in the reflectivity of multilayer structures at 6.7 nm.

Extreme ultraviolet (XUV) multilayers based on the constructive interference of reflected light are being investigated nowadays for several applications. In particular, these are ultrasensitive detection of materials by x-ray fluorescence [1], XUV telescopes for space research [2,3], optics for high-intensity free electron lasers (FEL) [4,5], and XUV photolithography (XUVL) [6,7]. The latter technology is required for fabrication of the new-generation chip patterns with improved spatial resolution.

For future XUVL, a wavelength window selection around λ = 6.7 nm is based on optical properties of suitable materials yielding in theory high reflectivity [8]. According to that requirement, La/B-based multilayers (MLs) are chosen and studied by different research groups [9–14]. However, so far in practice those MLs suffer from rather limited reflectivity. Note that reflectivity is directly relevant for the XUVL throughput, since it scales to the power of the number of mirrors.

The main reason for the limited performance of 6.7-nm MLs so far is the significantly reduced thickness of the layers with respect to the previous generation of 13.5-nm Mo/Si MLs [15]. Thus the detrimental effect of morphological roughness and intermixing between materials (including interdiffusion with subsequent compound formation) is significantly more pronounced: at least 0.5-nm-thick transition zones were found between La and B [16]. Assuming such a width at both interfaces, the calculated [17] absolute drop of peak reflectivity would be about 12% for La/B while only about 3% for Mo/Si multilayers. Nevertheless, using diffusion barriers or chemical passivation of materials, interdiffusion and compound formation on interfaces can be reduced. For instance, deposition of carbon diffusion barriers on the La-on-B_4C interface reached 58.6% at 6.66 nm but at 20.9° off-normal AOI [18], corresponding roughly to 56.5% at normal incidence, based on theoretical extrapolation. Nitridation of the whole La layer allowed to reduce the B-on-La interface, with a reflectivity of 57.3% at 1.5° off-normal angle of incidence (AOI) being achieved at 6.65 nm [16]. Also, reflectivity of 58.1% at 6.645 nm at off-normal AOI = 10° was demonstrated for LaN/B_4C multilayer [10], corresponding roughly to 57.5% at normal incidence. Notably, the theoretical maximum reflectivity, calculated [17] using experimental optical constants for pure B [19] and La [20], is about 80% (λ = 6.65 nm, AOI = 1.5° off-normal, s-polarized light), indicating the prospects for further improvement.

In this Letter, we report about an essential increase of reflectivity of LaN/B multilayer structures achieved by taking into account the processes at the LaN-on-B interface in the system with nitridated La. In particular, a hybrid deposition process that allows the fine tuning of the growth in combination with time-dosed layer passivation is demonstrated, resulting in a reflectivity of 64.1% at 1.5° off-normal AOI, the highest value reported to date to the best our knowledge.

The deposition of multilayers was performed using DC magnetron sputtering onto natively oxidized super-polished Si substrates (RMS ~2.0 ± 0.1 Å) in a chamber with a base pressure of 1×10^{-8} mbar. The working gas pressure was ~2×10^{-3} mbar. Deposition rate was about 0.05 nm/s for LaN and 0.03 nm/s for B. The composition deposited layers was checked by XPS, and La(N) showed about 5 atomic % of oxygen. IMD modelling [17] demonstrated that such contamination does not reduce reflectivity at 6.x nm wavelength. Therefore, the oxygen contamination was considered acceptable as were the stated above deposition rates in vacuum 1×10^{-8} mbar. All multilayers were covered with a 2-nm B layer to prevent oxidation.

We selected a system with nitridated La that up to date provided the highest reflectivity at near normal incidence (1.5° off-normal). Nitridation can be implemented either by using atomic nitrogen N and/or ion species N_x^+ due to their high reactivity, with the formation of LaN compound being energetically very favorable (enthalpy of formation ΔH = −303 kJ/mol). Initially, the nitridation of La was implemented by nitrogen-ion-assisted deposition or post-treatment of La layers using an ion source [21]. But the usage of an ion source has a limitation in achieving sufficiently low ion energy in order to avoid intermixing with the underlying layer. For this reason penetration of nitrogen through the entire multilayer period was observed in [21]. To solve this problem, we employed DC magnetron sputtering in N_2 gas environment to fully passivate La that previously [16] resulted in a significant reflectivity gain. Here the principle of nitridation remains the same. In a plasma with the presence of N_2 gas, ionization and/or splitting of N_2 molecules occurs via various electron-impact reactions [22]. The most abundant products of those reactions, N°, N^+, and N_2^+, form lanthanum nitride when impinging on a La surface.

In order to prevent intermixing between layers to the maximum extent, from general considerations full-passivated lanthanum nitride is preferred. This requirement means that all free chemical bonds of La are filled with N so the probability for interaction with the adjacent boron layers is minimized. In our experiment, such a condition was verified with x-ray photoelectron spectroscopy. It is important to consider that although passivation of La by magnetron deposition in nitrogen atmosphere can successfully protect the B-on-La interface, it also introduces a risk of formation of a BN compound at the La-on-B interface. Furthermore, the probability of formation of LaB_x at that interface cannot be excluded either. Indeed, at the initial stage of the lanthanum layer deposition in nitrogen environment, there is significant probability that both lanthanum and nitrogen atoms first interact with the boron atoms of the substrate layer instead of forming lanthanum nitride (Fig. 1). Formation of both compounds is thermodynamically favorable, with the enthalpies of

formation being ΔH = −130 kJ/mol and ΔH = −253 kJ/mol for LaB_6 and BN correspondingly [23]).

To check formation of the suggested compounds during the deposition, we did x-ray photo-electron analysis (XPS). For that purpose, a Thermo Scientific Theta Probe instrument was used employing monochromatic Al-Kα radiation. The in-depth analysis was done without ion sputtering to avoid destruction of the structure that provokes formation of compounds that initially were not present in the structure. For that, we performed angular resolved measurements with electron take-off angles from 27° to 79° relative to the surface normal.

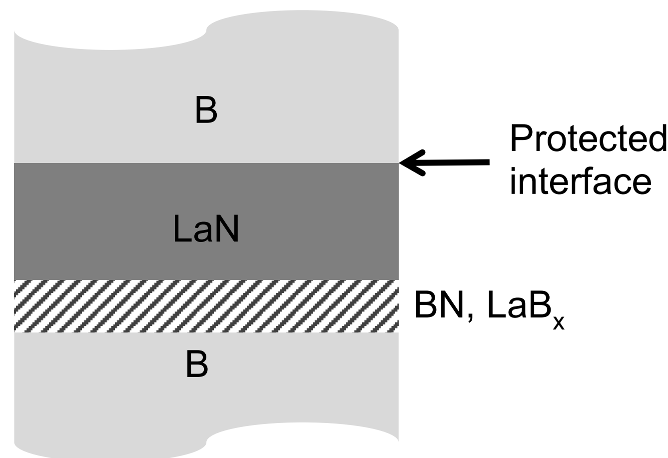

Fig. 1. Schematic representation of a part of the La/B-based multilayer with nitridated La. B-on-LaN interface is protected from chemical interaction, while BN and lanthanum borides may form at the LaN-on-B interface.

In the XPS measurement the probing depth is in the order of 5 nm, so only the top multilayer period was analysed. To detect LaBx, the XPS peaks of both B and La could be used. However unfortunately LaBx and LaN cause similar energy shift relatively to the La 4d doublet, so only the B peak could be used to identify the formed compounds. Fig. 2 shows the measured spectrum of the B peak. A peak fitting procedure to separate different components present in the sample allowed to detect the presence of BN in the sample. By default a Shirley background was used in the fitting procedure. Only for La 3d a so-called 'smart background' from the Avantage software was used. This background is based on Shirley, but with the constraint that the background cannot cross the signal, which would be unphysical. Standard Gauss-Lorentz peaks were added, either based on reference compounds (such as e.g. B, BN) or the minimal number of peaks is added to obtain a 'featureless' residual signal. If required to obtain a consistent fitting of the peaks over the entire angular range, constraints on the peak position were defined, typically to fix the peaks with ±0.1 to ±0.2 eV from their reference value (based on reference samples / reference cases).

The angular-resolved XPS measurements showed that the detected BN compound stays mostly below the top LaN layer, not on the B-on-LaN interface. This

confirms that a certain amount of BN does form below LaN layer during the nitridation process.

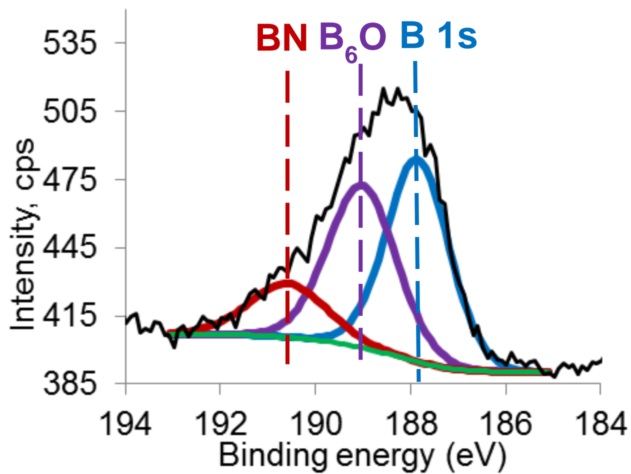

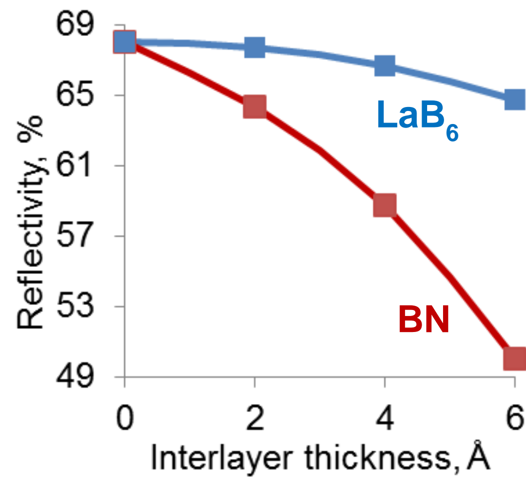

Fig. 2. XPS spectra measured from the top part of LaN/B multilayer including individual components used in the fitting procedure. The BN component is clearly present. B1s represents the elemental boron peak. Boron suboxide (corresponding to B_6O) is observed due to oxidation of the top B layer.

Fig. 3. Calculated peak reflectivity of LaN/B MLs with BN and LaB_6 as interlayers on the LaN-on-B interface. λ = 6.65 nm, AOI = 1.5 degrees off-normal. An effective roughness/diffused layer of 0.5 nm is taken for each interface.

Based on these findings, we synthesized a structure that excludes direct contact of nitrogen species with the underlying B layer at the LaN-on-B interface. The simplest way to realize that was to initially delay lanthanum nitridation. This effectively introduced a lanthanum interlayer at the LaN-on-B interface. It is known that in this case, chemical interaction of lanthanum with the underlying boron layer will result in the formation of a LaB_x interlayer [16]. To check the effect of that, we calculated [17] the reflectivity of multilayer structures for different thicknesses of LaB_6 interlayers and compared that to the effect of BN interlayers at LaN-on-B interface assuming effective roughness/diffused zones of 0.5 nm, as suggested in [16]. The calculations show (Fig. 3) that BN interlayers cause a significantly higher reflectivity drop compared to LaB_6. So in case of the formation of LaB_6 (instead of BN) compound at the LaN-on-B interface, we should expect gain in the ML reflectivity. Following the idea described above, 0.3 nm of La was first deposited on top of the boron layer followed by full-passivated LaN to complete the period (Fig. 4). The thickness of 0.3 nm was selected, as a minimally needed thickness to form a closed layer. XPS analysis shows almost full reduction of BN peak.

The soft x-ray reflectivity of the fabricated multilayer was measured at the radiometry laboratory of the Physikalisch Technische Bundesanstalt (PTB) [24,25] using

synchrotron radiation of the BESSY storage ring in Berlin, Germany. It showed that the used approach yielded 64.1% at 1.5° off- normal AOI (Fig. 5).

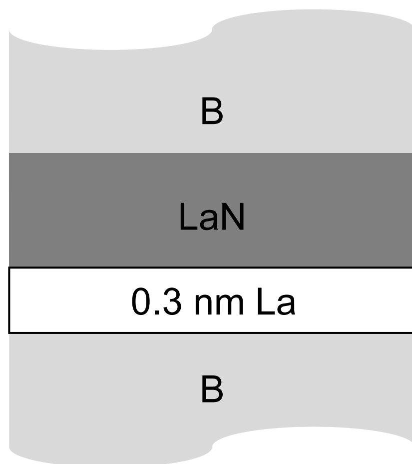

Fig. 4. Schematic representation of a part of the La/B-based multilayer produced according to the delayed nitridation scheme. Deposition of 0.3 nm La without nitridation is meant to reduce formation of unfavorable BN at LaN-on-B interface.

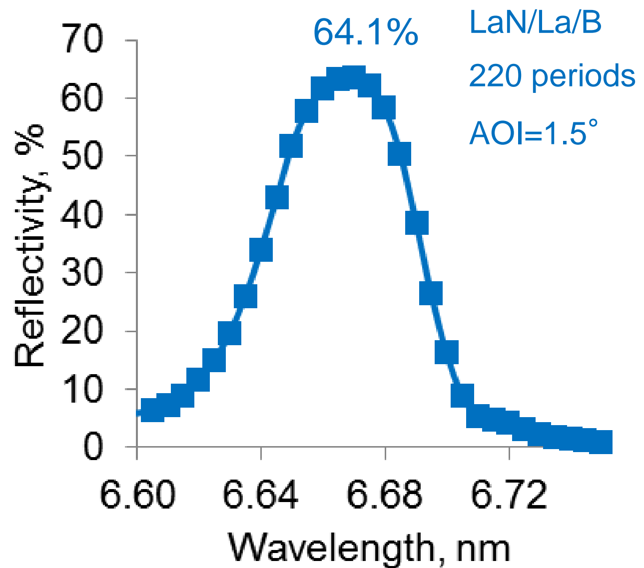

Fig.5. Measured reflectivity of a 220-periods B\La\LaN (materials stated in the sequence of deposition) ML with La interlayers of 0.3 nm introduced at the LaN-on-B interface (Fig. 3). The measurement was performed at 1.5 deg off-normal AOI at PTB.

This value is about 7% higher than the previously achieved best result of 57.3% at 1.5° off-normal AOI [16] obtained for a fully nitridated lanthanum layer. This gain is in qualitative agreement with the calculations presuming that about 0.4 nm of BN interlayer is substituted with about a similarly thick LaB_6 interlayer. This is also qualitatively confirmed by XPS measurements. BN was the dominant compound detected at LaN-on-B interface in the system with fully nitridated lanthanum layer. In the system with the delayed nitridation of lanthanum, lanthanum boride becomes predominantly present. Further details on this will be described in a separate publication.

To summarize, nitridation of the lanthanum layer in La/B multilayers is shown to protect the B-on-La interface from the formation of optically unfavorable LaB_x compounds at that interface. However, XPS measurements showed that the nitridation process results in the formation of an unfavorable BN compound at the opposite LaN-on-B interface. To prevent interaction of nitrogen species with boron atoms of the underneath layer, a short delay in the nitridation was used at the initial stage of the La layer passivation. The thus synthesized B\La\LaN multilayer mirrors showed a reflectivity of 64.1% at 6.65 nm measured at 1.5 degrees off-normal incidence. The

gain in reflectance is explained by formation of a more-optically favorable lanthanum boride compound instead of BN at LaN-on-B interface. The gain in reflectance shown and the analysis of the obtained structures are expected to lead to further gains in reflectance, a process similar to Mo/Si-based multilayers at 13.5 nm used in extreme ultraviolet lithography.

Acknowledgments: ASML; Carl Zeiss SMT GmbH; Foundation for Fundamental Research on Matter (FOM) (now part of the NWO, the Netherlands Organisation for Scientific Research); Industrial Focus Group XUV Optics; Malvern-PANalytical; Province of Overijssel; TNO; University of Twente.

Dr. Christian Laubis and colleagues at Physikalisch-Technische Bundesanstalt (PTB) are acknowledged for doing the reflectivity measurements.

References

1. M.K. Tiwari, K.J.S. Sawhney, and G.S. Lodha, Spectrochimica Acta Part B 65, 434 (2010)
2. D. Martinez-Galarce, P. Boerner, R. Soufli, J. Harvey, M. Bruner, J. Lemen, E. Gullikson, B. De Pontieu, N. Choi, M. Fernandez-Perea, N. Katz, S. Baker, E. Prast, S. Khatri, and J. Kong, 2nd International Conference on Space Technology (2011), p. 1.
3. K. Uji, I. Yoshikawa, K. Yoshioka, G. Murakami, and A. Yamazaki, Proceedings of SPIE 8528, 85281M (2012)
4. M. Barthelmess and S. Bajt, Applied Optics 50, 1610 (2011)
5. Y. Socol, G. N. Kulipanov, A. N. Matveenko, O. A. Shevchenko, and N. A. Vinokurov, Physical Review Accelelerators and Beams 14, 040702 (2011)
6. E. Louis, A. E. Yakshin, T. Tsarfati, and F. Bijkerk, Progress in Surface Science 86,
   1. 255 (2011)
7. V. Banine, A. Yakunin, and D. Glushkov, “Next generation EUV lithography: Challenges and opportunities” in International Workshop on Extreme Ultraviolet Sources, Dublin, Ireland (2010)
8. I.A. Makhotkin, E. Zoethout, E. Louis, A.M. Yakunin, S. Muellender, and F. Bijkerk, Journnal of Micro/Nanolithography, MEMS and MOEMS 11, 040501 (2012)
9. Y. Platonov, J. Rodriguez, M. Kriese, E. Gullikson, T. Harada, T. Watanabe, and H. Kinoshita, Proceedings of SPIE 8076, 80760N (2011)
10. P. Naujok, S. Yulin, N. Kaiser, and A. Tuennermann, Proceedings of SPIE 9422, 94221K (2015)
11. M.M. Barysheva, V.N. Polkovnikov, N.N. Salashchenko, S.D. Starikov, Yu. A. Vainer, and S. Yu. Zuev, Bulletin of the Russian Academy of Sciences: Physics 77, 24 (2013)
12. I.A. Makhotkin, E. Zoethout, E. Louis, A.M. Yakunin, S. Muellender, and F. Bijkerk, Optics Express 20, 11778 (2012)
13. T. Tsarfati, R.W.E. van de Kruijs, E. Zoethout, E. Louis, and F. Bijkerk, Thin Solid Films 518, 1365 (2009)
14. C. Montcalm, P.A. Kearney, J.M. Slaughter, M. Chaker, H. Pépin, and C.M. Falco, Applied Optics 35, 5134 (1996)

15. J. Bosgra, E. Zoethout, A.M. van der Eerden, J. Verhoeven, R.W.E. van de Kruijs, A. E. Yakshin, and F. Bijkerk, Applied Optics 51, 8541 (2012)
16. I.A. Makhotkin, E. Zoethout, R.W.E. van de Kruijs, S.N. Yakunin, E. Louis, A.M. Yakunin, V. Banine, S. Muellender, and F. Bijkerk, Optics Express 21, 29894 (2013)
17. D.L. Windt, Computers in Physics 12, 360 (1998)
18. N.I. Chkhalo, S. Kuenstner, V.N. Polkovnikov, N.N. Salashchenko, F. Schaefers, and S.D. Starikov, Applied Physics Letters 102, 011602 (2013)
19. M. Fernandez-Perea, J.I. Larruquert, J.A. Aznarez, J.A. Mendez, M. Vidal-Dasilva, E. Gullikson, A. Aquila, R. Soufli, and J.L. Fierro, Journal of the Optical Society of America 24, 3800 (2007)
20. B. L. Henke, E.M. Gullikson, and J.C. Davis, Atomic Data and Nuclear Data Tables 54, 181 (1993)
21. T. Tsarfati, R.W.E. van de Kruijs, E. Zoethout, E. Louis, and F. Bijkerk, Thin Solid Films 518, 7249 (2010)
22. D. Guettler, “An investigation of target poisoning during reactive magnetron sputtering”, Ph.D. thesis, Institut fuer Ionenstrahlphysik und Materialforschung (2008)
23. A.I. Efimov, Khimiya (1983)
24. F. Scholze, C. Laubis, C. Buchholz, A. Fischer, S. Ploeger, H. Wagner, and G. Ulm, Proceedings of SPIE 5751, 749 (2005)
25. C. Laubis, A. Barboutis, M. Biel, C. Buchholz, B. Dubrau, A. Fischer, A. Hesse, J. Puls, C. Stadelhoff, V. Soltwisch, and F. Scholze, Proceedings of SPIE 8679, 867921 (2013)

Chapter 4: Structure of high-reflectance La/B-based multilayer mirrors with partial La nitridation

We investigate a hybrid thin film deposition procedure that significantly enhances reflectivity of La/B based nanoscale multilayer structures to be used as Extreme UV mirrors at 6.7 nm wavelength and beyond. We have analyzed the La-nitridation process in detail, and proposed a growth mechanism and deposition procedure for full, stoichiometric passivation of La, avoiding the formation of optically unfavorable BN formation at the LaN-on-B interface. A partial nitridation was applied and studied as a function of the nitridation delay.

4.1 Introduction

The La/B-based multilayers have the potential to serve as mirrors for 6.x nm wavelength XUV lithography [1] and various applications, for instance, XUV telescopes for space research, [2,3] ultrasensitive analysis of materials by x-ray fluorescence [4] or optics for high-intensity free electron lasers (FEL) [5,6]. Different researchers achieved notable reflectivity at 6.x nm, dealing with different methods to control the interlayer quality. Examples include a LaN/B_4C system showing 58.1% at 6.645 nm at off-normal AOI 10°. [7], and the deposition of carbon barriers on the La-on-B4C interface yielded 58.6% at 6.66 nm, measured at 20.9° off-normal AOI [8]. For LaN/B reflectivity of 57.3% was achieved at 6.65 nm, measured already at near-normal incidence of AOI=1.5° off-normal [9]. A significant step towards the application-desired reflectivity of ~70% has been made by the so called delayed (partial) nitridation of La developed and demonstrated in ref. [10]. The obtained 64.1% reflectivity at AOI=1.5° off-normal, λ = 6.65 nm is a record value so far. The aim of this paper is gaining a deeper insight into the processes taking place at the interfaces during the partial nitridation. We first explore conditions required for the complete passivation of La layers. Then we focus on the formation of compounds during the full nitridation process of La layers. Finally the partial nitridation processes is investigated in terms of the formed compounds and their influence on 6.x nm reflectivity as a function of the nitridation delay.

4.2 Experimental

The deposition of multilayers was performed using DC magnetron sputtering onto natively oxidized super-polished Si substrates (RMS ~2.0 ± 0.1 Å) in a vacuum chamber with a base pressure of 1×10^{-8} mbar. The coater had no load lock. In order to protect the targets, especially, La, from atmosphere they were kept in vacuum-sealed packages and as quickly as possible installed inside the chamber. Right before each deposition the targets were cleaned by pre-sputtering till stable discharge parameters (current, voltage) and stable deposition rates measured by Quartz-Crystal Microbalances (QCM) were achieved. The working gas pressure was $\sim 2 \times 10^{-3}$ mbar. Deposition rate was about 0.03 nm/s for La, 0.05 nm/s for LaN, and 0.03 nm/s for B. All multilayers were covered with a 2.0 nm B layer to prevent oxidation. For all experiments, including XUV

reflectivity measurements, 50-period multilayers were used (instead of 220-period full stacks).

Thermo Scientific Theta Probe instrument was used for XPS measurements employing monochromatic Al-Kα radiation. Two types of XPS measurements were done: employing the ion depth-profiling and non-destructive measurement (angle resolved or AR XPS) of as-deposited samples. The XPS depth-profiling, using 0.5 keV Ar ions, was aimed to assess the in-depth distribution of chemical elements. The non-destructive measurement was used to avoid changes in the structure that provoke formation of compounds that initially were not present in the structure. For that, we performed angular resolved measurements with electron take-off angles from 27° to 79° relative to the surface normal. In the XPS measurement, the probing depth is in the order of 5 nm, so only the top multilayer period was analysed. The measured top layers were representative for the deeper layers in the multilayer. Indeed, sputter-cleaning of the samples (removing about 0.5 nm top contaminated part of the B layer) with subsequent analysis of XPS spectra revealed that there is no contamination of B or LaN by O or C within the XPS detectability. However, it is important to notice that a small part of the top B layer would still react with N_2 from atmosphere, with small amount of BN being formed at the surface. The signal from BN compound was present also for the elemental B reference sample, which set the lowest limit of BN detectability in the multilayer itself.

For the determination of the multilayers period, the grazing incidence X-ray reflectivity (GIXRR) was measured, employing PANalytical X'Pert X-ray diffractometer with a four-bounce monochromator (Cu-Kα radiation, 0.154 nm).

4.3 Synthesis of fully-passivated LaN

To minimize the chemical interaction with B layers in a multilayer, La should be fully passivated, i.e. as many La bonds as possible should take part in LaN compound formation. The passivation of La is implemented by the reactive magnetron sputter deposition of La with the addition of nitrogen gas into the chamber [9]. To find out the nitrogen pressure required during the deposition, modelling of the reactive sputtering process could be employed, for instance as developed by S. Berg et al. [11]. However, without precise values of the La and LaN sputtering yields (reactive deposition), the sticking coefficient of nitrogen to lanthanum, without taking into account nitrogen ion implantation into the target, etc., accurate calculations seem to be impossible. Moreover, in the plasma N°, N^+, and N_2^+ are produced via various electron-impact reactions [12], and positively charged species impinge the La target, neutralize (with certain probability) and reflect back, in the direction of the growing La layer [13], performing additional nitridation of deposited La. Modern advanced models of reactive deposition, for instance [14], require extraction of certain parameters by fitting the experimental data [15], which is time consuming. Therefore in this work we applied an experimental approach to determine conditions required for the complete passivation of La.

The required partial pressure of N_2 for this was found empirically by varying the pressure and employing XPS analysis of the atomic percentage of N in the multilayer.

In Fig. 1 XPS depth-profiles of nitrogen are plotted. For the case of 6 sccm N_2, saturation of La with N clearly was not reached, implying that B would still react with La on both interfaces due to the favorable LaB_x formation, with the enthalpy of formation of the stoichiometric LaB_6 compound being $\Delta H(LaB_6)$=-130 kJ/mol [16]. The presence of LaB_6 in non-passivated La/B multilayers was confirmed in [17] by wide-angle x-ray diffraction analysis. For the under-saturated LaN, the measured soft x-ray reflectivity around 6.7 nm wavelength at AOI of 1.5° off-normal was only about 14.0±0.5% for a 50-period multilayer stack, where the indicated error bar covers the typical reflectance reproducibility. The relatively low value is explained by the formation of La bonds with B, enhancing the interface layer thickness and reducing the optical contrast. Further increase of the N_2 flow higher than 12 sccm seems to result in the saturation of the N content in La (same N percentage in La on Fig. 1 for 12-21 sccm). This could be explained by the fact that La will not take more N during the reactive sputter deposition than needed to form a stoichiometric nitride. It was expected that a fully saturated LaN would result in an improved optical contrast due to reduced chemical interaction between the adjacent layers. Indeed for the N_2 flows 12-18 sccm the formation of a fully saturated La nitride resulted in a gain of the reflectance up to 18.5±0.5% at the same wavelength.

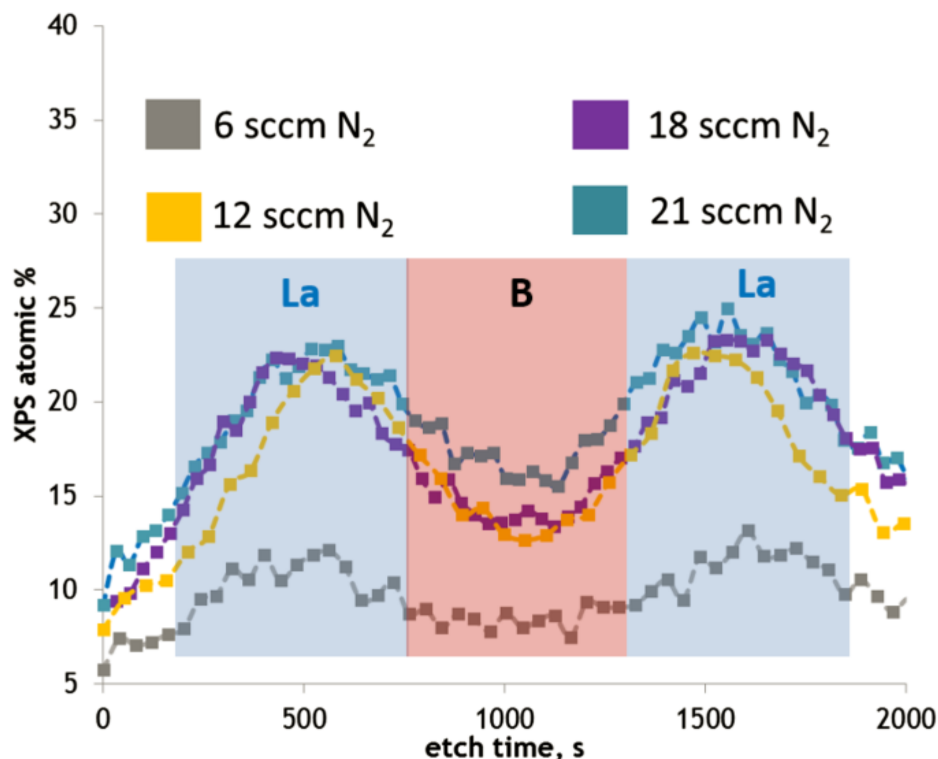

Fig.1. Nitrogen atomic percentage depth-profiles obtained by XPS for LaN/B multilayers deposited with 6, 12, 18 and 21 sccm of N_2 flow during La deposition.

However, further increase in N_2 flow resulted in a reflectivity loss. Namely, for an N_2 flow of 21 sccm the reflectivity dropped to ~12.5% and this is even lower than it was for the under-saturated case. Markedly, for the N_2 flow of 21 sccm nitrogen is already

detected in-between the La layers at the XPS depth-profile (see Fig. 1, B layer), indicating that the nitrogen atoms are present in the boron layers and/or at the interfaces. Note that due to significant alteration of the structure during depth-profiling by ion intermixing and probable sputter-induced compound formation the accurate composition of the samples could not be determined from this measurement.

4.4 BN formation

In order to reveal the compounds formed in the deposited stack, a AR-XPS measurements of as-deposited samples was employed. The measured spectra of B1s clearly showed the energy shift typical for the presence of the BN compound. The intensity of the corresponding BN peaks increases with the higher N_2 flows used for LaN deposition. For the adequate comparison of the BN amount of the multilayers with somewhat different periods, it had to be taken into account that the thicker B and LaN layers absorb more radiation of the probing X-ray beam in the XPS analysis. Moreover, a different degree of oxidation of the cap and the first LaN layer could make comparison of the absolute atomic percentage of BN unreliable. As a solution, the peak area ratios of BN to total B (elemental B1s and the B- compound(s)) were calculated. Their comparison is represented in Fig. 2a. The empirically obtained ratio for elemental B is also plotted as a reference where BN is present at the surface due to the exposure of the sample to atmosphere. As observed in Fig. 2a, the peak area ratio BN/total B increases in the whole N_2 flow range explored, indicating the amount of BN increasing with N_2 flow, from a certain onset value on. This can be explained by the fact that at higher N_2 flows there is more N available which interacts with B at the initial stage of LaN deposition.

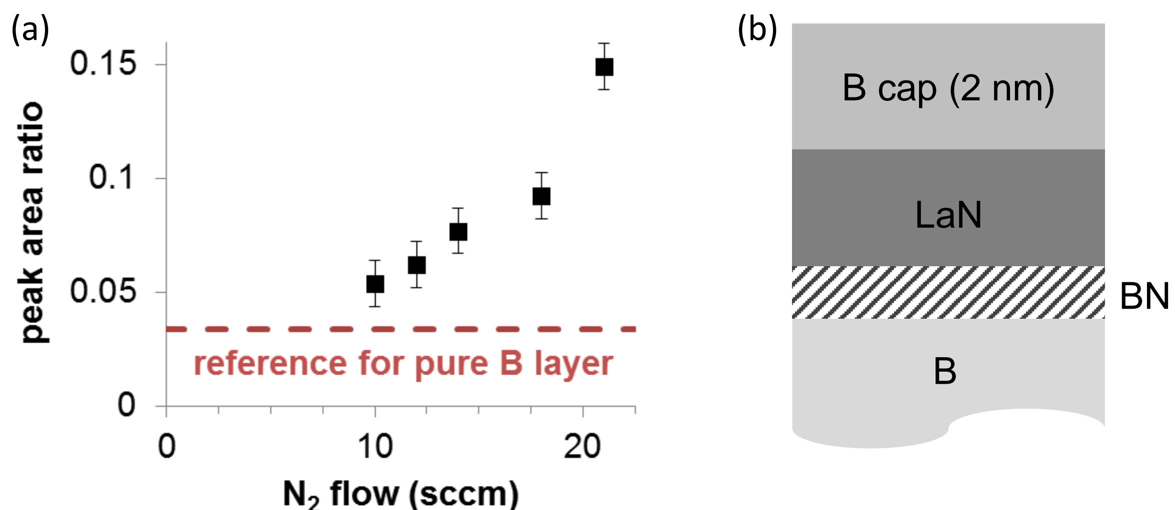

Fig. 2. (a) Ratios of fitted XPS peaks (B1s BN/total B1s) versus the N_2 flow employed during the deposition of LaN. The mentioned ratio for a deposited layer of elemental B is plotted with a dash line (for reference). **(b)** Schematic representation of the multilayer top layers as analysed by AR-XPS.

There are two “types” of interfaces in LaN/B multilayers: B-on-LaN and LaN-on-B. In order to reveal at which of them the most of BN is formed, AR-XPS measurements were done. The XPS spectra collected when the probing beam was at a more grazing angle clearly demonstrated less BN amount. That means that most BN is formed on the deeper-situated, LaN-on-B interface. In case most of the BN would be at the B-on-LaN interface, the BN signal should increase relative to La signal with more grazing angles. That is not observed in practice. The supportive schematic representation is sketched in Fig. 2b.

It is also possible to follow the trend of the amount of the formed BN at the interfaces by determining an effective expansion or compaction of the period due to the compound formation for various deposition conditions. The calibrated deposition rates at different nitrogen flows inherently takes into account any LaN thickness-effect due to different saturation of LaN with nitrogen. A dedicated set of samples was deposited varying N_2 flow values. In every deposition run a few stacks were deposited on top of each other, each one having a different LaN thickness. From GIXRR measurements periods of the stacks in every individual deposition run were determined. The extracted period values were plotted versus the LaN deposition times used for different stacks deposited in the one deposition run. An example of such analysis for a deposition with N_2 flow of 14 sccm is presented on Fig. 3.

The points were fitted with a linear regression. The slope of the line, about 0.04 (nm/s), determines the deposition rate of LaN. Extrapolation of the line to zero yields a value (~2.3nm) corresponding to a B layer thickness plus a certain value related to interface compaction or expansion. The latter was obtained by subtracting a known from a separate calibration deposited B thickness. In our experiment this value is positive that means an effective expansion of the multilayer period. It is important to note that this approach does not allow to judge about the width of the interface, because the depth of interdiffusion and real densities of the formed materials are not known.

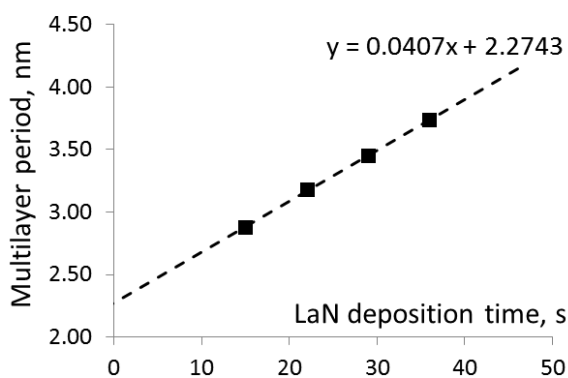

Fig.3. Periods of the stacks for different deposition time of LaN layers in the stacks. The LaN layers were deposited with 14 sccm N_2 flow.

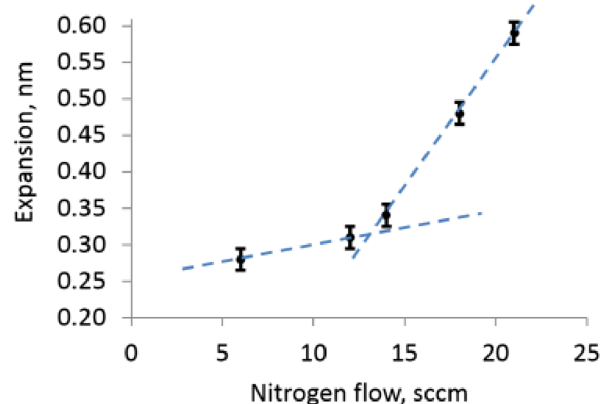

Fig.4. Effective expansion of the multilayer period versus N_2 flow used for La nitridation.

On Fig. 4 the determined above effective multilayer period expansion versus nitrogen flow used for La nitridation is plotted. The expansion is clearly not linear with the N_2 flow, and can be considered as two processes as indicated by the two lines with different slopes at the graph on Fig. 4. To explain this we consider a factor of competition between different atomic interactions during La deposition on B in N_2 environment. During this, two simultaneous processes are expected to occur: the interaction of B with La and interaction of B with N. The enthalpies of formation of the corresponding compounds are 130 kJ/mol (LaB_6) and 253 kJ/mol (BN), respectively [16]. Therefore, here we disregard the La-B interaction which is less favorable from thermodynamics point of view. At the initial stage of LaN layer deposition, if the N_2 flow is low, La takes significant part of the overall amount of N to form LaN. The remaining part is consumed by B to form BN, which causes the multilayer period to expand. The combination of these two processes results in the observed period expansion rate at low N_2 flows on Fig. 4. At higher N_2 flows, we observe a saturation in the amount of N in La. As shown above, La cannot take more N than needed to form stoichiometric LaN compound. As a result, after LaN is fully saturated, all the remaining (due to further increased N_2 flow) nitrogen species are available to react with B to form BN. At this stage the BN formation is greatly enhanced, that corresponds to the steeper slope on the Fig. 4.

4.5 Special scheme of La nitridation (“delayed” nitridation)

In Ref. 10 the effect of a thin BN interlayer on the LaN-on-B interface was calculated, and a significant drop of 6.x nm reflectivity due to this BN was shown. This loss can be explained by comparing the optical constants of B and BN at 6.70 nm wavelength. The absorption coefficients for B and BN are $\beta(B) \sim 4.1x10^{-4}$, $\beta(BN) \sim 8.9x10^{-4}$ [18], which means that BN absorbs 6.7 nm radiation more than 2 times stronger than B. The refraction coefficient for boron nitride ($\delta(BN) \sim 5.4x10^{-3}$) is ~4 times higher than that for B ($\delta(B) \sim 1.3x10^{-3}$). This means that instead of working as a spacer, BN reduces the optical contrast with the reflector layer, La(N), which also contributes to reflectivity losses. So, from an application point of view, it is important to notice that the standard reactive deposition of LaN in nitrogen atmosphere cannot in practice yield the highest possible reflectance of LaN/B multilayers. The formation of optically unfavorable boron nitride is inevitable even at relatively low nitrogen flows. But the latter should be high enough to obtain, as already mentioned above, a fully-passivated (saturated) LaN, i.e. to have it chemically inert to the maximum possible degree.

To prevent interaction of nitrogen species with B atoms of the underneath layer, we synthesized structures in such a way to avoid direct contact of N with the underlying B layer at the LaN-on-B interface. The simplest way to realize that was to delay the process of lanthanum nitridation. Effectively this should introduce a pure La layer on the B layer. Below we investigate the effect of this layer on the underlying interface and its impact on the reflective properties of the multilayers. A range of La thicknesses of 0.1 to 0.8 nm was taken for this experiment before starting the La nitridation. The actually deposited amount of La was a little larger to compensate for the interaction of La with the underlying B. To determine the moment when this interaction is

complete, compaction of the period was taken into account as described above for expansion. For the deposition of LaN we selected the conditions of the fully-passivated LaN (N_2 flow 12 sccm).

To determine if there is a reduction in the BN formation on the LaN-on-B interface, AR-XPS analysis was performed. The ratio of the fitted XPS B1s BN to total B1s peaks was taken for comparison (as described above). The resulting BN/total B ratio as a function of the La thickness is shown in Fig. 5.

The small error bars in the Figure 5 account for reproducibility of the peak fit with fixed constraints on the peaks. The bigger error bars stay for different fitting results with varied constraints, i.e. the uncertainty of the peak fitting model. The dashed line represents a reference BN/B ratio measured for a single layer boron film, where BN is present due to the exposure of the sample to atmosphere. The probed depth corresponds up to approximately 5 nm [19] of the top part of the structure. Strictly, the measured for this top part may not be exactly multiple of the bilayer thickness. So, the fitted percentage cannot be attributed to the composition of a bilayer.

As seen in Fig. 5 for La thickness of 0.1 nm the BN/total B ratio has the same value within the error bars as the “reference” LaN/B multilayer with fully passivated La layers. This means that 0.1 nm La did not noticeably reduce the BN formation.

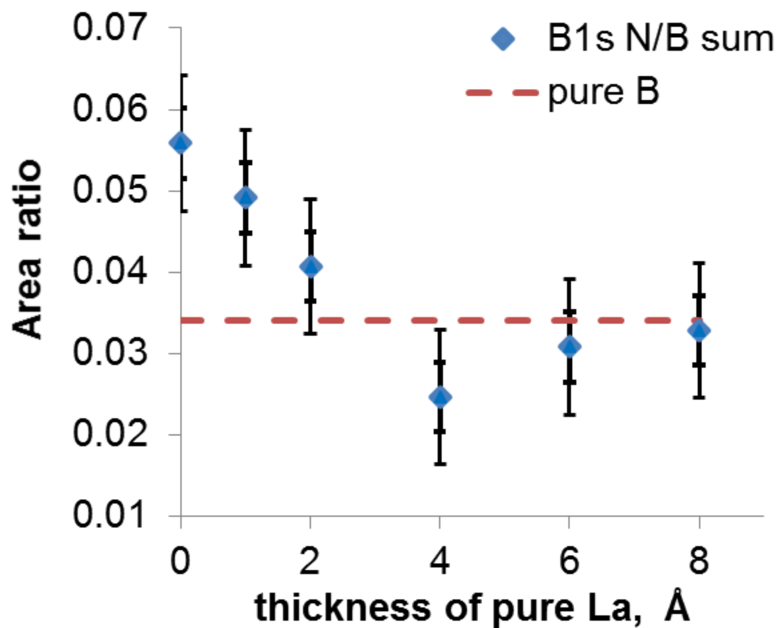

Fig.5. Ratio of the fitted B1s BN to total B1s XPS peak for different La thickness in the multilayers with delayed nitridation prepared at 12 sccm of N_2.

This is in agreement with the reflectivity measurement of this sample that showed 16.2±0.5% versus 17.2±0.5% % for the multilayer with fully passivated La. Starting from 0.3 nm of La, the BN/total B ratio becomes close to the elemental B reference, which suggests that these La thicknesses lead to a significant reduction of the amount of BN formed at the interface. This result is supported by a sharp increase in the reflectance

of the multilayers to 21.5±0.5% at 6.75 nm. From this it becomes obvious that the La thicknesses of 0.3 nm and higher are sufficient to form a structure with a closed layer, which prevents interaction of B with the nitrogen species.

It should be mentioned that introducing the lanthanum layer directly on the B layer will cause a chemical interaction of La with the underlying B layer, resulting in the formation of a LaB_x interlayer. Our calculations showed that reflectance of the multilayer would clearly decrease with the increase of LaB_x interlayer thickness [10]. Therefore it could be expected that the reflectivity of the multilayers would also decrease with the increase of the non-passivated La thickness, or larger delay in nitridation. This is provided the entire non-nitrided La would interact with B. However, as mentioned above, the multilayers with partial nitridation having La thickness in the range 0.3-0.8 nm demonstrated the same reflectivity within run-to-run reproducibility of ±0.5%. This points to the fact that as soon as a certain very thin LaB_x interlayer is formed, it does not grow anymore with the increase of the deposited La thickness. And as shown in [10] such a LaB_x interlayer is optically more favorable than the BN formed in case of complete La nitridation, resulting in a significantly enhanced reflectance.

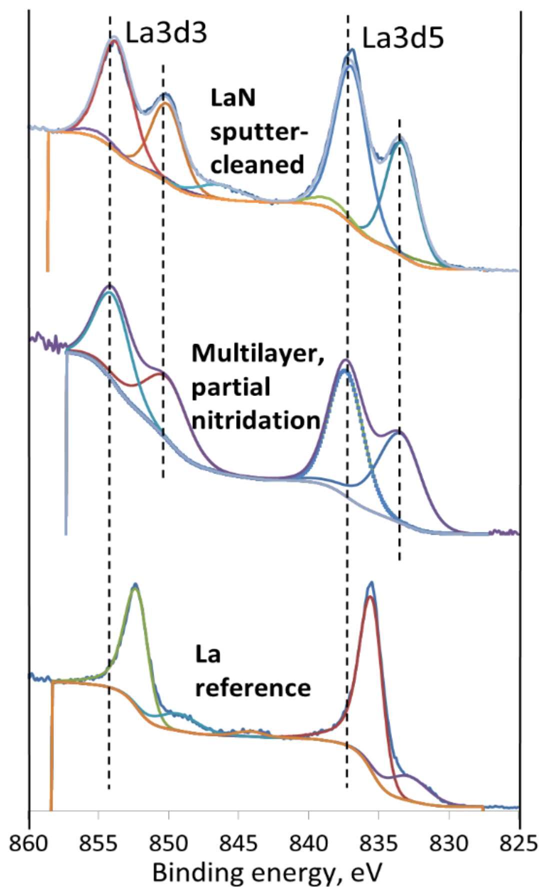

Fig. 6. Fitted La3d XPS spectra from sputter-cleaned LaN reference layer (top), multilayer with partial nitridation (middle) and the sputter-cleaned elemental La reference layer (down).

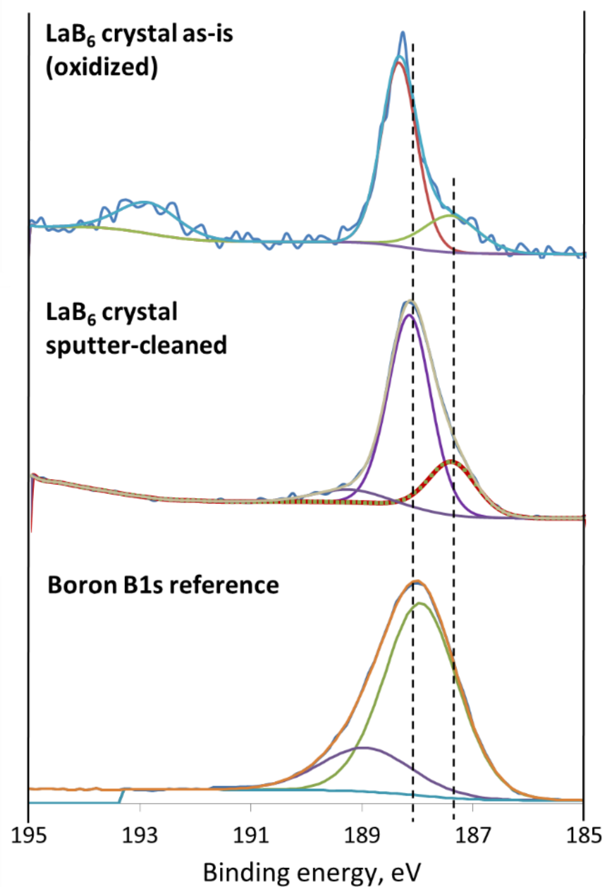

Fig. 7. Fitted B1s spectra from as-introduced (oxidized) LaB6 reference crystal (top), the latter measured after sputter-cleaning (middle) and elemental B reference (down).

To find out what is in fact formed on the interface as a result of the applied delayed nitridation, XPS analysis was employed. In Fig. 6 a fit of La3d measured spectra for one of the samples fabricated with delayed nitridation is plotted together with the spectra from La and LaN references. All peaks of the fitted spectrum for the sample with delayed nitridation coincide with the ones of LaN sputter-cleaned reference, but the exact fit depends on the constraints set on the fitting procedure. To fit the mentioned La3d spectrum from the partial nitridation sample the width of Gaussians had to be bigger than for fitting the spectrum from LaN reference. Low intensity side-peaks (shoulders) towards lower binding energies for both peaks from La3d doublet from La reference could be associated with La oxide.

Fig. 6 shows that the main La3d peaks for the elemental La reference has a position in-between the La peaks from the delayed nitridation sample. Since all La XPS peaks of the multilayer samples are rather broad, it is not possible to perform a unique peak fitting to prove or disprove the presence of elemental La. Therefore, fitting of the XPS spectra solely cannot be employed for tracing the elemental La, in this particular case. Below on Fig. 8 La3d spectra from the samples with ~0.2 and ~0.8 nm thick La are compared.

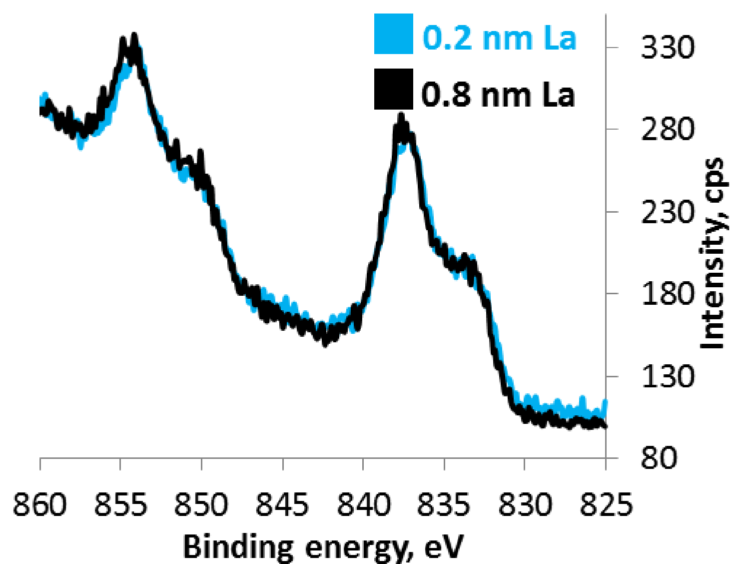

Fig.8. La3d XPS spectra from delayed nitridation samples with ~0.2 and ~0.8 nm La thickness.

In the XPS measurements no differences in the position of peaks and their intensity could be observed. This means that the chemical composition and the amount of materials are the same within the accuracy of the XPS measurement. It is anticipated that elemental La is mostly nitridized by the subsequent deposition of LaN. The reasons for nitridation of La by LaN deposition on top of it could be the following. First, nitridation is chemically-driven by direct interaction with reactive nitrogen species. Experiments with a thick La layer [20] revealed that the exposure of a La layer to N_2 gas already leads to the formation of a LaN stoichiometric overlayer with a

thickness of 0.5±0.2 nm. The second reason, in the case of LaN reactive magnetron sputter deposition, is the presence of relatively high-energy nitrogen neutrals [13] reflected from the La target which serve as an additional source of nitridation of the deposited elemental La, as mentioned above. The remaining question is why the nitrogen species do not penetrate deeper inside the B layer. We suggest that all arriving nitrogen species are trapped inside the elemental La with the subsequent formation of LaN. As soon as LaN is formed, it serves as a good diffusion barrier against further penetration of nitrogen species.

We also made an attempt to trace the anticipated on La-on-B interface LaB_6 by XPS. The La3d spectrum from a LaB_6 crystal was collected for the purpose of reference (not shown). The main fitted La3d5/2 peak for a sputter-cleaned (oxide and other surface contaminants removed) LaB_6 crystal appears at 837.5 eV, which is in agreement with literature values: 837.3 eV in Ref. 21, or 837.5 eV in Ref. 22. The positions of those peaks almost coincide (within ~0.2 eV) with the peaks in the La3d spectrum of the partial nitridation samples (and by so also with the peaks from our LaN reference, see Fig. 6). This makes tracing LaB_6 in the particular samples impossible if analysing XPS spectra from La levels. Due to that the XPS spectra of B1s were also analysed. In Fig. 7 the B1s spectrum from a sputter-cleaned LaB_6 crystal is presented together with the oxidized (as-is) LaB_6 crystal to demonstrate that the binding energy for the main (highest intensity) LaB_6 peak decreases just by ~0.2 eV due to ion surface treatment to sputter the oxide. This confirms no significant structure and composition changes due to this cleaning procedure. The main B1s peak from this LaB_6 reference has a binding energy in-between B1s elemental reference value (see Fig. 7) and sub-oxide of B (fitted at about 189 eV peak for B1s reference in Fig. 7), and, in principle, may even overlap with boron sub-oxide of a certain stoichiometry. However, sub-stoichiometric boron oxides are inevitably present in the multilayer samples (due to exposure to atmosphere). Therefore, a possible contribution of LaB_6 to the B1s spectrum cannot be traced by spectrum fitting in our particular case. The side peak fitted in the B1s spectrum from LaB_6 reference at ~187.4 eV, has a larger separation from the B1s elemental peak (~187.9 eV), but the low intensity of this side peak even for a pure LaB_6 reference, in combination with the broad nature of 1S peaks, suggests that the contribution from a few-monolayer-thick LaB_6 layer below other layers will not be visible in the measured spectrum at all. Moreover, the real stoichiometry of the formed lanthanum boride is unknown, so the formed compound may have deviation of binding energy from the expected for the stoichiometric one. So, additional experiments are required.

4.6 Summary

We have investigated a hybrid thin film deposition procedure that significantly enhances the reflectivity of La/B based multilayer structures to be used as reflecting elements at 6.7 nm wavelength and beyond. The procedure is a refinement of using fully nitrided La layers. It was found that La will not take more N than needed for the formation of a stoichiometric LaN compound, however excessive N_2 during the La

growth results in the formation of optically unfavorable BN at the LaN-on-B interface. To avoid this, the so-called delayed (partial) nitridation at the initial stage of La growth was applied and studied as a function of the nitridation delay. A range of 0.1 to 0.8 nm thicknesses of the non-nitrided elemental La was explored. For La thicknesses ∼0.3 nm and thicker clear reduction of the BN content on LaN-on-B interface was observed by AR-XPS. This observation was correlated with a noticeable improvement of the 6.x nm reflectivity of the 50-period multilayer structures from 17.2±0.5% to 21.5±0.5%, λ≈6.75 nm. For full (220 periods) stacks, as reported [10], the increase was from 57.3% [9] to 64.1%, AOI=1.5°, λ≈6.66 nm. The calculated [10] theoretical maximum about 80% for an ideal multilayer structure leaves a significant space for future improvements. The mechanism of the partial nitridation is explained as the prevention of N to interact with the underlying B layer by forming a closed layer of elemental La. It has been concluded that a part of this non-passivated La layer forms a thin LaB_x compound at the interfaces with B, though this LaB_x is proven to be optically more favorable at LaN-on-B interface than BN.

Acknowledgements

We acknowledge the support of the Industrial Focus Group XUV Optics at the MESA+ Institute at the University of Twente, notably the industrial partners ASML, Carl Zeiss SMT GmbH, Malvern-PANalytical, TNO, as well as the Province of Overijssel and the Foundation FOM (now part of the NWO, the Netherlands Organisation for Scientific Research).

Dr. Christian Laubis and colleagues at Physikalisch-Technische Bundesanstalt (PTB) are acknowledged for doing the reflectivity measurements.

References

1. V. Banine, A. Yakunin, and D. Glushkov, "Next generation EUV lithography: Challenges and opportunities" in International Workshop on Extreme Ultraviolet Sources, Dublin, Ireland (2010)
2. D. Martinez-Galarce, P. Boerner, R. Soufli, J. Harvey, M. Bruner, J. Lemen, E. Gullikson, B. De Pontieu, N. Choi, M. Fernandez-Perea, N. Katz, S. Baker, E. Prast, S. Khatri, and J. Kong, 2nd International Conference on Space Technology (2011)
3. K. Uji, I. Yoshikawa, K. Yoshioka, G. Murakami, and A. Yamazaki, Proceedings of SPIE 8528 , 85281M (2012)
4. M.K. Tiwari, K.J.S. Sawhney, and G.S. Lodha, Spectrochimica Acta Part B 65, 434 (2010)
5. M. Barthelmess and S. Bajt, Applied Optics 50 , 1610 (2011)
6. Y. Socol, G.N. Kulipanov, A.N. Matveenko, O.A. Shevchenko, and N.A. Vinokurov, Physical Review of Accelerators and Beams 14, 040702 (2011)
7. P. Naujok, S. Yulin, N. Kaiser, and A. Tuennermann, Proceedings of SPIE 9422, 94221K (2015)
8. N.I. Chkhalo, S. Kuenstner, V.N. Polkovnikov, N.N. Salashchenko, F. Schaefers, and S. D. Starikov, Applied Physics Letters 102, 011602 (2013)

9. I.A. Makhotkin, E. Zoethout, R.W.E. van de Kruijs, S.N. Yakunin, E. Louis, A.M. Yakunin, V. Banine, S. Muellender, and F. Bijkerk, Optics Express 21 , 29894 (2013)
10. D.S. Kuznetsov, A.E. Yakshin, J.M. Sturm, R.W.E. van de Kruijs, E. Louis, and F. Bijkerk, Optics Letters, Vol. 40, No. 16 (2015)
11. S. Berg and T. Nyberg, Thin Solid Films 476 (2005)
12. Dominik Güttler, "An investigation of target poisoning during reactive magnetron sputtering", PhD thesis, Institut für Ionenstrahlphysik und Materialforschung, Forschungszentrum Dresden-Rossendorf e.V., Dresden (2008)
13. K. Sarakinos, J. Alami, P.M. Karimi, D. Severin, and M. Wuttig, Journal of Physics D: Applied Physics 40 (2007)
14. K. Strijckmans and D. Depla, Journal of Physics D: Applied Physics 47 (2014)
15. K. Strijckmans, W.P. Leroy, R. De Gryse, and D. Depla, Surface & Coatings Technology 206 (2012)
16. A. I. Efimov, "Properties of inorganic compounds", Handbook, Khimiya (1983)
17. S.L. Nyabero, R.W.E. van de Kruijs, A.E. Yakshin, I.A. Makhotkin, J. Bosgra, and F.Bijkerk, Journal of Micro/Nanolithography, MEMS and MOEMS 13(1), (2014)
18. B.L. Henke, E.M. Gullikson, and J.C. Davis, Atomic Data and Nuclear Data Tables Vol. 54 (no.2) (1993)
19. Stefan Hüfner, "Photoelectron Spectroscopy", 3 edition, Springer (2003), ISBN 3-540-41802-4
20. E. Zoethout, "Lanthanum-nitride: creation at room temperature", presentation in FOM Institute Differ, 09 April 2013 (not published)
21. S.J. Mroczkowski, "Electron emission characteristics of sputtered lanthanum hexaboride", J. Vac. Sci. Technol. A, Vol. 9, No. 3 (1991)
22. R. Kanakala, "Exploring the synthesis of hexaborides: The basis of a new chemistry for the preparation of electro-optical materials", UMI Dissertations Publishing (2008)

Chapter 5: Thermal stability of high-reflectance La/B-based multilayers for 6.x nm wavelength

We have investigated the thermal stability of La/B-based (LaN/La/B) multilayer structures with partial-layer nitridation of La, a method shown earlier to result in enhanced reflectivity. The structures were annealed in the temperature range 100–500°C for 70 h. They showed period drifts by 0.005 nm at 100°C to 0.06 nm at 500°C. A reflectivity loss of more than 2% was only observed after annealing above 300°C. The study included separate investigation of B-on-LaN and LaN-on-La-on-B interfaces.

5.1 Introduction

In the XUV wavelength region, a single layer or surface of any material cannot provide high reflectivity of light. This requirement is, however, of crucial importance for systems with complex optical path including numerous reflections. An example is XUV lithography, which is highly desirable to further reduce the size of integrated circuits, decrease their power consumption, and increase productivity of electronic components [1]. This application demands high reflectivity multilayer mirrors that are built on the principle of constructive interference of light reflected from interfaces between layers of different materials. These materials are selected based on the maximum possible difference in their refractive index and low absorption. La/B-based multilayer mirrors are considered to have perspective for next-generation extreme UV photolithography at 6.x nm wavelength [1].

Similar to Mo/Si mirrors for 13.5 nm wavelength, the new 6.x nm systems have requirements on the thermal stability of the mirrors. The thermal load may result in interdiffusion at the interfaces and the formation of compounds [2] that reduce the optical contrast and thus the reflectivity [3]. Moreover, these processes may affect the period of the stack, detuning these Bragg mirrors from the centroid wavelength of operation. Passivation of La to form LaN compounds was applied previously [4] to minimize interaction between La and B thus enhancing optical contrast between the layers by reducing the interface zones between them. The conditions for reactive sputter deposition of fully passivated LaN were investigated [5]. The highest, to our best knowledge, normal-incidence reflectivity so far reached is 64.1% at 6.65 nm, measured at 1.5° with respect to the sample surface normal [6]. This has been achieved by applying a partial nitridation procedure for a LaN/B multilayer, which includes deposition of 0.3–0.8-nm elemental La on B followed by a fully passivated [5] LaN layer. This new structure has two interfaces, B-on-LaN and LaN-on-La-on-B, of which the properties under elevated temperatures are yet unknown.

Some studies of thermally induced changes in LaN/B multilayers in the temperature range 250–400°C were performed in Ref. 3. An increase in the period was observed in the range of a few picometers to tens of picometers. Interdiffusion processes were found to be slower in LaN/B multilayers than in La/B, which was also correlated with a significantly smaller decrease of the reflectance of LaN/B under elevated temperatures. To explore these stability issues in greater detail, in this work a LaN/La/B multilayer was investigated with LaN/B as a reference multilayer in order

to reveal any changes due to the partial nitridation. Dedicated structures based on single layers were produced to study interdiffusion and compound formation at the interfaces separately. Grazing-incidence hard X-ray reflectivity (GIXRR), XUV (at-wavelength) reflectivity measurements, X-ray photoelectron spectroscopy (XPS), and High-resolution Rutherford Backscattering Spectroscopy (HR-RBS) were the experimental techniques employed.

5.2 Experimental

A dedicated set of full-stack (220 periods of ~3.5 nm) LaN/B and LaN/La/B multilayers were deposited by DC magnetron sputtering [7] on super-polished (root mean square roughness 0.2 nm) Si wafers following the conditions in Refs. 4 and 6, respectively. The investigated range of annealing temperatures was from 100 to 500°C. The annealing time for all the temperatures was about 70 h, because the multilayer period changes observed by GIXRR during the annealing at the highest temperature of 500°C saturated after this time. After this saturation, interdiffusion and related heat-induced processes may still continue but at a significantly slower rate. The study of the long-term thermal stability requires a dedicated research.

Under the elevated temperatures, the period change is assumed to be associated with interdiffusion and subsequent formation of compound(s). This assumption is based on previously obtained results for Mo/Si-based [8] and La/B-based [3] multilayers.

To be able to monitor small period changes of the multilayers during annealing, GIXRR measurements have been performed in-situ, employing a PANalytical Empyrean X-ray diffractometer (Cu-Ka radiation, 0.154 nm). To minimize the enhanced oxidation and other contamination at elevated temperatures, the sample was placed under a dome which was continuously flushed with nitrogen. A detailed description of the thermal stage has been outlined earlier [9]. To prevent misalignment of the sample due to thermal expansion of the heating plate and its support, a re-alignment procedure was performed before each GIXRR scan.

Low-order Bragg peaks might shift at elevated temperatures as a result of changes in the refraction of the analyzed multilayer due to changes in the average density of the stack and evolution of the interface roughness caused by interdiffusion. This shift could result in misinterpretation of the multilayer period expansion. However, our estimates [8] showed that the effect of the changing refraction on the higher orders Bragg peaks can be neglected. Therefore the multilayer period values were extracted from GIXRR curves by fitting the higher order Bragg peaks with the simplified Bragg equation [10] to evaluate the multilayer period drift originating from interdiffusion and formation of compounds.

In order to assess the error of determination of the period, a partial derivative of the Bragg's equation is taken. The calculation is done taking 0.001° angular uncertainty and 0.15×10^{-3} nm wavelength uncertainty. The angular uncertainty includes the sample alignment accuracy. The second contribution into the error corridor comes from the fitting procedure, and its uncertainty is assessed to be about 0.003 nm. The total uncertainty calculated as the root mean square of the two

contributions is 0.005 nm or ±0.0025 nm. Notably, the first order Bragg peak was not employed in the fitting procedure due to the relatively high influence of refraction on its position [8]. The effect of bulk material expansion (and resulting multilayer period increase) at elevated temperatures was compensated by using tabulated values of expansion coefficients of materials [11,12] like in previous work [3]. It was determined by WAXRD that the layers in the multilayers had an amorphous structure. Therefore thermal expansion coefficients for amorphous materials were used.

At-wavelength (XUV) reflectivity, measurements of the as-deposited and annealed samples were performed at the Physikalisch-Technische Bundesanstalt (PTB, Berlin) [13,14] employing synchrotron radiation from BESSY-II. The angle of incidence (AOI) in these measurements was fixed at 1.5° with respect to the surface normal of the sample.

To determine interdiffusion of elements and formation of compounds in the samples as a result of annealing, XPS was used, employing a Thermo Scientific Theta Probe instrument with monochromatic Al-Ka radiation. The binding energy scale is calibrated to a measured binding energy of the Ag3d5/2 peak of 368.2 eV. The atomic percentages are calculated taken into account elemental sensitivity factors and dependence of the information depth on photoelectron energy according to Scofield sensitivity factors, as well as the transmission function of the analyzer. Non-destructive XPS measurements were done on the as-deposited structures and the structures were annealed at selected temperatures within the 100–500°C range.

XPS sputter depth-profiles were measured only for the samples annealed at 500°C because higher temperatures result in enhanced interdiffusion, such that the chance to resolve the changes was higher. The etching was done using Ar^{+} ions with an energy of 0.5 keV.

Due to the typical XPS probing depth of about 5–6 nm [15,16] in a non-destructive measurement of a 3.5 nm-period multilayer, a few interfaces were probed, which complicated the analysis and induced some ambiguity in determining the interface from which the signal originates. Therefore, for the studies of the B-on-LaN interface, which is present both in the reference LaN/B as well as in LaN/La/B multilayers, dedicated samples containing a few layers were additionally deposited.

The sample deposition and vacuum annealing studies were performed with a home-built deposition system in-vacuo connected to the XPS instrument via a sample transfer system. The base pressures in the deposition, sample transfer, and XPS systems were 5×10^{-10} mbar or lower. The films were deposited by DC magnetron sputtering in the same conditions as the full stack multilayers. The sample annealing was carried out with a heater element integrated in the sample holder, while the temperature was measured by an N-type thermocouple clamped to the sample surface.

In addition to XPS, High-Resolution Rutherford Backscattering Spectroscopy (HR-RBS) was employed. Since conventional RBS with a depth resolution of ~5–50 nm [17] cannot be used to judge sub-nm diffusion of elements between layers, HR-RBS [18] was performed at the Ion Beam Center (IBC) of the Helmholtz-Zentrum Dresden-Rossendorf. In that scheme, C^{2+} ions of 2.02 MeV hit the sample under an impact angle

of 17.5° with respect to the surface and undergo (forward) scattering at the target nuclei. Taking into account the geometry of the experiment, the technique can also be referred to as Rutherford Forward Scattering. Under a scattering angle of 35.8°, the scattered particles are analyzed by means of a magnetic spectrometer of the Browne–Büchner type [19]. The energy resolution of the magnetic spectrometer used in the HR-RBS study was 4 KeV, which translates into a depth resolution of below 1 nm in the surface proximity. HR-RBS measurements were carried out before and after annealing. Two dedicated samples representing the structures with and without partial nitridation were used: Si wafer/8 nm B/0.4 nm La/1.0 nm LaN/2.5 nm B and Si wafer/8 nm B/1.4 nm LaN/2.5 nm B, correspondingly.

5.3 Period expansion

In Fig. 1, the period changes for the LaN/B and LaN/La/B multilayers due to annealing-treatment are presented. These data are corrected for the bulk material thermal expansion.

Comparison of the period changes for LaN/B (a) and LaN/La/B (b) reveals qualitatively the same behavior in the entire temperature range studied: an initial "immediate" effective period expansion and a gradual further increase of the period in time. However, the partial nitridation system has a slightly larger period expansion at 400–500°C out of the error-corridors. After about 70 h, the period change significantly slows down for both structures at all temperatures investigated. Longer-term thermal stability requires further studies.

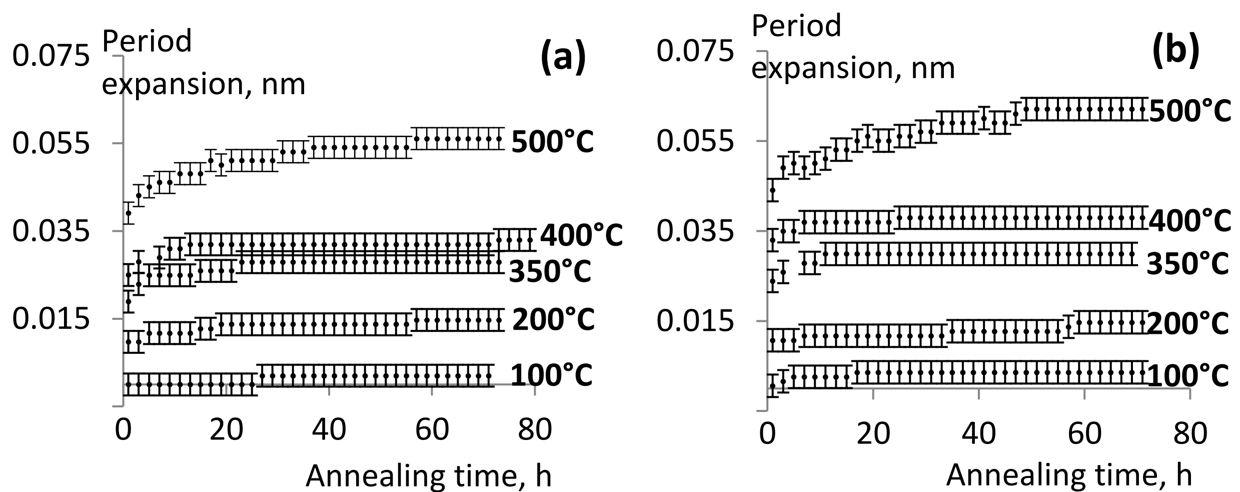

Fig.1. Period change of (a) LaN/B and (b) partial nitridation (LaN/La/B) multilayers extracted from GIXRR in-situ measurements during annealing. The total uncertainty is about 0.005 nm (shown as the vertical error bars).

5.4 6.x nm reflectivity (PTB)

At-wavelength (XUV), reflectivity data was measured for as-deposited and annealed LaN/B and LaN/La/B samples at selected temperatures 100, 200, 350, and

500°C. The absolute difference between the peak reflectivity values for as-deposited and annealed samples is plotted in Fig. 2. The peak reflectivity values measured at PTB have an uncertainty of 0.1% absolute [20] which in Fig. 2 is well within the size of the plotted points. At 100°C, the reduction of R is within 1%, for 200°C within 1.5% both for LaN/B and LaN/La/B. The observed higher absolute R drop for LaN/La/B at 500°C vs. LaN/B is correlated with a larger effective expansion of the period for LaN/La/B (Fig. 1), and might be related to (poly)crystallization of main material(s) and/or interlayer(s) which would result in enhanced interdiffusion/layer roughness. Those processes are out of the scope of this paper.

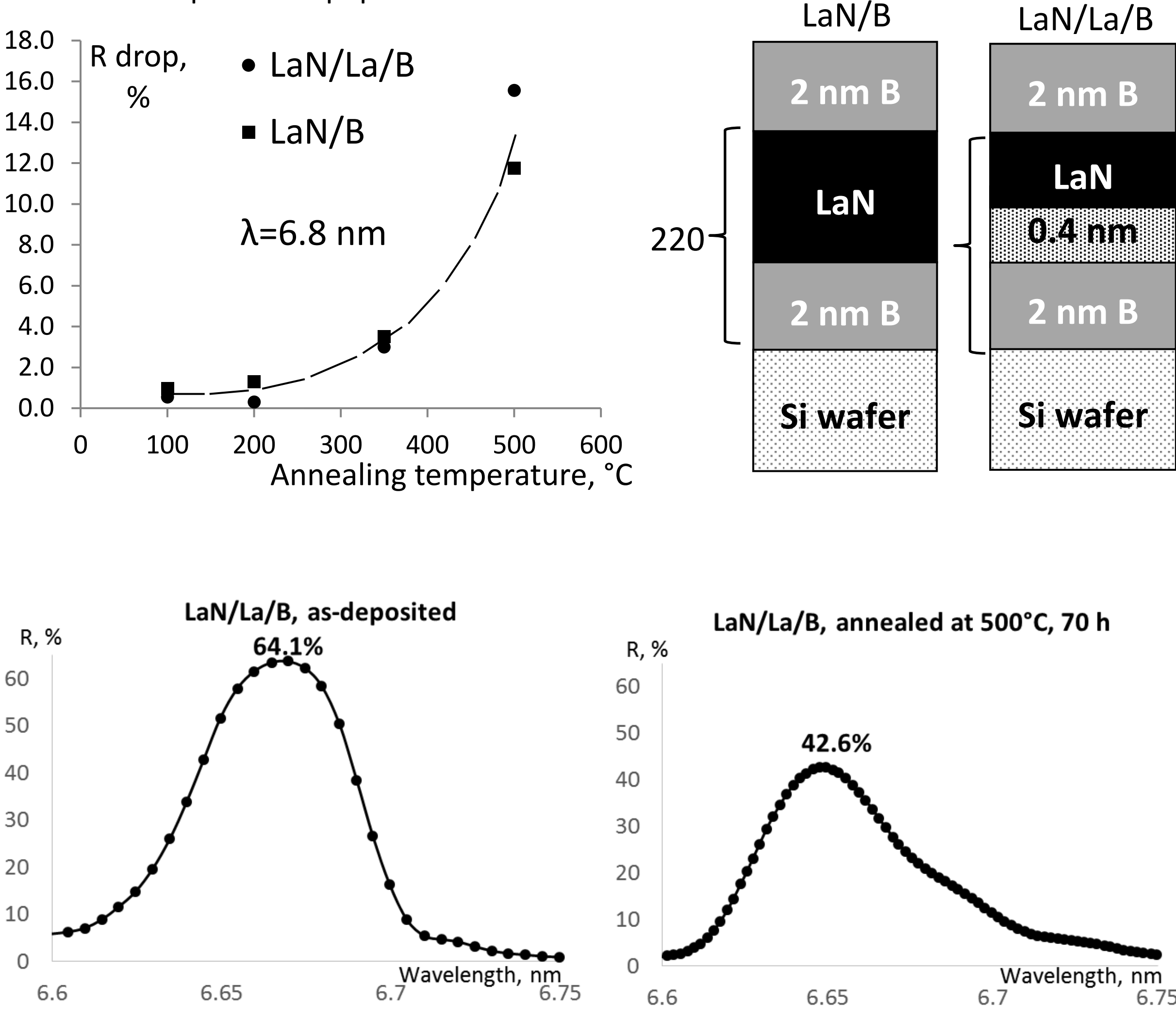

Fig.2. On the left, above: absolute drop of the peak reflectivity value for reference (LaN/B) and partial nitridation (LaN/La/B) multilayers. The dash line serves as a guide to the eye to mark the general dependence of R on the annealing temperature. On the right, above: schematic structures of LaN/B and LaN/La/B multilayer mirrors. Below: reflectivity measured for LaN/La/B (partial nitridation) multilayers measured as-deposited (left) and after annealing at 500°C for 70 h (right).

From general considerations, the at-wavelength reflectance drop depends on the particular compound(s) formed, their exact composition and density, position in

the bilayer, width, and concentration profile of the elements at the interfaces in between the "bulk" layers. The nature of broadened reflectivity peak for annealed at 500°C versus the peak from as-deposited multilayer was not investigated. Hypothetically, it could be explained by intermixing and compound formation, resulting in (extra) interlayers of different optical properties versus as-deposited state. Since all the multilayers in this work are capped with a ≈2 nm B layer, a small part of the R drop comes from enhanced absorption of radiation in the capping layer. Based on the known experimental evidence, a 0.5–0.6 nm thick BxOyCz layer is modeled [21] as the top part of the B cap in the as deposited samples, and the drop of R is well within 0.2%. As will be shown below by non-destructive XPS measurements of the annealed multilayers, at 500°C, stoichiometric B_2O_3 is formed on top of the B cap. Calculations show that the reflectivity drop for the worst case, when all 2 nm thick B would be fully oxidized (which is not observed in experiment), would be within 1.5%. So, the largest part of the reflectivity loss is related to changes in the multilayer itself in the entire temperature range studied.

5.5 Non-destructive XPS spectra

The multilayer samples were annealed employing a special setup of the diffractometer, as described above. Here we will show an example of non-destructive XPS measurements of as-deposited and annealed multilayers at 500°C. An annealing temperature of 500°C was chosen to have higher chances for an observable interdiffusion effect. An example of the fitted B1s spectrum from a LaN/B multilayer is plotted in Fig. 3. For the as-deposited structure, the peak modeled at a binding energy of about 188.0 eV corresponds to elemental boron. The peak modeled at about 188.8 eV accounts for under-stoichiometric boron oxide (boron sub-oxide), being formed due to natural oxidation of the top B layer by atmosphere gases. The next modeled peak towards higher binding energies corresponds to BN which is formed (mostly) on the LaN-on-B interface for the as-deposited samples. The spectrum for the as-deposited partial nitridation (LaN/La/B) structure has only one additional feature compared to the spectrum for the reference LaN/B: the reduced amount of BN compound. This was demonstrated and discussed in detail in [5].

The spectrum of the annealed multilayer at 500°C shows pronounced reduction of the elemental boron amount, which is explained by enhanced oxidation of the top B layer at elevated temperature. The peak appearing at around 192.4 eV stands for stoichiometric boron oxide B_2O_3. The peak at about 189.3 eV for the annealed samples is considered to come from a boron sub-oxide which is somewhat richer in oxygen than the one for the as-deposited state. This explains the shift of peak to higher energy.

Unfortunately no conclusions could be drawn on the formation of compound(s) inside the multilayer at elevated temperatures. Discrimination of the compounds (namely, observed BN) at different interfaces is very difficult since XPS is probing a few interfaces of the 3.5 nm period multilayer, given the probing depth of about 5–6 nm. Additional uncertainty of quantification of BN comes from the low intensity of the BN peak in-between the high-intensity B oxide peaks (B_xO, B_2O_3 in Fig. 3) on B1s spectra. This contamination of the initially 2 nm thick B layer cannot be etched away without

the risk of intermixing B with the underlying layer(s). So, annealing of the samples in a nitrogen flushed atmosphere as used in this research resulted in significant contamination of the top layer, which did not allow analysis of the BN content with sufficient accuracy. For this reason, further non-destructive XPS analysis was done in vacuum, employing special structures for separate analysis of interfaces, which is described below in the section “Dedicated studies….”.

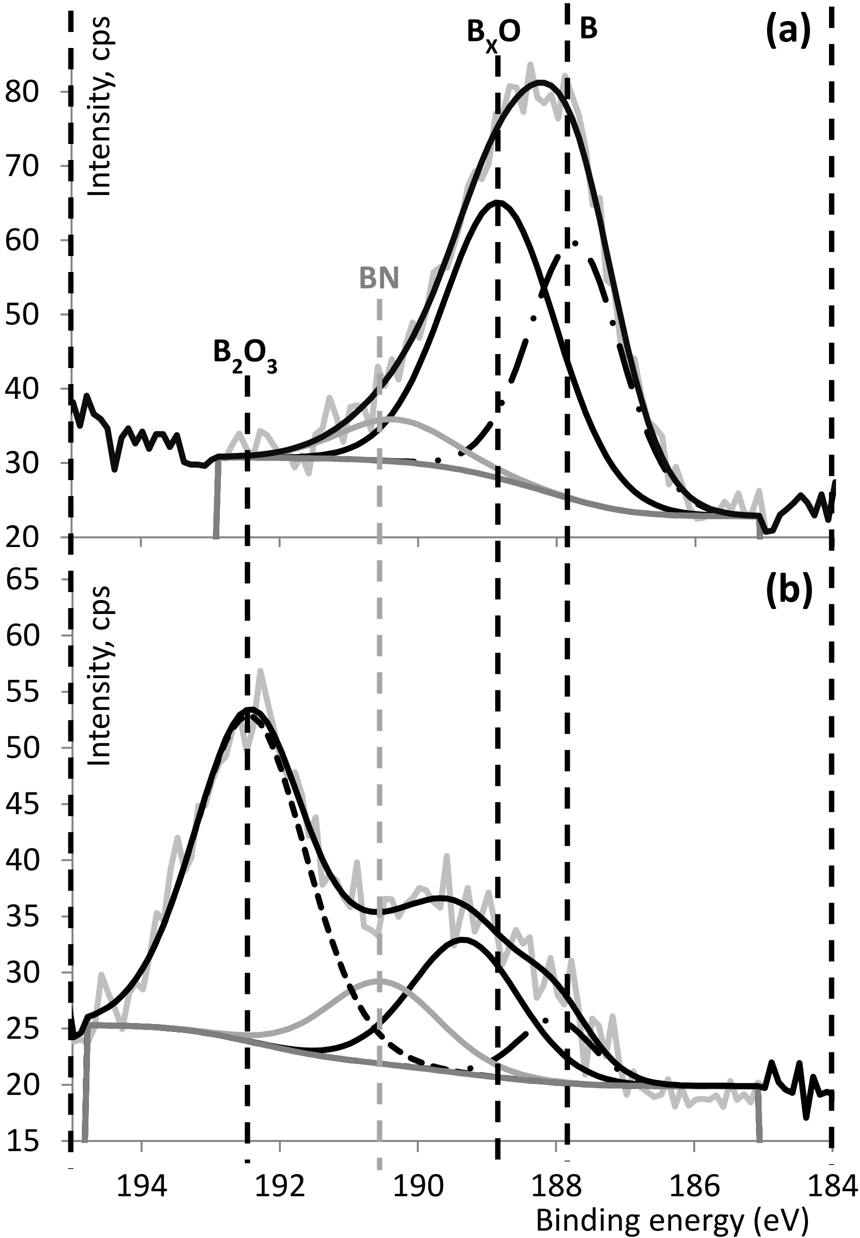

Fig.3. B1s spectra measured for (a) as-deposited LaN/B multilayer and (b) LaN/B multilayer annealed at 500°C. The spectra are fitted with peaks corresponding to B, B_xO, BN, and B_2O_3.

5.6 XPS depth-profiles

In addition to non-destructive XPS, we also carried out depth-profile measurements by XPS. The results of the analysis are presented at Fig. 4. Due to reduced ion etching rate of the oxidized B in the annealed samples, the profiles have been shifted along the time (thickness) x-axis for the sake of visual comparison.

Annealed samples show a significantly reduced percentage of B in comparison to the as-deposited structures at the initial stage of depth-profiling for both LaN/B and LaN/La/B multilayers. This is explained by oxidation of the top B layer at elevated temperature. Deeper lying bilayers (periods) did not suffer from oxidation, according to the XPS depth-profile of oxygen atomic percentage (not shown), therefore they could be compared for as-deposited state with the state after annealing. Unfortunately, due to the measurement noise, uncertainties in the XPS spectra fitting procedure, and, most notably, intermixing caused by ion-etching, no conclusions based on difference between the profiles before and after annealing can be made on interdiffusion of chemical elements due to annealing.

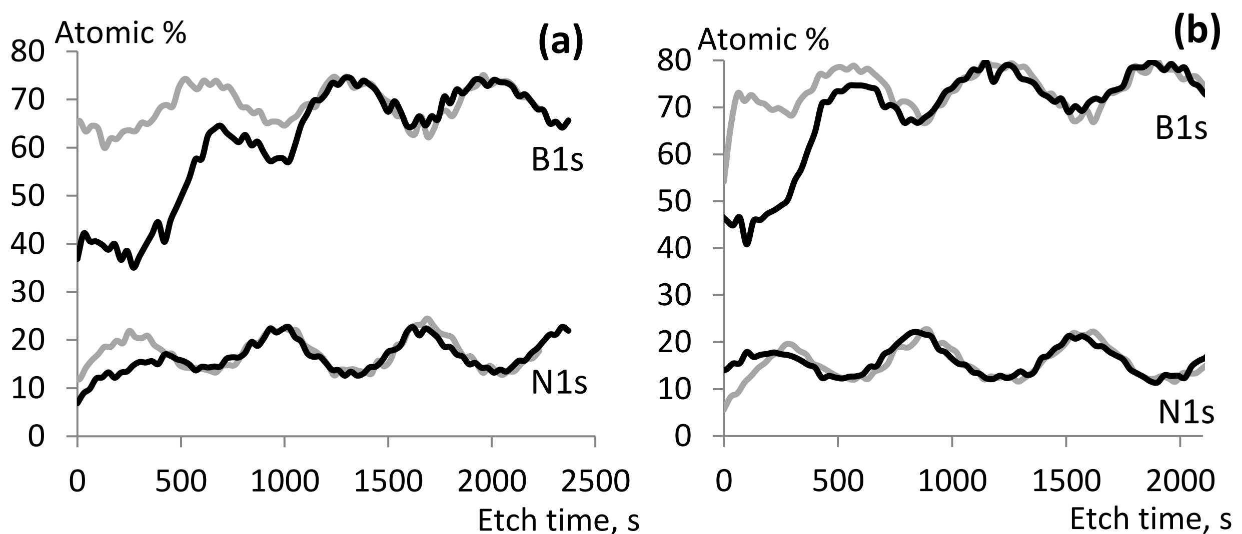

Fig.4. XPS depth-profiles for as-deposited (grey lines) and annealed 500°C, 70 h (black lines) (a) LaN/B and (b) LaN/La/B multilayers. The atomic percentage of nitrogen and boron is extracted from, respectively, analysis of N1s- and B1s-related fitted peaks of XPS spectra.

5.7 Non-destructive HR-RBS

To avoid the uncertainty introduced by the depth profiling procedure, non-destructive HR-RBS was employed on specially prepared test structures with only a few layers. The results are presented in Fig. 5 together with the schematic representation of the structures of the samples used here specifically. Thicknesses of top B layers and La-based layers in the structures are about as in the 3.5 nm period multilayers. Only the thickness of the B layer deposited first on the wafer deviates significantly, being 8 nm. However, from our experiments it is known that B with this thickness stays amorphous,

and does not show measurable (by AFM) development of roughness compared to 2 nm B films. Therefore, the conclusions made from the study of these dedicated test structures are considered directly applicable for the 3.5 nm period multilayers.

Only the part of the measured spectrum corresponding to La is shown (the response from the Si wafer is of no interest). The conducted HR-RBS measures the signal from La only due to the specially selected mass of the probing ions (C^{2+}). As seen, within the measurement uncertainty there is no clear difference between the peaks from the LaN-on-La-on-B structure before and after annealing. The same observation holds for the B-on-LaN sample (not shown here). Therefore, from the obtained profiles we can conclude that for the annealing up to 500°C interdiffusion of La is within the sub-nm resolution of the HR-RBS measurement. For lower temperatures, interdiffusion would then occur within an even smaller range.

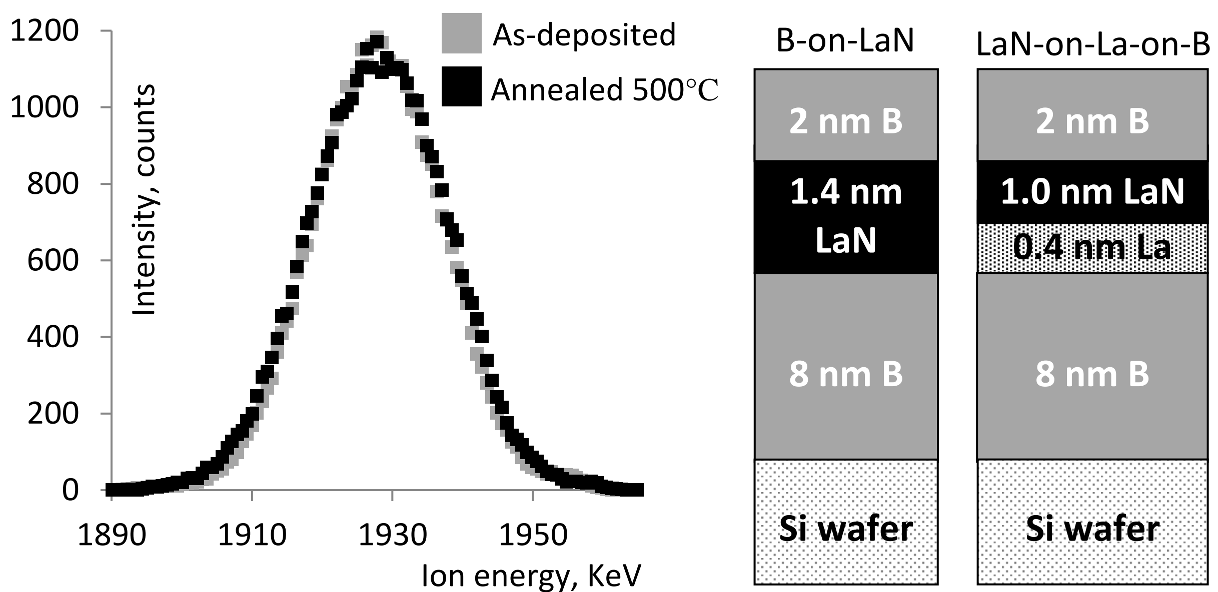

Fig.5. On the left: HR-RBS peaks for a LaN-on-La-on-B sample in the as-deposited state and after annealing in vacuum as described above. On the right: the schematic representation of the structure of measured with HR-RBS samples.

5.8 Dedicated study of B-on-LaN and LaN-on-La-on-B interfaces

To resolve chemical processes taking place at different interfaces we deposited two other dedicated model structures, namely, B/LaN/Si (2 nm B/7 nm LaN/Si wafer) and LaN/La/B/Si (1.0 nm LaN/0.4 nm La/8 nm B/Si wafer). A schematic representation of the structures is shown in Figs. 6(a) and 6(b). As outlined in section "Experimental," these structures represent two interfaces in the multilayer structure with partial nitridation. B/LaN/Si allows to probe solely the B-on-LaN interface. The other structure represents the LaN-on-La-on-B interface. The structures were measured with non-destructive XPS directly after deposition and after annealing at temperatures up to 300 °C. Temperatures above 300°C were considered to be of no further practical interest for the reason of a pronounced reflectivity loss (more than 3% absolute in peak value).

Furthermore, at higher temperatures there exists a significant risk of recrystallization of the constituting materials that can result in an accelerated diffusion process (for instance, [22]), which would confirm that higher temperatures have little practical interest. Note that in the current work, no attempt was made to trace lanthanum boride formation by XPS [23]. The partial overlap of the B1s peak of LaB_6 with the relatively broad B1s peak of elemental boron, overlap of the La4d peak of LaB_6 with La4d peaks of La and LaN, and overlap of La3d 3/2 and La3d 5/2 peaks of LaB_6 with corresponding La3d peaks of LaN are known [5]. In combination with the very low intensity of the signal from the B1s side peak specific for LaB_6, even for a reference LaB_6 crystal [5], few-Ångström-thick LaBx interlayers in practice are untraceable with XPS. All investigated samples have a layer of LaN, and from our earlier studies we know that the N1s peak of BN partially (but significantly) overlaps with the N1s of LaN. And due to the high intensity of the N1s peak from a nanometer-thick LaN layer, distinguishing the N1s peak from BN is an extremely complicated task. Therefore, we chose to fit BN in the B1s spectrum, where only some overlap with sub-stoichiometric B oxide may occur.

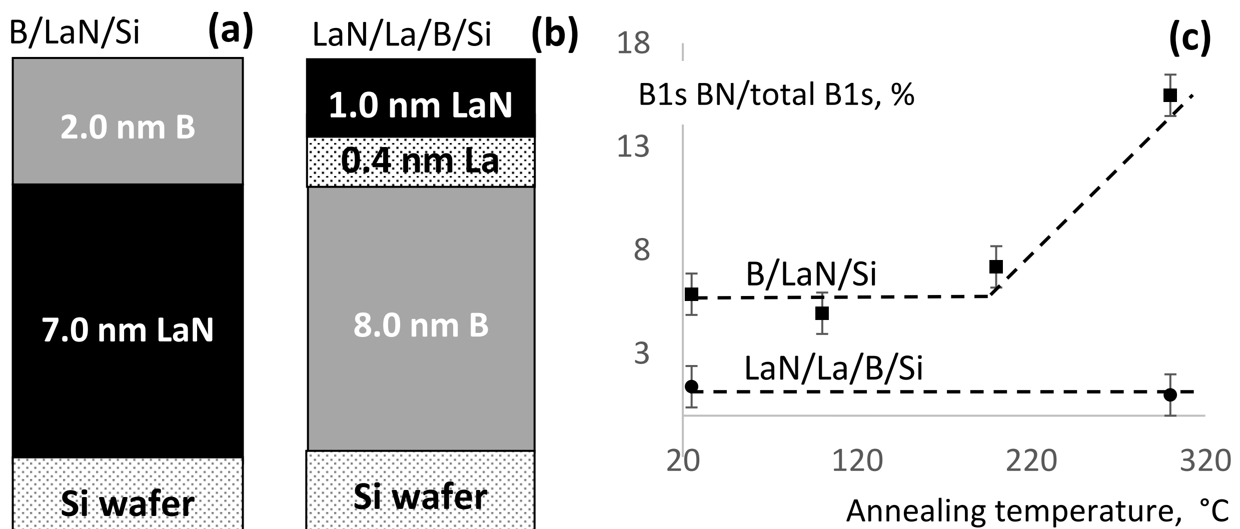

Fig.6. Schematic structures of samples employed for the study of (a) B-on-LaN and (b) LaN-on-La-on-B interfaces. (c) B1s(BN)/total B1s peak area ratio of XPS peaks versus annealing temperature for the structures (a) and (b). The annealing time was 70 h for every point. The dash-lines are a guide to the eye.

The B-on-LaN/Si-substrate structure was used to study the B-on-LaN interface. We analysed the B1s XPS spectra measured for the as-deposited samples and samples annealed for 70 h at 100, 200 or 300°C. The results are presented in Fig. 6(c). The BN content was assessed as the B1s(BN)/total B1s peak area ratio. For temperatures 100–200°C, the amount of BN stays constant as for the as-deposited structure within the analysis error bars. The presence of BN for the as-deposited sample is explained by exposure of the top B layer to atmosphere, and was observed for a single B film

reference as well [3]. However, for 300°C a pronounced increase of BN content is observed. So, at 300°C diffusion on that interface was clearly activated.

The LaN/La/B/Si wafer structure was used to study the LaN-on-La-on-B interface. Figure 6(c) includes results of analysis of B1s XPS spectra for the as-deposited and 70 h annealed samples. The sample on Fig. 6(b) contains a B layer deeper in its structure and therefore does not show the initial BN offset observed for the counterpart structure. The samples (a) and (b) from Fig. 6 have different structure (in particular, different materials of layers on top of the tested interface) and the intermixing at different elevated temperature might further change in-depth distribution of elements. Therefore, the absolute values of the B1s(BN)/B1s total peak area ratio for samples (a) and (b) should not be compared to each other. A straightforward approach to detect chemical changes was chosen then. It is considered significant that the BN content does not change at 300°C within the error bars of analysis compared to the as-deposited state. Therefore, in contrast to the B-on-LaN interface, interdiffusion on the LaN-on-La-on-B interface at 300°C is not yet activated to result in resolvable formation of BN compound. It is important to note that interdiffusion at elevated temperatures can also lead to the formation of a ternary LaxByNz compound. The XPS binding energy in that case might be very close to the one for BN. However, investigation of this possibility is out of the scope of the current paper.

5.9 Discussion

In this section, we discuss the results of a separate study of B-on-LaN and LaN-on-La-on-B interfaces. The losses of peak reflectivity of multilayers by 1.0% at 100°C and 1.5% at 200°C (both absolute) cannot be explained by contamination of the B cap known from XPS measurements, notably, since no B_2O_3 was observed, therefore, they should be related to changes in the stack itself. For details see section "6.x nm reflectivity (PTB)." Modelling [21] shows that the drop of peak R about 1% could be explained by increase of BN thickness on the B-on-LaN interface by about 0.5 Å. The other (LaN-on-La-on-B) interface is not included in the model here, since it is not yet activated for (inter)diffusion at 100–200°C. In XPS this would correspond to about 2.5% of BN from total B, since the total thickness of B is about 20 Å. The error bars of XPS analysis are about ±1% (error due to Poisson statistics of about ±0.7% plus uncertainty of the fits). So the expected amount of the formed at 100–200°C BN cannot be resolved by XPS. The drop of reflectivity by about 2% at 300°C (interpolated value in Fig. 2), according to modelling using [21] would correspond to an increase of the BN thickness on the B-on-LaN interface by about 1 Å, which is 5% of the total B thickness. The increase of BN in XPS quantification for 300°C was by about 8%. When comparing these two numbers we should keep in mind that thicknesses of sharp BN layers with bulk density in the model cannot be directly compared with B1s(BN)/total B1s measured with XPS, since the real densities and shape of the interface zones between the layers are, strictly, unknown. Therefore, within the existing uncertainties, reflectivity loss due to annealing (Fig. 2) at up to 300°C could be explained by the formation of BN compounds on the B-on-LaN interface.

At an annealing temperature above 200°C the B-on-LaN interface is clearly activated for diffusion while the other, LaN-on-La-on-B, not (see Fig. 6(c)). This difference in behaviour of the two interfaces seems surprising at first sight but could be understood if we consider the structure formed at the LaN-on-La-on-B interface as a result of the partial nitridation scheme. It was concluded in [5] that deposition of a thin La layer on top of B would result in the formation of LaB_x. We suggest that this LaB_x interlayer can act as a diffusion barrier between LaN and B to prevent fast interdiffusion at this interface. Note that at least up to 350°C there are similar losses of reflectivity for LaN/B and LaN/La/B. These structures have a common interface of B-on-LaN. The other interface is different for these structures and as determined in [6] there is BN formed at the LaN-on-B interface in the as-deposited LaN/B multilayers. From this we suggest that at temperatures up to 350°C the BN interlayer on the LaN-on-B interface may act as a similar diffusion barrier as LaB_x on the corresponding interface in the multilayers with partial nitridation. At 500°C, however, the reflectivity loss for LaN/La/B is noticeably higher than for LaN/B (Fig. 2), and that is correlated with higher effective multilayer period expansion for LaN/La/B at this temperature-point (Fig. 1). Therefore, we anticipate that at 500°C the diffusion barrier properties of a BN interlayer are better than that of LaBx, for instance because of possible LaB_x crystallization. However, the study at this high temperature should be a subject of a separate research.

5.10 Summary and conclusions

Thermal stability of high-reflectance La/B-based multilayers for normal incidence 6.x nm wavelength was studied. Structures with full-layer (LaN/B) and partial-layer nitrided La (LaN/La/B) were annealed in the temperature range 100°C to 500°C. Both type of structures showed similar period drifts by 0.005 nm at 100°C to 0.06 nm at 500 °C that significantly slowed down at 70 h. The observed period drifts were associated, as in previous studies, with interdiffusion and formation of compound(s). These drifts were accompanied by reflectivity losses of about 2% at 200°C to more than 12% at 500 °C. Notably, at 500°C reduction of reflectivity for the structure with the partial-layer nitrided La was clearly higher than for the full-layer nitrided La.

Separate investigation of B-on-LaN and LaN-on-La-on-B interfaces was done by XPS on dedicated samples at temperatures up to 300°C. In the temperature range 100–200°C, no additional compound formation was resolved for both interfaces. However, at 300°C clear increase of BN compound was observed at the B-on-LaN interface. Notably, the (partial-layer nitrided) LaN-on-La-on-B interface was still not activated for interdiffusion at that temperature. This result could be explained by the as-deposited formation of a LaB_x interlayer at that interface that is suggested to slow down interdiffusion.

Acknowledgments

HR-RBS measurements and their analysis were carried out at IBC at the Helmholtz-Zentrum Dresden – Rossendorf e.V., a member of the Helmholtz Association. We

would like to thank Gregor Hlawacek, Richard Wilhelm, and René Heller for their contribution and valuable discussions.

Dr. Christian Laubis and colleagues at the Physikalisch-Technische Bundesanstalt (PTB) are acknowledged for doing the reflectivity measurements.

We acknowledge the support of the Industrial Focus Group XUV Optics at the MESA+ Institute for Nanotechnology at the University of Twente, notably the industrial partners ASML, Carl Zeiss SMT GmbH, Malvern-PANalytical, TNO, as well as the Province of Overijssel and the Foundation FOM (now part of the NWO, the Netherlands Organisation for Scientific Research).

References

1. V. Banine, A. Yakunin, and D. Glushkov, “Next generation EUV lithography: Challenges and opportunities” in International Workshop on Extreme Ultraviolet Sources, Dublin, Ireland (2010)
2. E. Louis, A.E. Yakshin, T. Tsarfati, F. Bijkerk, Progress in Surface Science 86, 255 (2011)
3. S.L. Nyabero, R.W.E. van de Kruijs, A.E. Yakshin, I.A. Makhotkin, J. Bosgra, and Fred Bijkerk, Journal of Micro/Nanolithography, MEMS and MOEMS 13(1), 013014 (2014)
4. I.A. Makhotkin, E. Zoethout, R.W.E. van de Kruijs, S.N. Yakunin, E. Louis, A.M. Yakunin, V. Banine, S. Muellender, and F. Bijkerk, Optics Express 21, 29894 (2013)
5. D.S. Kuznetsov, A.E. Yakshin, J.M. Sturm, R.W.E. van de Kruijs, and F. Bijkerk, AIP Advances 6, 115117 (2016)
6. D.S. Kuznetsov, A.E. Yakshin, J.M. Sturm, R.W.E. van de Kruijs, E. Louis, and F. Bijkerk, Optics Letters, Vol. 40, No. 16 (2015)
7. A.E. Yakshin, R.W.E. van de Kruijs, I. Nedelcu, E. Zoethout, E. Louis, and F. Bijkerk, Proceedings of SPIE 6517, 65170I (2007)
8. S. Bruijn, R.W.E. van de Kruijs, A.E. Yakshin, and F. Bijkerk, Applied Surface Science 257 (2011)
9. R. Resel, E. Tamas, B. Sonderegger, P. Hofbauer, and J. Keckes, Journal of Applied Crystallography 36, 80 (2003)
10. C. Kittel, Introduction to Solid State Physics, John Wiley & Sons (1971)
11. David R. Lide (ed), CRC Handbook of Chemistry and Physics, 84th Edition, CRC Press. Boca Raton, Florida, 2003; Section 4, Properties of the Elements and Inorganic Compounds; Physical Properties of the Rare Earth Metals
12. Touloukian, Y. S., Thermophysical Properties of Matter, Vol. 12, Thermal Expansion, Plenum, New York (1975)
13. F. Scholze, C. Laubis, C. Buchholz, A. Fischer, S. Ploeger, H. Wagner, and G. Ulm, Proceedings of SPIE 5751, 749 (2005)
14. C. Laubis, A. Barboutis, M. Biel, C. Buchholz, B. Dubrau, A. Fischer, A. Hesse, J. Puls, C. Stadelhoff, V. Soltwisch, and F. Scholze, Proceedings of SPIE 8679, 867921 (2013)
15. S. Hüfner, Photoelectron Spectroscopy, 3 ed., Springer (2003), ISBN: 3-540-41802-4

16. N.N. Greenwood, A. Earnshaw, “Chemistry of the elements”, ISBN 978-0750633659, Second Edition, Elsevier (1997)
17. H.R. Verma, Atomic and Nuclear analytical Methods, Springer (2007)
18. M. Vieluf, F. Munnik, C. Neelmeijer, M. Kosmata, and S. Teichert, Thin Solid Films 520 (2012)
19. R. Grötzschel, C. Klein, O. Kruse, Nuclear Instruments and Methods in Physics: Section B, Vol. 183 (2001)
20. C. Laubis, A. Kampe, C. Buchholz, A. Fischer, J. Puls, C. Stadelhoff, and F. Scholze, Proceedings of SPIE, Vol. 7636 (2010)
21. D.L. Windt, Computers in Physics, Vol. 12(4), 360-370 (1998)
22. I. Nedelcu, R.W.E. van de Kruijs, A.E. Yakshin, and F. Bijkerk, Journal of Applied Physics 103, 083549 (2008)
23. T. Tsarfati, R.W.E. van de Kruijs, E. Zoethout, E. Louis, and F. Bijkerk, Thin Solid Films 518, 7249 (2010)

Chapter 6: Grazing-incidence La/B-based multilayer mirrors for 6.x nm wavelength

We studied a possibility of fabricating LaN/B grazing incidence multilayer mirrors for ~6.7 nm radiation at a relatively large angle of incidence (AOI=77° off-normal). LaN/B multilayers with a periodicity of 15 nm were successfully fabricated. But when stored in air for one week they showed strong deterioration of the surface accompanied by oxidation of the topmost LaN layers, even though the multilayer was capped with a thin B film. In a series of experiments with variable LaN thickness it was found that the B protective properties depend on the thickness of the underlying LaN layer. Based on these experiments a 15nm LaN/La/B multilayer with a passivation layer of only 0.4 nm of LaN was fabricated, which did not show any deterioration of the surface within a testing period of half a year. An initial reflectivity of 74.5% at ≈6.66 nm, AOI=77° off-normal was achieved, which was reduced by 0.5% absolute in half a year, due to contamination of the top B layer.

6.1 Introduction

La/B-based multilayers have a potential to be used as mirrors in XUV telescopes for space research [1,2], for ~6.x nm wavelength XUV lithography [3], and various other applications, for instance, optics for high-intensity free electron lasers (FEL) [4,5] or ultrasensitive analysis of materials by x-ray fluorescence [6]. Recently, a significant improvement of the reflectivity at-wavelength was made using a special passivation scheme of La by nitrogen, which resulted in about 64% reflectivity at near normal incidence (AOI=1.5° off-normal [7, 8]). At the same time, some applications, for instance, the EIS-TIMER beamline [9] at the FERMI@Elettra FEL [10] also require mirrors for grazing-incidence geometry. For this application, the authors fabricated [11, 12] a 4.8 nm period La/B_4C multilayer for AOI=45° and achieved 54.4% reflectivity at ≈6.7 nm. In [13] 66.5% was demonstrated for a 7.3 nm period La/B stack at λ≈6.7 nm and off-normal AOI=61.3°. In this work we study the possibility of fabricating a grazing incidence multilayer structure for a larger angle of incidence, which implies a larger period. Investigating the effect of this on the structure, reflectivity and environmental stability of the resulting multilayer is the aim of this work.

AOI, °	La/B_4C, %	La/B, %	Δ, % (abs.)
77	62.6	79.2	16.6
65	65.3	79.5	14.2
45	65.9	79.6	13.7

Table 1. Peak reflectivity for La/B_4C and La/B multilayers calculated at different angles of incidence. Experimentally obtained optical constants of La [15], B [16] and B_4C [17] were used. Number of periods and gamma-ratio (La-based layer thickness / bilayer thickness) were optimized for each multilayer. The value Δ indicates the absolute peak reflectance difference between B_4C- and B-based multilayers.

Table 1 shows calculations [14] of the maximum theoretical reflectivity (zero roughness of layers and no intermixing) for La/B_4C and La/B multilayers in a range of different angles of incidence. Elemental B-based multilayers shows significantly higher peak reflectivity compared to B_4C-based multilayers. At AOI=77°, for instance, the gain by using elemental B is 16.6% (absolute). Due to that, La/B is taken in our work as the basis for grazing-incidence multilayers. Normal-incidence LaN/B multilayers (with passivated La) showed higher experimental reflectivity [13] and better experimental thermal stability [18] than La/B, and therefore LaN/B was the starting point for our experiments. A stack with a period of about 15 nm was chosen, reflecting at the off normal AOI=77°.

6.2 Experimental

The deposition was performed by DC magnetron sputtering [19] onto natively oxidized super-polished Si wafers (RMS roughness ~0.2 nm). The base pressure in the vacuum chamber was 1 x 10^{-8} mbar. The highly reactive La target, as well as the B target, was cleaned before each deposition by pre-sputtering till stable discharge parameters (voltage, current) and stable deposition rate assessed by Quartz-Crystal Microbalances (QCM) were reached. For storage outside of the vacuum chamber the La target was kept in a vacuum-sealed package to prevent its strong oxidation [20]. The depositions were done with Ar as a working gas, with the pressure being about 2 x 10^{-3} mbar. The deposition rates were 0.03 nm/s for La and B, and 0.05 nm/s for LaN. The conditions for the synthesis of the fully-passivated LaN are taken from our past work [8]. La target was used both for La and LaN deposition, with LaN being deposited by reactive sputtering in Ar + N_2 mixture. All the multilayers had 15 periods and were covered by a B capping layer of the same thickness as in the stack (about 9 nm for 15 nm period). All specified thicknesses in the described experiments are the nominal values for thicknesses deposited based on calibrated deposition rates, uncompensated for any additional effects.

The surface composition of the samples was determined by non-destructive X-ray Photoelectron Spectroscopy (XPS), using a Thermo Scientific Theta Probe Instrument employing monochromatic Al-Kα radiation. Since the XPS probing-depth is about 5-7 nm [21], and the top B layer (cap) is about 9 nm, these measurements probed exclusively the top B layer. Distribution of the elements inside the stack was assessed by XPS depth-profiling implemented by ion etching (Ar^+, 0.5 keV). XPS spot size (analyzed area) was about 400 µm, the take-off angle was varied to collect integrated signal in the range ±30° around average take-off angle 53° with respect to surface normal.

For visual monitoring of the surface condition of the samples, optical microscopy was employed, using a Nikon Eclipse ME600, in PC-controlled setup with NIS-Elements D 3.10 as the imaging software. The latter allows programmed high frequency measurements of the same spot to monitor surface changes in real time.

For measurements of the surface roughness of the samples, a Bruker Dimension Edge^{TM} Atomic Force Microscope (AFM) was used with special probe for high-resolution: Hi'Res-C14/Cr-Au by MikroMasch with spike radius about 1 nm.

The period of the multilayers was extracted by analysis of Bragg peak positions in grazing incidence hard X-ray reflectivity (GIXRR) curves, measured at a PANalytical Empyrean X-ray diffractometer (Cu-Kα radiation, λ≈0.154 nm).

The soft X-ray (6.x nm, at-wavelength) reflectivity (R) of the multilayers was measured at Physikalisch Technische Bundesanstalt (PTB) [22] using the synchrotron radiation of the BESSY storage ring in Berlin, Germany. The measurements were conducted for the as-deposited structures and after storage, in order to assess the degradation of the structures as well as the influence of the surface contamination. The influence of contaminants on 6.x nm R was estimated with IMD software [14] with an input from the XPS measurements and suggesting a certain layer model of the top part of the stack. To reconstruct the multilayer structure, a fit of at-wavelength GIXRR (measured at λ≈6.66 nm) was implemented with the IMD software [14] assuming an error-function form of the interface transition zones (σ roughness/diffuseness [14]). A differential evolution algorithm was used for fitting [23].

6.3 LaN/B multilayers

Our initial materials choice for depositing grazing incidence mirrors was LaN/B structure with a period of about 15 nm (6 nm LaN and 9 nm B).

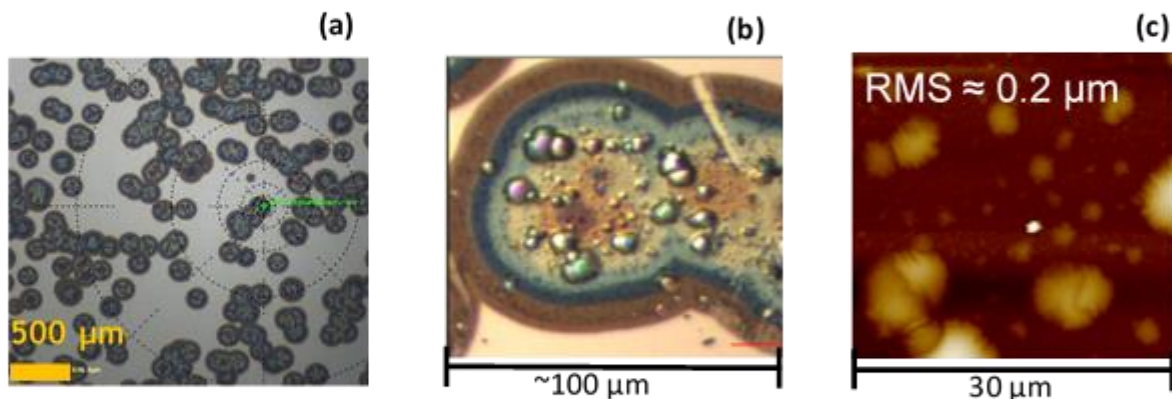

Fig. 1, (a) Optical microscope view on the surface of LaN/B; **(b)** Zoomed-in optical microscopy view of a defective zone; **(c)** 2D AFM in a defective zone.

However, after one week of storage of the deposited multilayer in air, circular-like defective zones were observed (Fig. 1, (a)). Zooming into a single defective zone using an optical microscope (Fig. 1, (b)) reveals numerous features inside the defective zone, which were determined by AFM to be elevations. According to the AFM measurement, the sizes of these elevations range from ~ 1 µm to ~10 µm in diameter and from ~10 nm to ~500 nm in height.

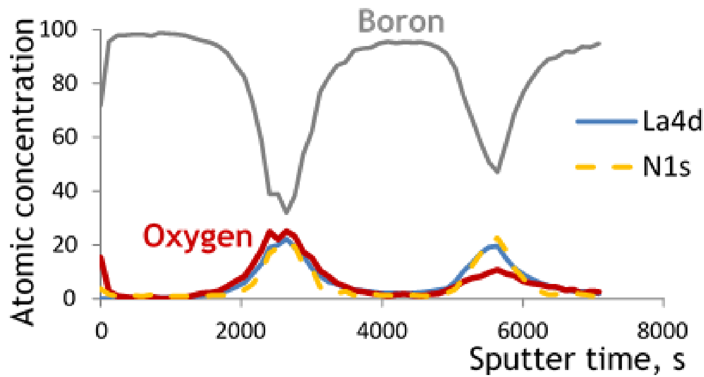

Fig. 2. XPS depth-profile of LaN/B multilayer in one week after storage in air.

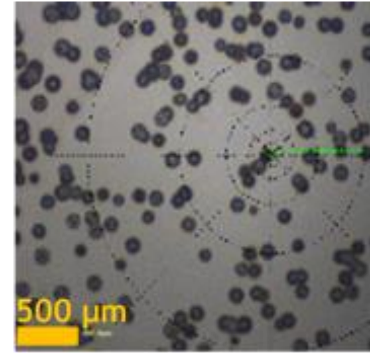

Fig. 3. Optical microscope view on the surface of LaN/B multilayer after depth profiling (Fig. 2).

2D AFM measurements inside the defective zone and between the elevations (Fig. 1, (c)) reveal severe roughening of the surface due to the presence of numerous features resulting in an RMS roughness of about 0.2 µm. Notably, the surface between the defects (bright areas on Fig. 1, (a)) remains flat, with the RMS roughness of that area being about 0.3 nm, like for the as-deposited structure. The XPS depth-profile in Fig. 2 shows the distribution of the chemical elements in depth in a sample with the developed defects. The probing spot of XPS was 400 µm and covered both defects and defect-free area shown on Fig.3. Note that after sputtering away the surface contamination, the atomic concentration of B reaches a value close to 100%. This suggests that the B layer is not oxidised. Furthermore this indicates that B is not delaminated in the defective areas, otherwise signal from the next layer would be visible. The presence of oxygen in the La-based layer directly under the B top layer is significant. The second from top La-based layer shows already a significantly reduced but still noticeable presence of oxygen. The optical view on the surface after the depth profiling (Fig. 3) was taken at exactly the same spot as shown in (Fig. 1, (a)) within half a minute after finishing the depth-profiling. Notably, the defective zones are still visible at exactly the same positions as on the imaged structure before sputtering. However, no measurable signal of La, N and O is present in the depth-profile after the first La-based layer (see Fig. 2, at around 4000s etching time). This allows us to make an assumption on probable blister-nature of the elevations (Fig. 1). If 100-500 nm high elevations would be filled in with a solid material, the atomic concentrations of La, N and O in XPS depth profile could not go to almost zero level in the B layer.

6.4 B protective properties

It is shown in the previous section that the LaN/B multilayers with about 6 nm thick LaN layers experience quick surface degradation when stored in air. To verify if the observed degradation is related to the presence of the LaN layer underneath the B capping layer, in the next deposition we replaced LaN with La. For that a 15 nm-period La/B multilayer was deposited. The latter shows no degradation of the surface in time

even after half a year of storage in air. The surface RMS roughness stays at the as-deposited value of about 0.3 nm. Based on this, it was proposed that the protective properties of the top B layer could depend on the material of the underlying layer.

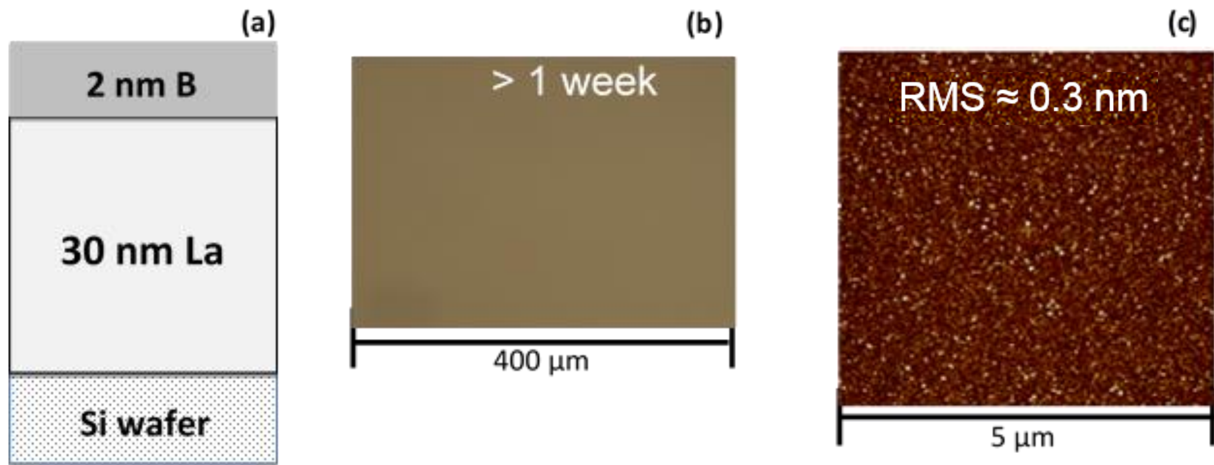

Fig. 4, (a) Schematic structure of the B-on-La sample; **(b)** Optical microscopy view of the La-sample after > 1 week of storage; **(c)** 2D AFM of the La-sample surface after > 1 week of storage.

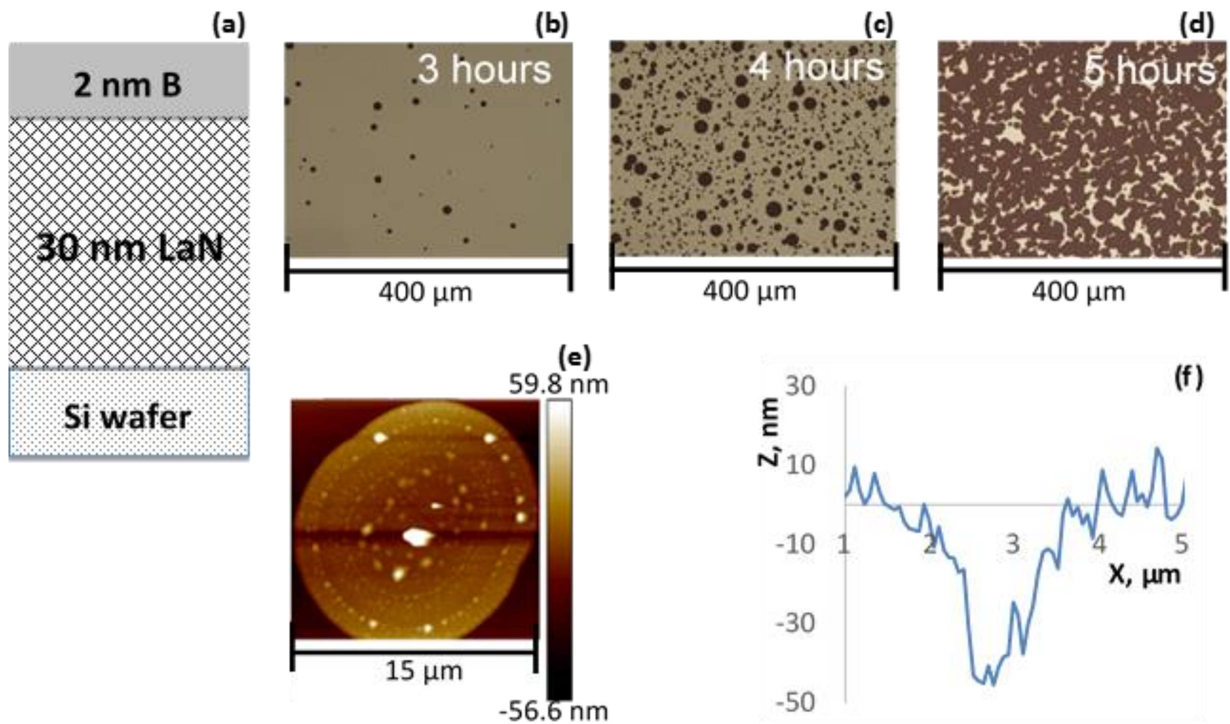

Fig. 5, (a) Schematic structure of the B-on-LaN-sample; **(b, c, d)** Optical microscopy pictures obtained 3, 4, 5 hours, respectively, after the deposition of the sample; **(e)** 2D AFM of defect, obtained 3 h after the deposition;
(f) AFM cross-section in the centre of a defect, obtained 5 h after deposition.

To check this and to exclude a possible influence of the multilayer underneath, a dedicated set of single-layer samples was fabricated. Their schematic structures are represented on Fig. 4, (a) and Fig. 5, (a). A relatively thin B cap was used to cover 30 nm thick La and LaN films to speed up the test. Initially the structures were covered with only 1.5 nm B, but they both showed quick degradation. At the next step the structures were fabricated with 2 nm B and this proved to be a proper thickness for this test. For the B-on-La sample (Fig. 4, (a)), after one week of storage no surface features were observed by optical microscopy (Fig. 4, (b)). The surface kept the as-deposited roughness with RMS of about 0.3 nm. The XPS depth-profile after 2 weeks of storage in air showed a typical value of about 5% of oxygen in La, the level usually observed in La in every deposition in a vacuum of about $1x10^{-8}$ mbar. On the contrary, the B-on-LaN-sample qualitatively demonstrates similar degradation features as the LaN/B multilayer described above. In a few hours time of storage in air, circular-like defective zones appeared at the surface (Fig. 5, (b)), and in-time the already existing defects were increasing in diameter while in the meanwhile new ones still appearing at various positions on the surface (Fig. 5, (c)). At the initial stage the defects have an elevation at the centre as determined by AFM measurement (Fig. 5, (e)). However, at a later stage, when the defects have grown in diameter enough to meet each other (Fig. 5, (d)), instead of an elevation there is a pinhole about 40 nm deep, as shown on the cross-section of the 2D AFM measurement (Fig. 5, (f)). This pinhole might explain the observed LaN/B stack oxidation through a few layers, however, when monitoring the LaN/B multilayer we did not observe any pinholes. Therefore, the precise mechanism of the development of the observed defects in the LaN/B multilayers has to be studied further. Importantly, our study did confirm that the protective properties of the top B layer depend on the underlying layer in case of a relatively thick (in our case 30 nm) LaN layer.

According to our in-situ X-ray reflectometry studies of La and LaN growth [24], when the LaN layer is 2 nm and thicker, it is found to have a reduced density compared to its bulk value. Therefore, we anticipated an increased porosity of the LaN layer, which facilitates penetration of oxygen species through the B top layer resulting in LaN oxidation. The suggested reason for the increased LaN porosity is competing growth of two different crystal structures, in particular, wurtzite (WZ) and zincblende (ZB), resulting in so called stacking faults. Moreover, the crystal structure of LaN, with the layer being 2 nm and thicker, is very close (from crystallographic view) to the structure of lanthanum oxide (La_2O_3), which might further facilitate oxidation of LaN. On the contrary, according to our results, La is found to have almost bulk density (therefore expected low porosity), with a dominant NaCl structure revealed.

6.5 La surface nitridation in single films

As shown above, 15 nm period La/B multilayers did not show any development of defects even after half a year storage in air. However, as found before for the normal-incidence multilayers, La/B multilayers demonstrated a significantly lower reflectivity at-wavelength compared to multilayers where the La layers were passivated to form LaN [13]. This was shown to be due to the reduced chemical interaction at the

interfaces and therefore higher optical contrast of the LaN/B stack. It was also shown in [7] that it is sufficient to passivate only the B-on-La interface to gain in reflectivity. Following this, as well as keeping in mind fast surface degradation when using a thick LaN layer, we designed a structure where only the surface of La would be passivated, rather than the entire layer. As outlined above, B protective properties were found to depend on the material of the underlying layer.To examine the dependence of B/LaN/La thin film degradation on LaN thickness, a dedicated series of samples was fabricated with various thickness of the LaN layer as illustrated in Fig. 6, (a – d). Note that the total thickness of the La-containing layer (La+LaN) was kept 30 nm for all the samples. A B layer thickness of 2 nm is chosen, as it is found in this work to be the most suitable choice for a short life time test of the structures under storage in air.

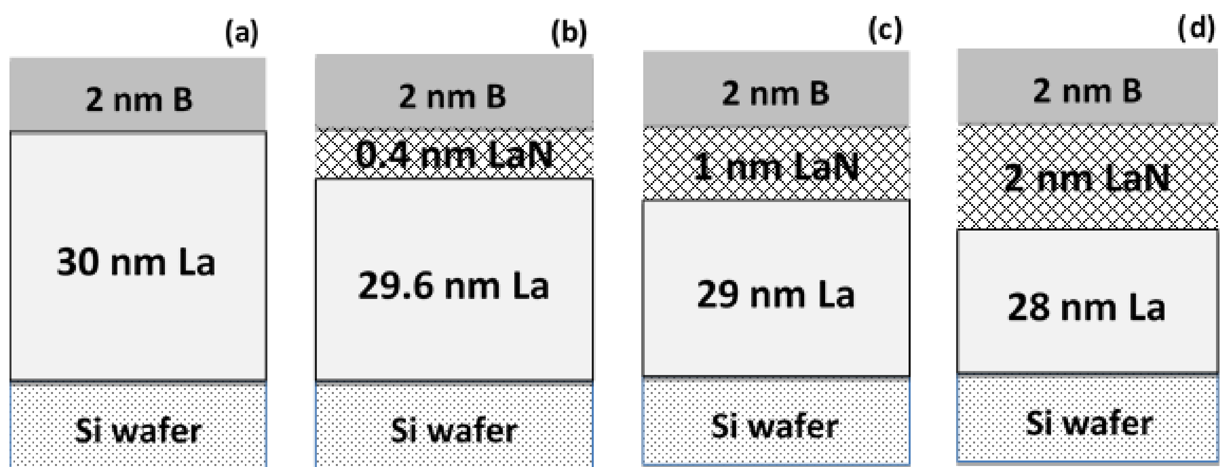

Fig. 6, (a) – (d): Schematic picture of the composition of the samples with variable thickness of the LaN layers for a short life time test under storage in air. The sample on Fig. 6, (a) is the same as the one represented on Fig. 4, (a).

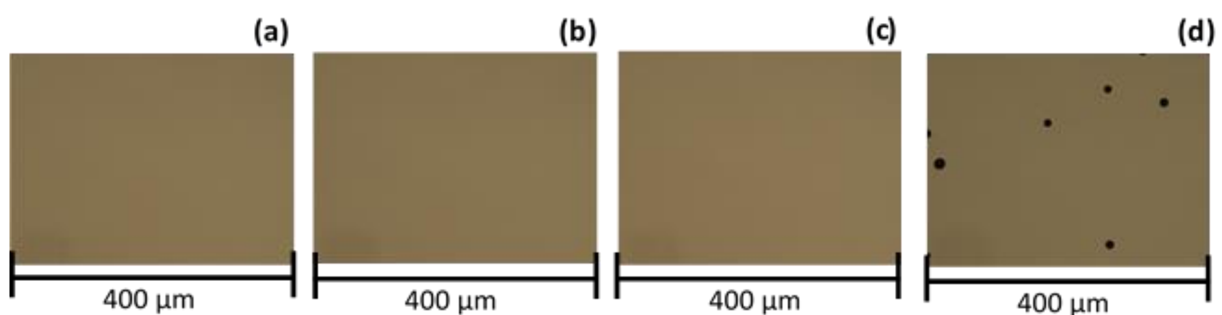

Fig. 7. Optical microscopy view of surfaces of the samples from Fig. 6 after 1 week storage in ambient atmosphere (air).

Fig. 7, (a – d) shows optical microscopy views of the surfaces of the test samples after 1 week of storage in air. As seen, only in the case of the sample with the 2.0 nm LaN layer some circular defects developed. The rest of the structures did not show any

traces of degradation, like in the case of the structures based on pure La. This result suggests that the protective properties of the B layer do depend on the thickness of the underlying LaN layer. Therefore, when using passivation of La by nitrogen in the grazing incidence multilayer structures, it is necessary to keep the thickness of LaN below 2.0 nm.

6.6 La surface nitridation in multilayers

Based on the results of the single layer tests, we fabricated two 15 nm period La/B-based multilayers, with only the top part of every La layer being nitrided, and one La/B multilayer without La nitridation as the reference. Two different thicknesses of LaN are used, 0.4 nm and 1 nm, to check which of the selected thicknesses is sufficient to completely prevent interaction of B with La on the B-on-La interface. Fig. 8 shows the at-wavelength reflectivity (the first Bragg peak) of these multilayers, measured at PTB [25].

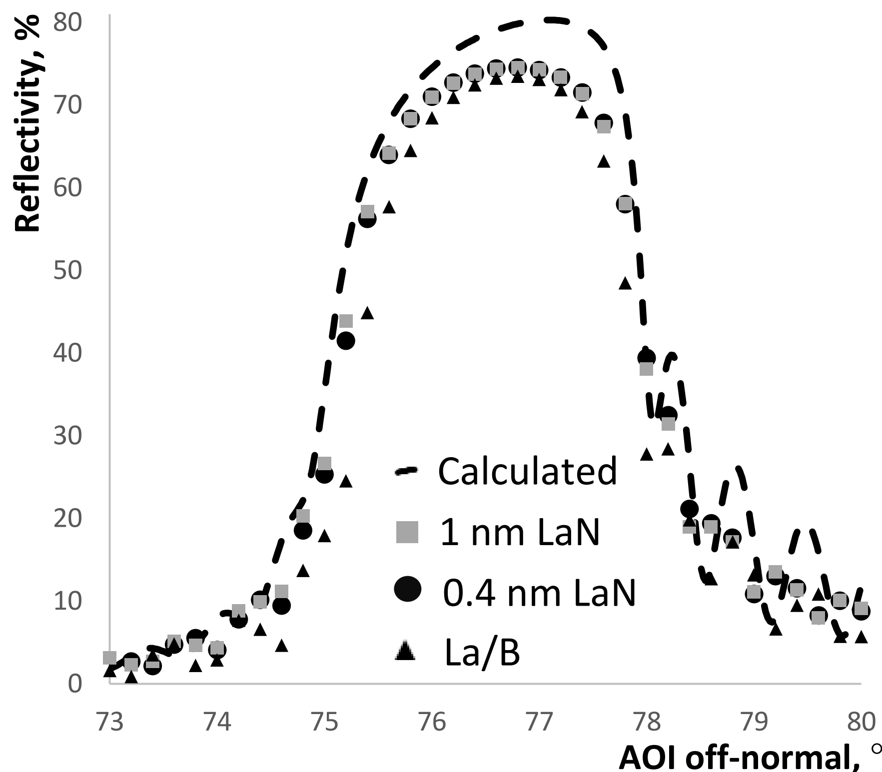

Fig. 8. Measured soft X-ray (λ ≈ 6.66 nm) reflectivity (first order Bragg) for two La/B-based multilayers with La surface nitridation and La/B, calculated curve for an ideal optimized structure included.

Both structures showed a reflectivity gain of 1% absolute with respect to the La/B multilayer (without La passivation). Notably, the achieved reflectivity is the same for both structures within the 0.05 uncertainty of the measurements [22]. From this we conclude that even 0.4 nm of fully-saturated LaN [8] is sufficient to passivate the B-on-La interface. The calculated [14] theoretical maximum for an ideal structure (bulk densities, zero roughness's/intermixing, zero layer thickness errors) is included in Fig. 8

as well. The theoretical maximum of about 79% leaves room for about 4.5% absolute possible gain for a further improved structure.

In order to reconstruct the structure of the obtained multilayer with La surface nitridation (0.4 nm LaN), a simplified fitting of the measured at-wavelength reflectivity was employed. The schematic representation of the model structure is shown in Fig. 9, (a). In our model, the stack consists of alternating La and B layers. LaN is not included into the model because the optical constants of LaN are very close to La, with the difference in reflectance being not significant to determine parameters of LaN layers (including thickness, density, chemical composition, etc). Since the exact real densities of the B and La layers in the deposited stacks are not accurately known, we do not rely on the measured optical constants [15, 16] used in the initial calculations (Table 1) but use the densities of B and La as the fitting parameters. The roughness/diffuseness (σ) [14] on the La-on-B and B-on-La interfaces is included in the fit with a composition-profile represented by an error-function. The top layer (contaminated upper part of B cap) is modelled as B_xO_y in accordance with the results of XPS analysis done in 1 month after the deposition, with stoichiometry, density and thickness being fitting parameters. Simultaneously with that, the thickness of the underlying elemental (not contaminated) part of the B cap is fitted as well. An initial attempt of the fit was not successful when implemented without a diffused interface between the contaminated top part of the top B layer and the underlying elemental B (σ(B_xO_y-on-B) in Fig. 9, (a)).

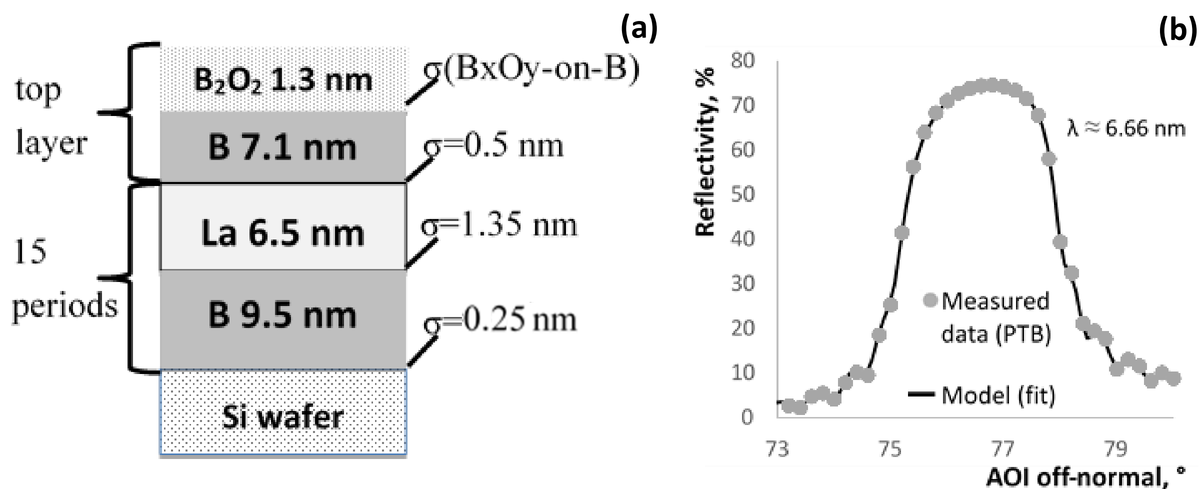

Fig. 9, (a) A schematic structural model of the LaN/La/B multilayer (with La surface nitridation, 0.4 nm LaN); **(b)** the measured (circles) at-wavelength reflectivity of the LaN/La/B (La surface nitridation) multilayer and its best fit (line) employing the structural model on Fig. 9, (a).

In this case, the modelled reflectivity peak in its top part is about at best 2% higher than the measured data. After introducing a diffused zone σ(B_xO_y-on-B), the fitted Bragg peak on its top part is within 0.3% absolute of the experimental data. The final best fit is presented in Fig. 9, (b) together with the experimental data. Parameters as obtained by the fit to be taken into further consideration are stated in Fig. 9, (a). It is noted that the stoichiometry of the B_2O_2 obtained by the fit is within the under-

stoichiometric (less rich in oxygen than B_2O_3) value concluded from the XPS analysis. The fitted densities of B and La are 2.0 and 5.2 g/cm3, respectively.

Asymmetry of interfaces cannot be resolved by this analysis, i.e. values of σ(B-on-La) and σ(La-on-B) can be „interchanged“ by applying intentional constraints on their ranges of allowed values and re-fitting the data. Still it is possible to assess the structural improvement done by the La surface nitridation. For this we model the structure only by varying the parameter σ(B-on-La).

As a result, the increase of reflectivity from R=73.5 % for the La/B multilayer to 74.5 % for the LaN/La/B multilayer could be modelled by a decrease of σ(B-on-La) from 1.5 nm to 0.5 nm. This means that the interface width of the B-on-La interface was effectively reduced by about 1 nm. This improvement of the structure by La surface nitridation is indeed significant. The relatively small reflectivity gain of absolute 1% is explained by the relatively large period of the structure compared to the improved width of the interface, and by grazing-incidence angle, at which reflectivity is less sensitive to interfacial/roughness effects compared to angles closer to normal incidence. Our calculations showed that the gain could reach 3-4% (absolute) in case of a grazing incidence multilayer with a lower period, in particular, about 8-9 nm.

6.7 Stability of La/B multilayers with La surface nitridation

The long-term stability of La/B-based multilayers with La surface nitridation (LaN 0.4 nm) to storage in air was studied by various techniques in half a year after the deposition. Below, these will be called aged multilayers. Optical microscopy revealed no defects or other features visible on the surface. The roughness of the surface did not change compared to the as-deposited samples, having an RMS value of ≈ 0.3 nm (measured by AFM). The XPS depth-profile for the aged multilayers showed a typical value of about 5% of oxygen in La, the level usually observed in La in every deposition in vacuum of about $1x10^{-8}$ mbar. To assess possible surface contamination of the top B layer, non-destructive XPS measurements are done for the as-deposited sample and for the aged multilayer. For both samples, O and C elements were found. Since the binding energies of the fitted N1s and O1s XPS spectra could not be assigned unambiguously to any compound, we considered B1s and C1s XPS spectra to identify the surface contamination after storage. These spectra are shown in Fig. 10 (a) and (b). On the B1s spectrum (a), clear oxidation of B is observed, however no stoichiometric boron oxide (B_2O_3) is found, expected at 193.1-193.7 eV [26]. Only an under-stoichiometric (B-rich) oxide is observed. The C 1s-orbital spectrum (b) reveals the presence of elemental carbon (ascribed to hydrocarbons on the surface), an oxidised carbon with the stoichiometry of about 1:1 (C1s O) and a rich in oxygen carbonate compound (CO_3). Quantification of the total O1s and C1s spectra shows similar percentages of both of them of about 13±1%. There is also a small amount of BN present in XPS spectra originating from the interaction with air, which is also observed for the reference B layer samples [8]. The measured percentages of contaminants after half a year of storage in air are totally related to the aging, since as-deposited samples do not show measurable by XPS amount of top layer contamination.

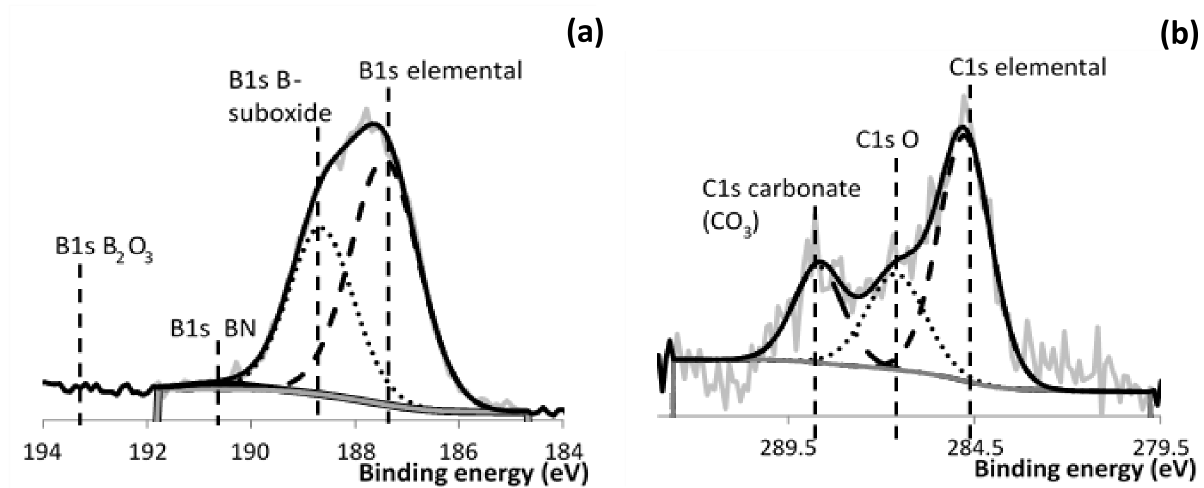

Fig. 10. Fitted XPS B1s **(a)** and C1s **(b)** spectra, measured as-introduced for the La/B-based multilayer with La surface nitridation (0.4 nm LaN) after half a year storage in air.

The at-wavelength reflectivity was re-measured after the storage as well, and showed a reduced reflectivity by 0.5% (absolute) in the very top part of the Bragg peak. To be able to explain this drop in reflectivity by increased roughness/diffuseness at interfaces, the e.g. roughness parameter σ(B-on-La) in the model would need to be increased from 0.5 to 1.3 nm. However, in this case the FWHM would decrease from 2.895° to 2.701°, so by as much as 0.2°. In reality the measured FWHM for the aged multilayer got reduced from 2.895° to 2.868°, so by only about 0.02-0.03°. A similar behaviour was observed if involving the densities of the La and B layers and the gamma-ratio into the fitting procedure. This means that the reflectivity loss of the aged multilayer could most likely not be explained by an evolution of the internal structure. The remaining cause, which we have to consider, is surface contamination and oxidation of the top layer due to storage in air, as confirmed by the presence of hydrocarbons with CO and CO_3 groups at the surface, as detected by XPS. All these factors are very difficult to describe in an unambiguous model. But, keeping in mind that in our simulations we observed a strong sensitivity of the very top part of the reflectivity peak to surface contamination, we consider surface contamination as the most likely reason for the observed reflectivity drop of 0.5% in the aged multilayers.

6.8 Summary

We studied the possibility of fabricating LaN/B multilayers for ~6.7 nm radiation at an AOI=77° off-normal. LaN/B multilayers of 15nm period were successfully fabricated, but showed strong deterioration of the surface when stored in atmosphere, even though the multilayer was capped with a 9 nm thick B layer. It was shown by XPS that this deterioration is accompanied by oxidation of at least two of the topmost LaN layers. In a series of short lifetime experiments on tri-layer LaN/La/B films with various LaN thicknesses, it was found that the B protective properties depend on the thickness of the underlying LaN layer. It was shown that for a thickness of this LaN less than 2 nm

no deterioration of the surface is observed. Thicker LaN is likely to have a higher porosity of the film, leading to enhanced oxygen diffusion. Based on these experiments, two 15nm LaN/La/B multilayers with a LaN passivation layer of only 0.4 nm and 1.0 nm were fabricated. The multilayers with 0.4 nm LaN were chosen for temporal stability study and showed no deterioration of the surface within a testing period of half a year of storage in air. An initial reflectivity of 74.5% at ≈6.66 nm, AOI=77° off-normal was achieved for the as-deposited structure. This reflectivity reduced by 0.5% absolute in half a year of storage in air. IMD [14] simulations suggested that this reflectivity loss entirely can be explained by contamination of the top B layer.

Acknowledgments

We acknowledge the support of the Industrial Focus Group XUV Optics at the MESA+ Institute for Nanotechnology at the University of Twente, notably the industrial partners ASML, Carl Zeiss SMT GmbH, PANalytical, as well as the Province of Overijssel and the Foundation FOM (now part of NWO, the Netherlands Organisation for Scientific Research).

Dr. Christian Laubis and colleagues at the Physikalisch-Technische Bundesanstalt (PTB) in Berlin are acknowledged for doing the reflectivity measurements.

References

1. D. Martinez-Galarce, P. Boerner, R. Soufli, J. Harvey, M. Bruner, J. Lemen, E. Gullikson, B. De Pontieu, N. Choi, M. Fernandez-Perea, N. Katz, S. Baker, E. Prast, S. Khatri, and J. Kong, 2nd International Conference on Space Technology, p.1 (2011)
2. K. Uji, I. Yoshikawa, K. Yoshioka, G. Murakami, and A. Yamazaki, Proceedings of SPIE 8528, 85281M (2012)
3. V. Banine, A. Yakunin, and D. Glushkov, International Workshop on Extreme Ultraviolet Sources, Dublin, Ireland (2010)
4. M. Barthelmess and S. Bajt, Applied Optics 50, 1610 (2011)
5. Y. Socol, G.N. Kulipanov, A.N. Matveenko, O.A. Shevchenko, and N.A. Vinokurov, Physical Review Accelerators and Beams 14, 040702 (2011)
6. M.K. Tiwari, K.J.S. Sawhney, and G.S. Lodha, Spectrochimica Acta Part B 65, 434 (2010)
7. D.S. Kuznetsov, A.E. Yakshin, J.M. Sturm, R.W.E. van de Kruijs, E. Louis, and F. Bijkerk, Optics Letters, Vol. 40, No. 16 (2015)
8. D.S. Kuznetsov, A.E. Yakshin, J.M. Sturm, R.W.E. van de Kruijs, E. Louis, and F. Bijkerk, AIP Advances 6, 115117 (2016)
9. F. Bencivenga and C. Masciovecchio, Nuclear Instruments and Methods in Physics Research Section A 606(3), 785 (2009)
10. E. Allaria, C. Callegari, D. Cocco, W. M. Fawley, M. Kiskinova, C. Masciovecchio, and F. Parmaigiani, New Journal of Physics 12(7), 075002 (2010)
11. P. Naujok, S. Yulin, A. Bianco, N. Mahne, N. Kaiser, and A. Tünnermann, Optics Express, Vol. 23, No. 4 (2015)

12. N. Kaiser, H.K. Pulker, "Optical Interference Coatings", chapter "Multilayer Coatings for EUV/Soft X-ray Mirrors", Springer-Verlag (2003)
13. I.A. Makhotkin, E. Zoethout, R.W.E. van de Kruijs, S.N. Yakunin, E.Louis, A.M. Yakunin, V. Banine, S. Müllender, and F. Bijkerk, Optics Express, Vol. 21, No. 24 (2013)
14. D.L. Windt, Computers in Physics 12, 360 (1998)
15. Yu. Uspenskii, J. Seely, N. Popov, I. Artioukov, A. Vinogradov, D. Windt, B. Kjornrattanawanich, Proceedings of SPIE, Vol. 5919, 59190S (2005)
16. M. Fernandez-Perea, J. I. Larruquert, J. A. Aznarez, J. A. Mendez, M. Vidal-Dasilva, E. Gullikson, A. Aquila, R. Soufli, and J. L. Fierro, Journal of the Optical Society of America, Vol. 24(12), 3800 (2007)
17. R. Soufli, A.L. Aquila, F. Salmassi, M. Fernández-Perea, E.M. Gullikson, Applied Optics 47, 4633-4639 (2008)
18. S.L. Nyabero, R.W.E. van de Kruijs, A.E. Yakshin, I.A. Makhotkin, J. Bosgra, F. Bijkerk, Journal of Micro / Nanolithography, MEMS and MOEMS 13(1), 013014 (2014)
19. E. Louis, A.E. Yakshin, T. Tsarfati, and F. Bijkerk, Progress in Surface Science 86 (2011)
20. N.N. Greenwood, A. Earnshaw, "Chemistry of the elements", Elsevier (1997)
21. S. Hüfner, "Photoelectron Spectroscopy", Springer (2003)
22. F. Scholze, C. Laubis, C. Buchholz, A. Fischer, S. Ploeger, H. Wagner, and G. Ulm, Proceedings of SPIE, Vol. 5751, 749 (2005)
23. M. Björck, Journal of Applied Crystallography 44, (2011)
24. B. Krause, D.S. Kuznetsov, A.E. Yakshin, S. Ibrahimkutty, T. Baumbach, and F. Bijkerk, Journal of Applied Crystallography 51 (2018)
25. C. Laubis, A. Barboutis, M. Biel, C. Buchholz, B. Dubrau, A. Fischer, A. Hesse, J. Puls, C. Stadelhoff, V. Soltwisch, and F. Scholze, Proceedings of SPIE, Vol. 8679, 867921 (2013)
26. A.V. Naumkin, A. Kraut-Vass, S.W. Gaarenstroom, and C.J. Powell, "NIST X-ray Photoelectron Spectroscopy Database", (2012)

Chapter 7: In situ and real-time monitoring of structure formation during non-reactive sputter deposition of lanthanum and reactive sputter deposition of lanthanum nitride

Lanthanum and lanthanum nitride thin films were deposited by magnetron sputtering onto silicon wafers covered by natural oxide. In situ and real-time synchrotron radiation experiments during deposition reveal that lanthanum crystallizes in the face-centred cubic bulk phase. Lanthanum nitride, however, does not form the expected NaCl structure but crystallizes in the theoretically predicted metastable wurtzite and zincblende phases, whereas post-growth nitridation results in zincblende LaN. During deposition of the initial 2–3 nm, amorphous or disordered films with very small crystallites form, while the surface becomes smoother. At larger thicknesses, the La and LaN crystallites are preferentially oriented with the close-packed lattice planes parallel to the substrate surface. For LaN, the onset of texture formation coincides with a sudden increase in roughness. For La, the smoothing process continues even during crystal formation, up to a thickness of about 6 nm. This different growth behaviour is probably related to the lower mobility of the nitride compared with the metal. It is likely that the characteristic void structure of nitride thin films, and the similarity between the crystal structures of wurtzite LaN and La_2O_3, evoke the different degradation behaviours of La/B and LaN/B multilayer mirrors for off-normal incidence at ~6.7 nm wavelength.

7.1 Introduction

Multilayer (ML) mirrors in the soft X-ray and extreme ultraviolet (XUV) regimes are employed for various applications, including XUV telescopes for space research [1, 2] beam-transport systems and focusing optics for free-electron lasers [3, 4], XUV lithography [5] and total-reflection X-ray fluorescence analysis (TXRF) [6].

Lanthanum and boron are very promising candidates for mirror applications focusing on wavelengths of around ~6.7 nm [7, 8]. Experimentally, a reflectance of 64.1% for near-normal incidence was obtained by a hybrid process combining non-reactive and reactive sputter deposition of La. Delayed nitridation of the La layer avoids the formation of undesired BN at the La-on-B interface, while a fully passivated LaN layer on top significantly reduces the B-on-La interface width [9, 10, 11].

For application purposes, the long-term stability of the multilayers is crucial. Lanthanum and lanthanum nitride are highly reactive under ambient conditions, while crystalline and amorphous boron particles are known to oxidize only within a limited thickness in the range 0.5–2 nm [12, 13, 14]. Therefore, a boron cap thicker than about 2–3 nm is expected to protect La/B and LaN/B multilayers from oxidation. Surprisingly, this approach works for normal-incidence mirrors (ML periods of around 3.5 nm) but not for grazing-incidence mirrors with larger thickness: while La/B structures with an ML period of 15 nm appeared to be stable to storage for at least six months, LaN/B multilayers with the same period showed strong surface degradation after one week of storage in air [15]. This thickness-dependent degradation behaviour suggests that the stability of the cap might be influenced by the properties of the underlying layer.

The main objective of this manuscript is to determine the crystalline phases and microstructures of La and LaN thin films. Only limited information is available on the local atomic ordering and microstructures of La and LaN thin films and nanostructures [11, 16, 17]. For bulk lanthanum, the low-temperature double hexagonal close-packed α phase (Inorganic Crystal Structure Database entry ICSD-641382; a = 3.772, c = 12.144 Å [18]) with a phase transition to a high-temperature face-centred cubic (f.c.c.) β phase (ICSD-41518; a = 5.32 Å [19]) at 566 ± 10 K was reported [20]. For lanthanum nitride, the NaCl structure with a = 5.293 Å (ICSD-641470 [21]) was reported. However, ab initio calculations predict the formation of other metastable phases at room temperature: a wurtzite (WZ) phase with a = 3.95–4.2 Å and c = 5.84–6.24 Å, and a zincblende (ZB) phase with a = 5.51–5.69 Å [22, 23].

Owing to the high reactivity of La and LaN, the crystal phases and microstructures of these materials are difficult to access. This problem can only be overcome by in situ analysis methods, avoiding any contact of the thin films with the highly reactive contaminants oxygen or nitrogen, with humidity, or with other surface contaminants such as hydrocarbons. In this paper, we report on the structural evolution of La and LaN single layers during thin-film formation. The chemical composition and bond structure of the layers were verified by X-ray photoelectron spectroscopy (XPS) measurements. Reflection high-energy electron diffraction (RHEED) measurements gave a first indication of the crystalline phases. The reactive and non-reactive sputter processes of lanthanum, and the post-growth nitridation of a lanthanum layer, were monitored by combined in situ and real-time synchrotron X-ray diffraction (XRD) and X-ray reflectivity (XRR) measurements [24, 25]. The phase formation and texture development could be determined and related to the simultaneously detected film thickness and roughness. This detailed understanding of structure formation during La and LaN thin-film deposition is required for a deeper insight into the structural details and long-term stability of ~6 nm multilayer stacks, for both normal and grazing incidence.

7.2 Experimental

7.2.1 Thin-film deposition

The La and LaN layers were deposited in a portable magnetron sputtering chamber dedicated to in situ X-ray experiments during reactive and non-reactive magnetron sputtering [26]. The base pressure of the ultra-high-vacuum (UHV) system was 1 × 10^{-6} Pa. The lanthanum target, with a diameter of 50 mm, was mounted at a distance of about 130 mm from the earthed 20 × 20 × 1 mm Si substrate. All substrates used for the in situ X-ray experiments were taken from the same wafer. Sample exchange was done using a loadlock, reducing the contamination of the La target to a minimum.

Before each deposition, the target was sputter-cleaned. During this period, the substrate was protected by a shutter. Non-reactive sputter deposition was done with a flux of 1.2 sccm (standard cubic centimetres per minute) argon, corresponding to a pressure of about 0.3 Pa. During reactive sputter deposition, a mixture of 0.6 sccm Ar and 1.2 sccm N_2 at a pressure of 0.55 Pa was used. The DC power at the La target was

kept at 20 W, resulting in a target voltage of 267 V during La deposition and 188 V during deposition of LaN. A similar voltage difference between reactive and non-reactive La sputtering was also observed by Haye et al. [27].

For the RHEED and XPS measurements, the sputter chamber was docked to a UHV cluster system with a base pressure of 1 × 10^{-8} Pa. The samples were transferred to the analysis chambers directly after growth, without exposure to ambient conditions. The XPS measurements were performed with a Phoibos 150 analyser and an unmonochromated XR-50 Mg Kα X-ray source from SPECS which was calibrated using the Ag 3d 5/2 peak. For the LaN coatings, a floodgun was used for charge compensation. The RHEED measurements were carried out at an electron energy of 10 keV, using an REG30 electron gun (Dr Gassler Electronic Devices).

The XRD and XRR experiments were performed at the MPI beamline of the Test Facility and Synchrotron Radiation Source ANKA, Karlsruhe, Germany (Stierle et al., 2004). The experimental setup and measurement geometry are shown in Fig. 1.

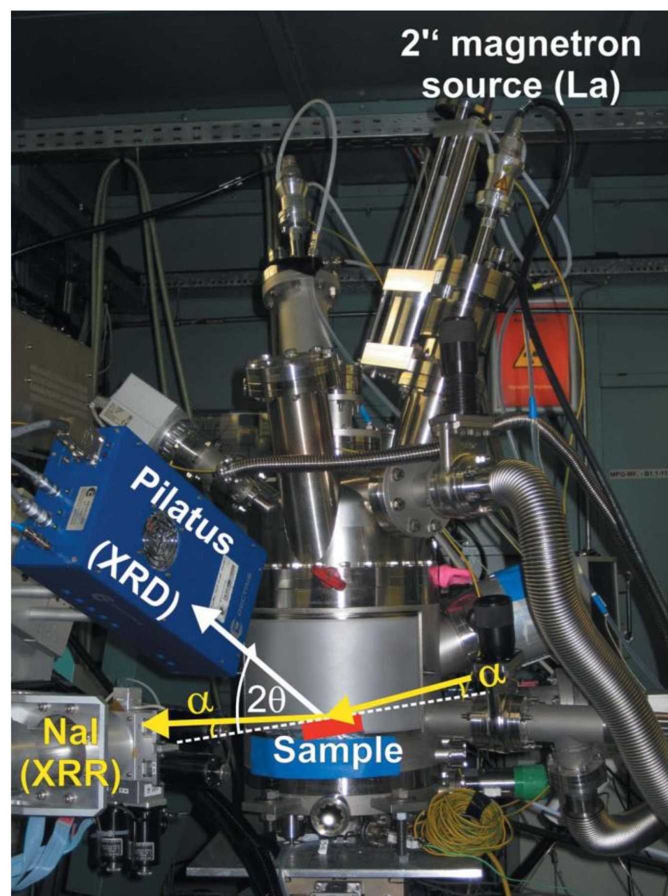

Fig. 1. Experimental setup and schematic of the measurement geometry. The sample horizontal is indicated as a dashed line. The incoming beam at an incident angle α is reflected onto a point detector (yellow arrows), while the diffracted signal (white arrow) is measured with a two-dimensional detector.

The sputter chamber was mounted in horizontal scattering geometry on a Huber 4 + 2 heavy-load diffractometer. Two detectors, an NaI scintillation detector and a Pilatus

100K detector (Dectris), were mounted with an angular offset of 24° on the same detector arm. For the time-dependent X-ray experiments during thin-film deposition, the incoming X-ray beam with a photon energy of 10 keV, an incident angle α = 1.5° and a beam size of 0.3 × 0.15 mm (horizontal × vertical) was reflected onto the scintillation detector. Simultaneously, the diffracted signal was measured with a two-dimensional detector, mounted at 2Θ = 27° and covering an angular range of about ±6° in the vertical direction and ±2° in the horizontal direction. Both data sets were recorded with a sampling frequency of 1 s. Before and after deposition, angular reflectivity scans and two-dimensional maps of the diffraction signal were measured. For the maps, the Pilatus detector was scanned in an angular range of ±30° in the horizontal direction and 0–40° in the vertical direction. The angular scans were done with automatic absorbers. The measured signal was normalized to the incoming beam intensity, which was monitored by an ionization chamber. The reproducibility of all observations was verified by the repeated deposition of films using identical growth conditions.

7.3 Results

7.3.1 Surface analysis

To verify the chemical composition and bond structure, XPS measurements were performed on thin films deposited under non-reactive and reactive sputter conditions. The results are shown in Fig. 2. For the reactively sputtered LaN film (black lines), the overview spectrum shows the lanthanum XPS peaks La 3d, La 4s, La 4p and La 4d, and the nitrogen peak N 1s (Fig. 2a). With the exception of the nitrogen peak, the same features are also observed for non-reactive sputter deposition of lanthanum (red lines). For both materials, an oxygen content of about 5 at.% was found at the sample surface, but quantification is difficult because the O 1s peak is superimposed on the strong La Auger signal. This problem is due to use of Mg Kα X-ray source, for the other setup employed in our research with Al Kα this overlap does not occur. Bond formation is revealed by an enlargement of the La 3d region (Fig. 2b). For non-reactive deposition, two well separated narrow peaks at binding energies of 835.7 ± 0.2 (La 3d 5/2) and 852.5 ± 0.2 eV (La 3d 3/2) are observed, as expected for metallic La [28]. For reactive sputtering both peaks showed a double-peak structure. The La 3d 5/2 peak is shifted to 833.3 ± 0.3 eV, which is lower than for metallic La, and a satellite peak with higher intensity occurs at 836.6 ± 0.2 eV. This satellite structure is a fingerprint of the chemical environment of La: $La(OH)_3$ formation leads to a smaller satellite peak, while La_2O_3 is characterized by two peaks of similar height [29]. The satellite peak with higher intensity observed here is characteristic of LaN [11, 30]. The La—N bond is also confirmed by the N 1s peak at 397 eV, which is typical for metal–nitrogen bonds.

The difference between reactively and non-reactively deposited films was also confirmed by RHEED measurements (see Fig. 3). For both film types, spotty RHEED patterns typical of the transmission of an electron beam through three-dimensional structures were observed. The non-reactively deposited La film shows the hexagonal pattern expected for f.c.c. La in the [111] orientation. For reactive deposition, a

different pattern with more pronounced intensity wings is found, which cannot be explained by LaN in the expected NaCl structure. Similar patterns are also observed for the deposition of La and LaN on boron, i.e. phase formation on Si wafers is also relevant for La/B-based multilayers.

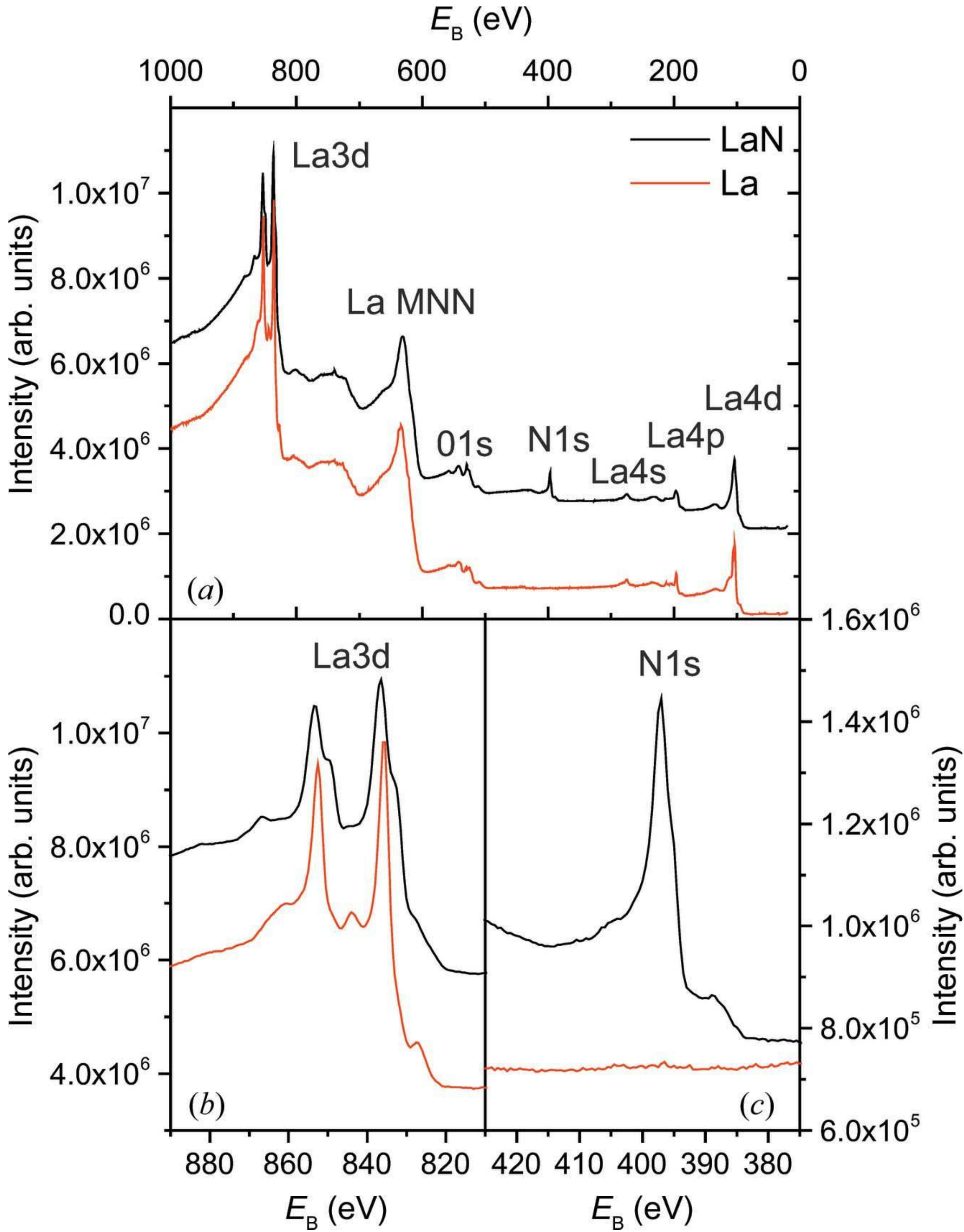

Fig.2. XPS spectra after non-reactive (red lines) and reactive (black lines) sputter deposition. (a) Survey spectra, (b) an enlargement around La 3d, and (c) an enlargement around N 1s.

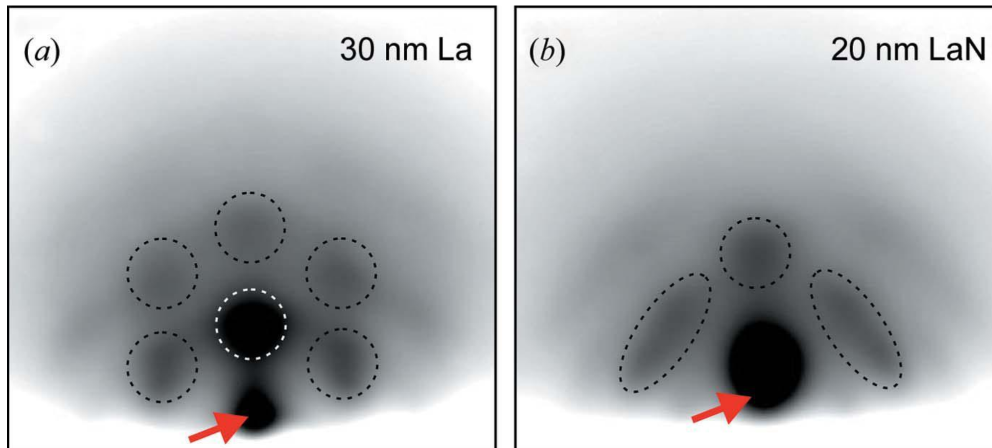

Fig.3. RHEED images of film growth by (a) non-reactive and (b) reactive deposition from a lanthanum target. The red arrows indicate the reflected electron beam. Characteristic diffraction spots are highlighted by dashed lines.

7.3.2. Crystalline phases

In situ synchrotron studies of the X-ray diffraction signal reveal a more detailed picture of the crystalline structure. Fig. 4 shows X-ray diffraction maps of (a) La and (b) LaN films with a thickness of 30 nm, measured directly after deposition while keeping the films under UHV conditions. The data are presented as q/χ maps, where χ is the angle to the surface normal and q is the scattering momentum transfer in a radial direction (corresponding to a 2Θ/ω scan). In this representation, a perfect stress-free crystalline powder would be characterized by horizontal lines representing the diffraction rings.

The La pattern (Fig. 4a) corresponds well to the f.c.c. [111] texture of the lanthanum β phase (indicated by yellow dots). The weaker intensity distribution above the central (111) peak indicates a coexisting [100] texture. Assuming thermodynamic equilibrium, the lanthanum β phase is expected at temperatures above ~566 K, which is well above our nominal substrate temperature of about 300 K during deposition. This can be explained in two ways: (i) for thin films the transition temperature might be shifted because of the energetic contributions of the surface and interface to the substrate; and (ii) the non-equilibrium sputter deposition process, where energetic particles are deposited on the growing film, often results in the growth of metastable phases. Once the β phase is formed, it is likely to be stabilized at room temperature owing to the extremely slow kinetics of the β-to-α phase transition [20].

The LaN pattern shown in Fig. 4(b) shows a much shorter distance between the two side peaks close to $q = 2$ Å^{-1} and $\chi = 70°$. The pattern cannot be explained by the expected NaCl structure, but agrees well with the theoretically predicted wurtzite and zincblende structures [22, 23]. Fig. 4(b) shows the calculated peak positions for [111]-oriented ZB LaN with $a = 5.6$ Å (yellow dots) and [002]-oriented WZ LaN with $a = 4.08$ Å and $c = 5.84$ Å (white dots).

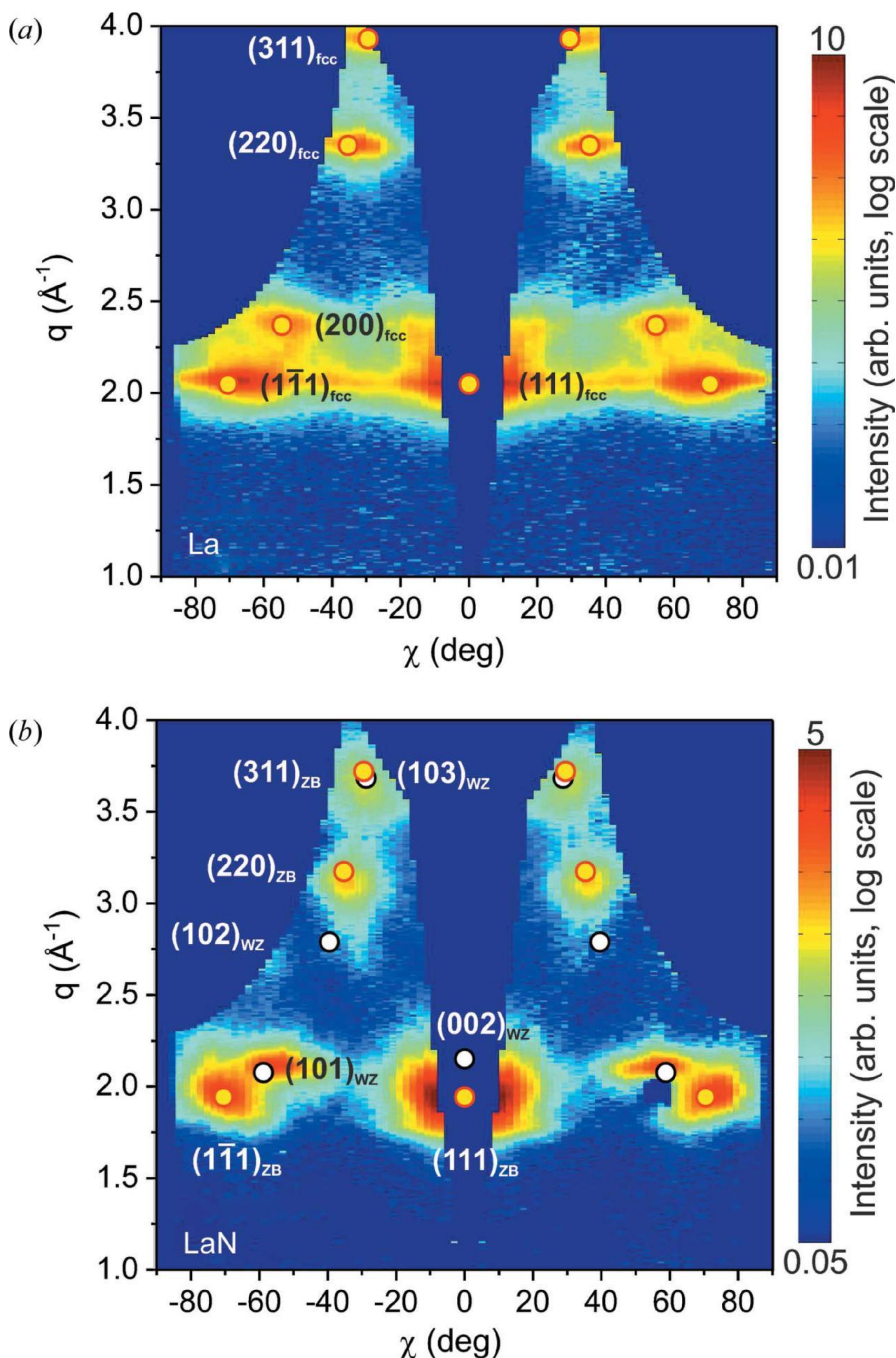

Fig. 4. Diffraction maps after (a) non-reactive and (b) reactive deposition, plotted as a function of the momentum transfer q and the angle χ to the surface normal. The non-reactive deposition results in a [111] textured f.c.c. La film. Yellow dots correspond to the expected peak positions. The pattern observed after reactive deposition can be explained by coexisting wurtzite and zincblende LaN in [002] and [111] orientations, respectively. The expected zincblende (yellow) and wurtzite (white) peak positions are indicated.

The observed structures are very interesting from the electronic point of view: while the expected NaCl structure is predicted to be metallic or semi-metallic, the WZ and ZB structures are expected to be semiconductors [23].

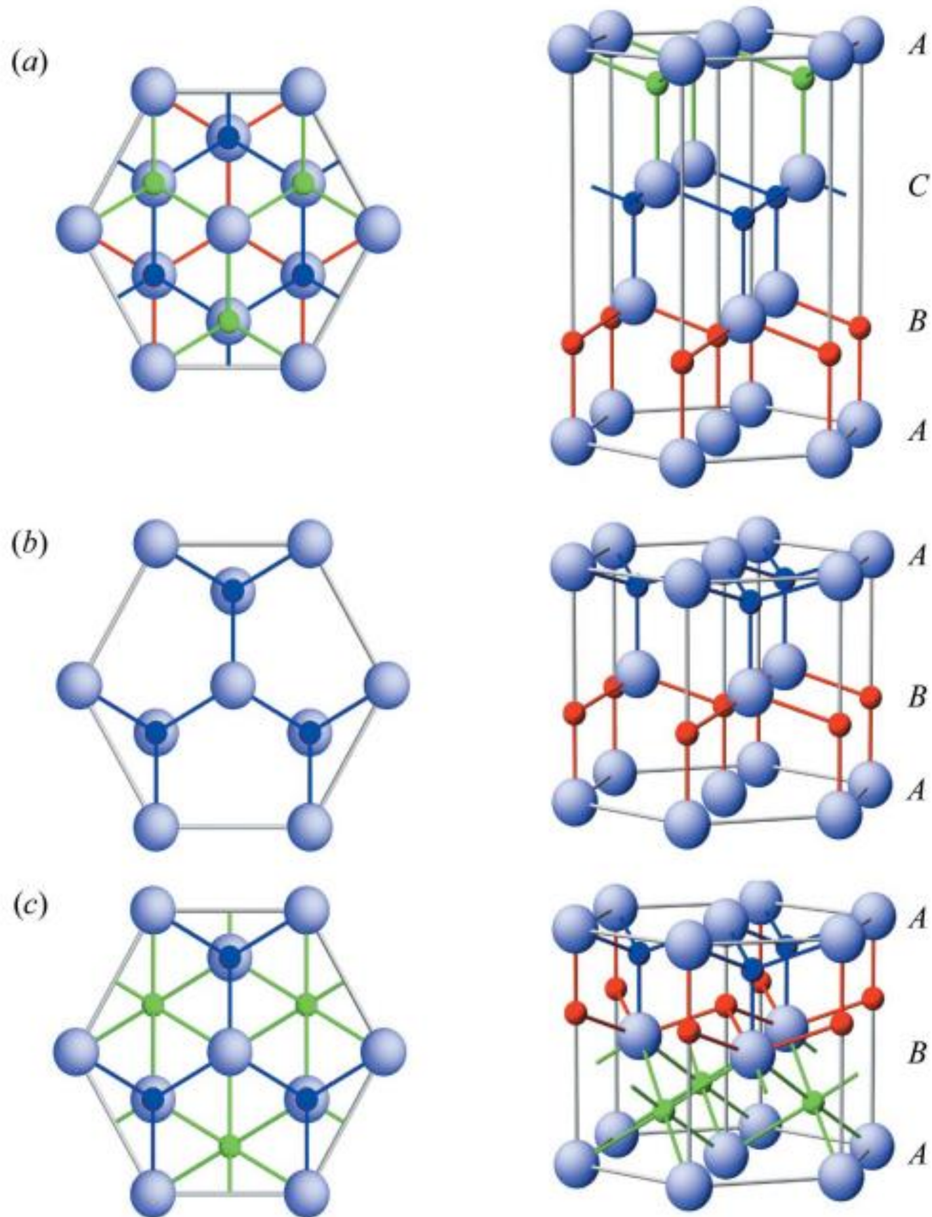

Fig. 5. Layer stacking of (a) the zincblende structure, (b) the wurtzite structure and (c) La_2O_3. The left-hand column shows top views and the right-hand column side views of the close-packed structures. Large light-blue balls correspond to lanthanum atoms and small balls to nitrogen or oxygen atoms. For better visibility, different colours indicate lattice sites in different atomic planes along the stacking direction.

The ZB structure has ABC layer stacking and the WZ structure AB layer stacking, as shown in Figs. 5(a) and 5(b), respectively. Both structures are close packed and directly related by stacking faults. A similar polytypism has been reported, for example, for GaN

[31], GaAs [32] and BN [33]. For electronic applications, coexisting phases are often undesired, while for hard coating materials such as BN, coexisting structures offer new alternatives to tune the material properties. Interestingly, the wurtzite structure of LaN has the same metal sublattice as La_2O_3 (Fig. 5c). It is possible that small oxygen impurities stabilize the metastable wurtzite structure, as known, for example, for the metastable tungsten β phase [34]. The similarity of the two crystalline lattices might also be relevant for the degradation mechanism of LaN under ambient conditions.

7.3.3 Structure formation during reactive and non-reactive deposition

The LaN layer thickness has a strong influence on the degradation behaviour of boron-capped LaN, while boron-capped La layers seem to be stable in the studied La thickness range of up to 15 nm [15]. Therefore, the thickness dependence of the structure formation was studied during thin-film deposition, employing a combination of in situ XRD and XRR. This approach has already been used successfully to understand the structure formation of $MoSi_X$/Si layer systems [25].

Fig. 6 shows the time-dependent diffraction signals close to the surface normal of the substrate ($\chi \approx 14°$), measured for (a)non-reactive and (b) reactive deposition. For better comparison, the deposition time has been converted into film thickness. The deposition rate was determined from the time-dependent XRR signal (see below). At thicknesses lower than 2–3 nm, both films show a weak and broad intensity distribution, indicating an amorphous layer or small disordered crystallites. During further deposition, in both cases the final texture is established within a few nanometres. For non-reactive deposition, an intense La(111) and a weak La(200) peak emerge. For reactive deposition, the intensity distribution remains broad but becomes slightly asymmetric, confirming the coexistence of LaN WZ and ZB phases already during early growth.

The time-dependent reflectivity signal, measured during non-reactive and reactive deposition, is presented in Fig. 7(a). The intensity was collected simultaneously with the XRD signal shown in Fig. 6. The experimental data are indicated by open symbols. They show characteristic oscillations which reflect the increasing film thickness. During one oscillation period τ, a film of thickness

$$D_\tau = \pi/|k_Z|, \quad (1)$$

is deposited, where $|k_Z|$ is the z component of the wavevector $k = 2\pi/\lambda$. At the incident angle $\alpha = 1.5°$ ($q = 0.2653$ Å^{-1}), each oscillation corresponds to the deposition of approximately 2.40 nm.

The time-dependent experimental data were fitted using the Parratt formalism, as described in detail [24, 25]. First, the angular reflectivity scans before and after deposition were fitted assuming a simple layer model. This was done for thick films of ~30 nm, and thin films where the deposition was interrupted close to the maximum of the time-dependent XRR signal. Based on these reference values, a time-dependent layer model was developed. The experimental data were reproduced by optimization of the thickness increase and roughness change during deposition. The fitted angular and time-dependent curves are shown as red lines in Fig. 7.

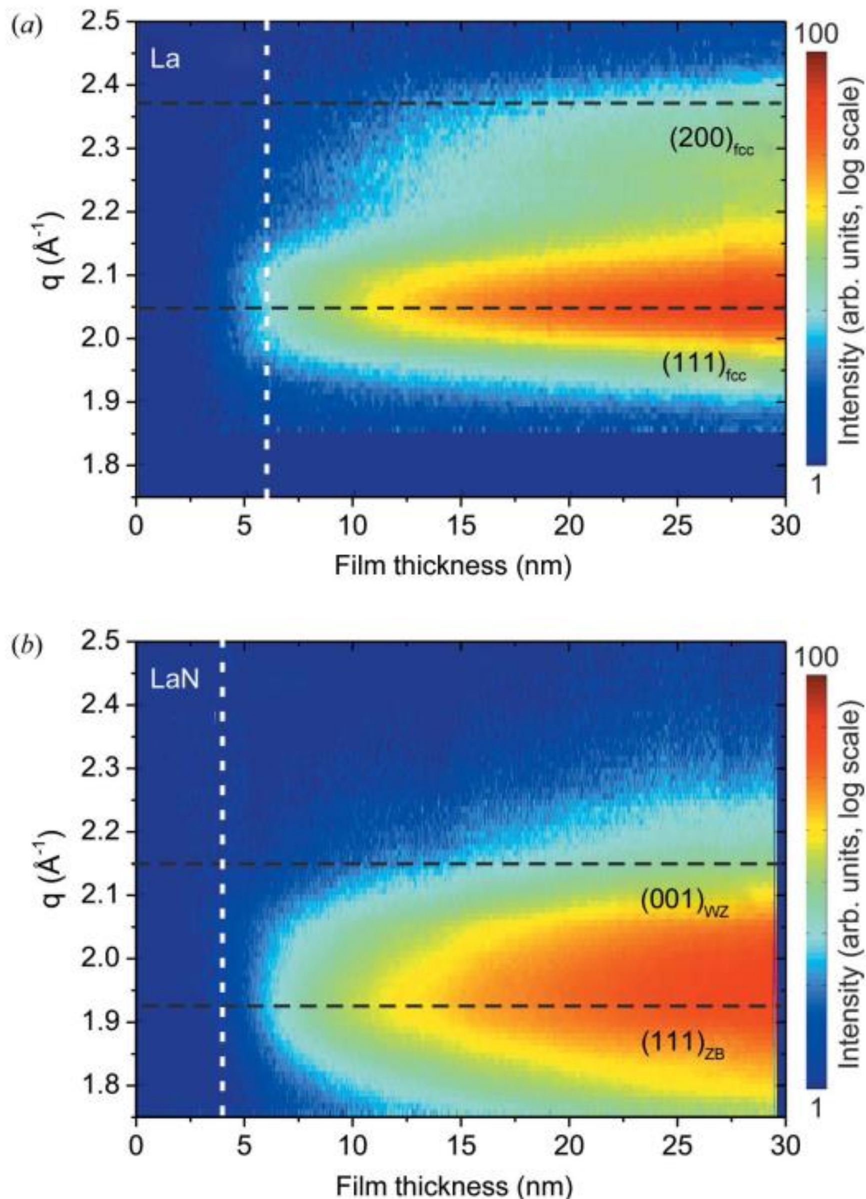

Fig.6. X-ray diffraction signals during (a) non-reactive and (b) reactive deposition, plotted as a function of film thickness. The nominal peak positions of the crystalline phases identified after growth are indicated by black dashed lines. The dashed white lines (vertical) indicate the film thickness with minimum roughness.

Table 1 summarizes the simulation parameters of the angular reflectivity curves. For the thick LaN film, a two-layer model was assumed. The other measurements could be reproduced with a single layer. The fit parameters for the substrate, consisting of silicon covered by a natural oxide layer, were the same for all samples.

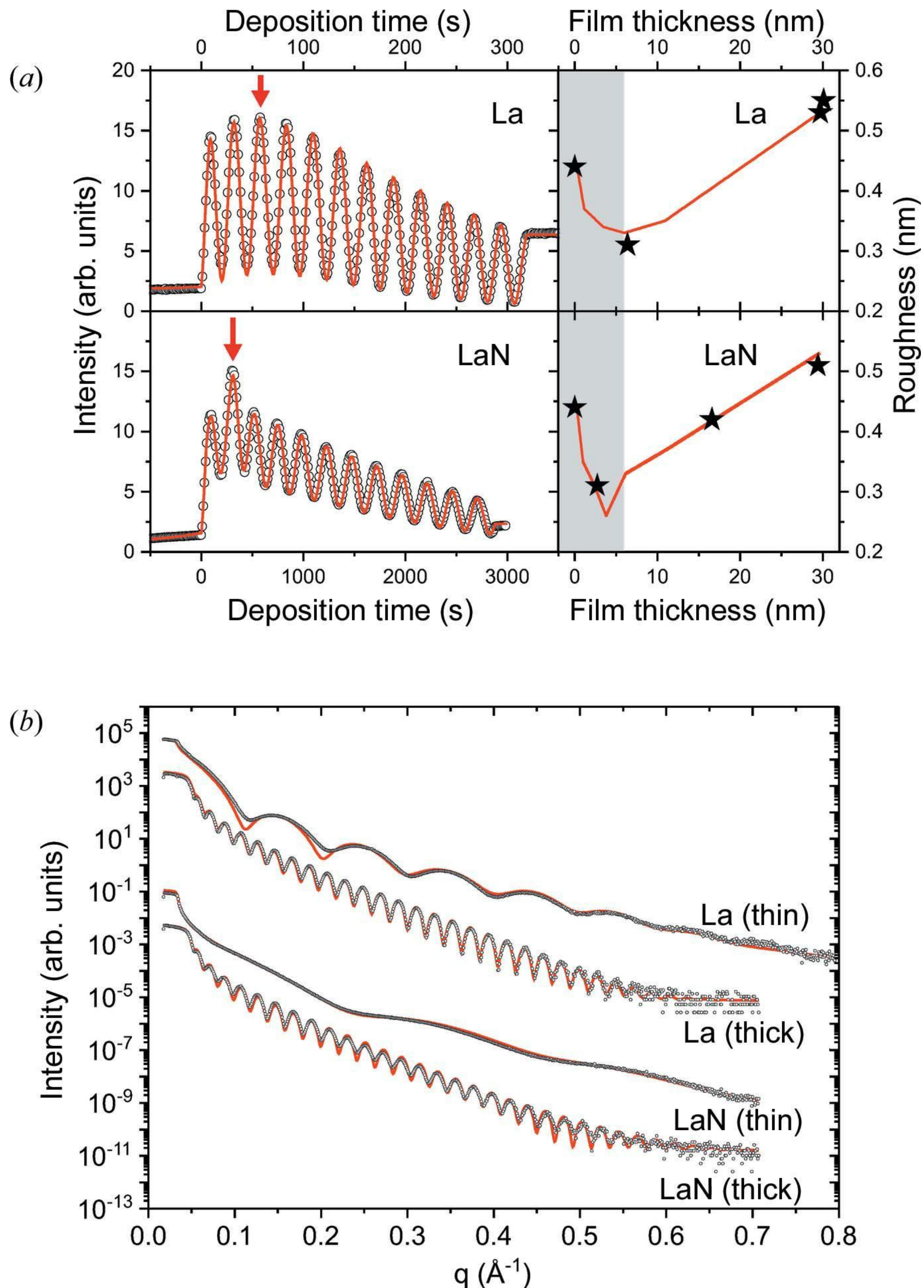

Fig.7. Experimental (open symbols) and simulated (red line) XRR measurements, (a) during and (b) after non-reactive and reactive deposition. The time-dependent measurements were performed at q = 0.2653 Å^{-1}. The roughness development with film thickness (extracted from the fit, red line) is shown on the right-hand side.

The expected δ values are δ(La) = 10.49 × 10^{-6} for f.c.c. and h.c.p. La, δ(f.c.c. LaN) = 11.81 × 10^{-6} for LaN with the NaCl structure, and (WZ/ZB) = 9.6–10.3 × 10^{-6} predicted for WZ and ZB LaN. Reference values determined from fitting complete angular XRR measurements at the indicated thickness are shown as black stars, and the initial growth regime is highlighted (grey background). The angular measurements were performed on thin and thick (~30 nm) La and LaN films. For the thin films, the deposition was interrupted close to the maximum intensity of the time-dependent measurements [red arrow in panel (a)]. The fit parameters are summarized in Table 1.

For La, the measured value is only slightly lower than expected. For LaN, the values are too low for the NaCl structure but can be explained by WZ and ZB LaN, in agreement with the diffraction data. For a pure LaN layer, the value is proportional to the mass density of the film. The slightly lower value of the LaN layer during the first few nanometres can be explained by porosity. Assuming that the subsequently deposited LaN (layer 2) has bulk density, the density of the first layer would be in the range of ~80% (thin film) to ~90% (thick film). However, owing to the low interaction with the SiO_X surface compared with B, it is not clear if this observation is relevant for multilayer formation. In agreement with our XPS measurements, a large oxide contribution can be excluded since all observed values are much lower than δ(La_2O_3) = 11.68 × 10^{-6}.

Sample	$\delta \times 10^{-6}$	d (nm)	σ (nm)
Si	5.44		0.44
SiO_x	4.48	0.18	0.44
La (thin)	10.01	6.37	0.31
La (thick)	10.08	29.7	0.53
LaN (thin)	8.67	2.76	0.31
LaN (thick, layer1/layer2)	9.43/10.67	0.88/28.42	0.31/0.51
La (thin, after nitridation)	10.13	6.73	0.35

Table 1. Real part correction of the refraction index, film thickness d and roughness used for the fit of the angular X-ray reflectivity measurements shown in Figs. 7(b) and 8(a).

From the fit of the time-dependent curves, deposition rates of 0.091 nm s^{-1} for non-reactive and 0.010 nm s^{-1} for reactive deposition were obtained. Taking into account automatic PC-controlled substrate shutter, maximum delay of 1 s might be taken as a total maximum delay between sending the command and actually having the shutter opened or closed. Therefore, maximum thickness errors ≈1Å for La and ≈0.1 Å max for LaN deposition. For both layers, an initial smoothing of the films was found, consistent with the fit parameters obtained for the angular XRR of the thin films. From our experience, it is known that ≈1 nm La or LaN form a continuous layer, therefore, it is not expected that the roughness versus film thickness graphs (Fig. 7, (a)) are affected by island growth. For LaN, the minimum roughness is reached at about 3 nm film thickness, and there is subsequently a continuous roughness increase which

can be explained by simultaneous texture formation. For La, the behaviour is similar but the roughness minimum is broader and shifted to a larger film thickness of 5–6 nm, which is slightly delayed with respect to the onset of texture formation.

Texture formation is often accompanied by facet formation. The surface morphology coarsens with increasing thickness, resulting in an increasing roughness, as observed for LaN and La. However, the detailed growth mechanisms of the two materials are different, as indicated by the delayed roughness transition observed for La. This delayed transition can be explained by grain-boundary diffusion taking place in competition with vertical grain growth. Because of this mechanism, the gaps between neighbouring grains are filled, leading to an additional smoothing effect [35]. Nitrides have a lower mobility than metals. After the onset of faceting, shadowing effects suppress the formation of grain boundaries, and a columnar film with small voids is formed [36, 37]. This growth model can explain the different efficiency of the B cap for thin and thick LaN films. At larger film thickness, the coating contains voids. Some of these voids reach up to the surface. If they are sufficiently large, they cannot be completely closed by the cap. At these points, the film can be attacked by oxygen and humidity. Once this process starts, the large volume increase due to hydroxide formation leads to a further destruction of neighbouring film areas, starting an avalanche-like degradation process. The proposed grain-boundary diffusion mechanism for La explains why, in this case, the formation of pores is suppressed, the B cap covers the entire film, and for larger film thicknesses no degradation is observed.

7.3.4 Nitridation of an already deposited La film

The reflectance of La/B multilayer structures is significantly improved by a combination of non-reactive and reactive La deposition. This process, also called partial (delayed) La nitridation, results in an La/LaN/B stack [10]. It is expected that such a stacking sequence can also be produced by post-growth nitridation. Therefore, a thin lanthanum film was exposed for 10 min to a nitrogen flux of 4 sccm. Fig. 8(a) compares the angular reflectivity curves measured before and after N_2 exposure. After nitridation, the oscillation minima are shifted to lower q, indicating a larger film thickness. A fit of the data revealed an increase in the film thickness of 0.35 nm.

To study the influence of nitridation on the crystalline structure, diffraction maps before and after nitridation were recorded. Fig. 8(b) shows the difference signal of the two maps, enhancing the relatively small intensity changes. The XRD intensity increases at the positions of [111] ZB LaN (yellow dots), while the intensity at the [111] f.c.c. La (white dots) decreases, indicating the transformation of the topmost atomic layers of La into LaN. For f.c.c. La, the volume per La atom is 37 Å^3, and for ZB and WZ LaN it is about 42 Å^3 [23]. Assuming that the volume increase is dominated by an expansion in the z direction where the atoms are free to move, a thickness increase of 0.35 nm would correspond to a nitride layer of 2.6 nm thickness. Interestingly, the texture of the La film is maintained even in the nitridized surface layer. This can be explained by the identical arrangement of La atoms in f.c.c. La and ZB LaN. The N atoms fill interstitial sites of the f.c.c. La lattice (see Fig. 5a). This indicates that the structure formation mechanism during post-growth nitridation is quite different from the

formation mechanism during deposition. During deposition, the crystallites of both WZ and ZB phases are formed during a competitive nucleation and growth process. During post-growth nitridation, the crystalline phase forms via diffusion of nitrogen atoms in the already established f.c.c. lattice of the lanthanum atoms.

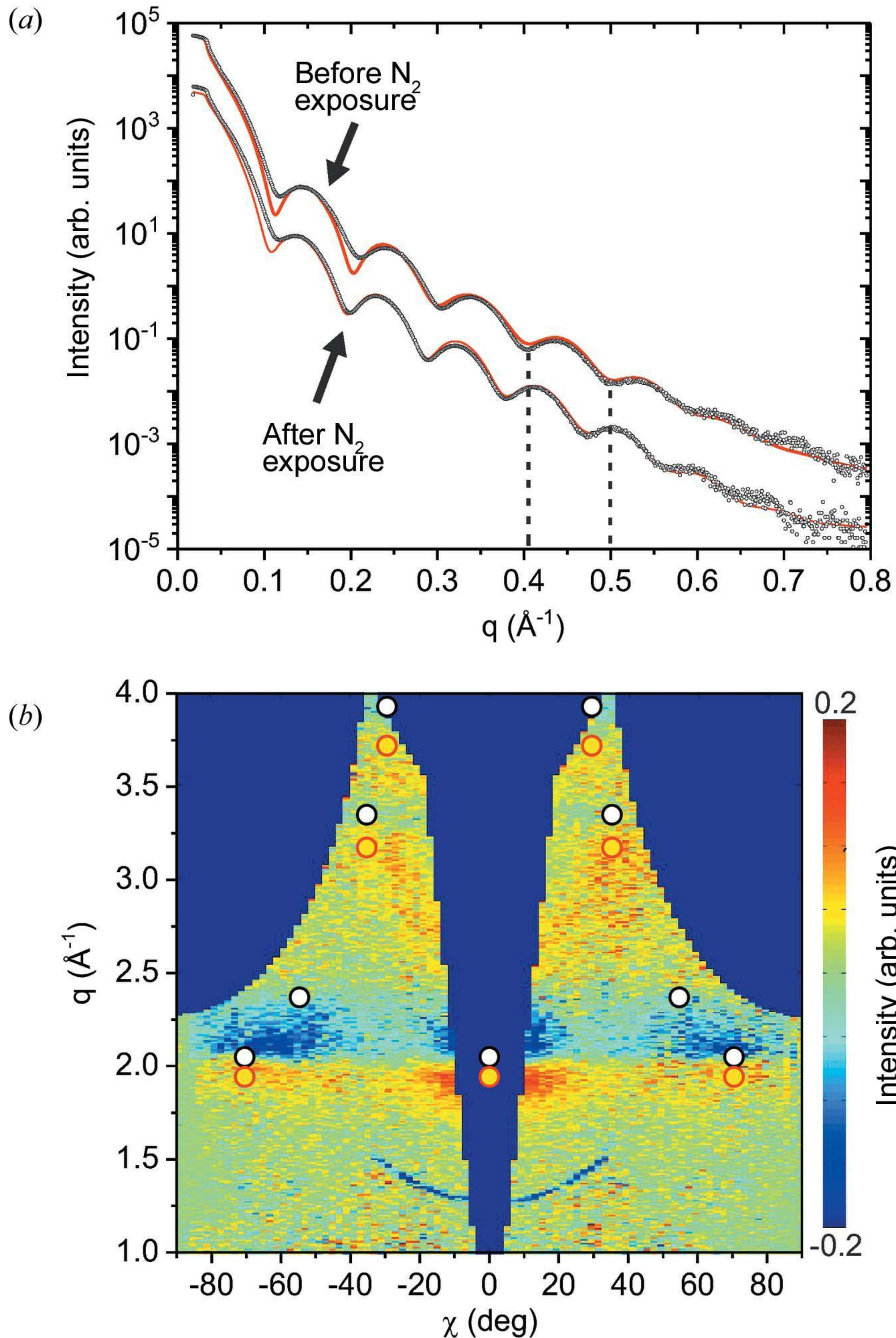

Fig.8. X-ray reflectivity curves measured before and after N_2 exposure of a 2.7 nm thick lanthanum layer. Dots correspond to experimental data and fitted curves are presented as red lines. The fit parameters are summarized in Table 1. To highlight the

change in the oscillation period, dashed lines indicate the positions of intensity minima before N_2 exposure. (b) Difference between the XRD maps after and before N_2 exposure. As a result of N_2 exposure, the intensity decreases at the positions of [111] f.c.c. La (white dots) and increases at the positions of [111] ZB LaN (yellow dots).

7.4 Summary and conclusions

Using in situ synchrotron methods during non-reactive and reactive sputter deposition, it was possible to determine the crystalline structures and textures of highly reactive La and LaN thin films. For La, a dominant [111] texture of the expected NaCl structure was identified, coexisting with a weaker [100] texture. For LaN, in agreement with theoretical predictions, the observed diffraction peaks were explained by coexisting metastable WZ[001] and ZB[111] textures. The ZB phase was also found after post-growth nitridation of f.c.c. La. After initial deposition of an amorphous or nanocrystalline disordered layer, La and LaN thin films show a roughness transition related to texture formation. For La, this roughness transition is slightly delayed compared with the onset of texture formation. This is attributed to the greater mobility of the pure metal compared with the nitride, resulting in a different growth mechanism. For metal growth, grain-boundary diffusion plays an important role, while for nitride growth, shadowing effects dominate.

On the basis of the above observations, two possible explanations for the degradation of B-capped thick LaN films were identified. (i) After the onset of texture and facet formation, LaN is expected to form a voided structure as a result of shadowing effects. Some of these voids reach up to the sample surface and cannot be completely closed by the cap, thus allowing direct contact between the film and ambient conditions. (ii) The crystalline structure might contribute to the stability of the films. The observed WZ LaN structure has the same metal sublattice as La_2O_3 , which might facilitate oxidation and subsequent hydridation. The post-growth nitridation of lanthanum, as a further development of the delayed nitridation process successfully employed to increase the reflectivity of thin LaN films, might solve the void problem since it maintains the dense structure of the initial film. Direct experimental evidence for the proposed LaN void structure is challenging, since the bulk densities of WZ and ZB LaN are not yet known. Commonly, this question would be addressed by cross-sectional scanning and transmission electron microscopy studies. In the case of La and LaN, these methods are complicated by the high reactivity of the films. Atomic force and scanning electron microscopy measurements of the capped structures cannot resolve the expected large aspect ratio of the voids and are unlikely to detect local widely separated defects. Indirect evidence, however, is given by optical microscopy, which reveals that sample destruction proceeds via radially extending and widely scattered areas.

Acknowledgements
The authors acknowledge the Test Facility and Synchrotron Light Source ANKA for provision of beam time, and thank the staff of the KIT institutes IPS and IBPT for support during the X-ray experiments. We are grateful for the support of the Industrial Focus Group XUV Optics at the MESA+ Institute at the University of Twente, notably the industrial partners ASML, Carl Zeiss SMT GmbH, Malvern Panalytical and NWO, as well as the Province of Overijssel.

References
1. J.L. Culhane et al., Solar Physiscs, Vol. 243, Iss. 1, 19-61 (2007)
2. J.R. Lemen et al., Solar Physics, Vol. 275, Iss. 1-2, 17-40 (2012)
3. A.J. Corso, P. Zuppella, D.L. Windt, M. Zangrando, and M.G. Pelizzo, Optics Express, Vol. 20, Iss. 7, 8006-8014 (2012)
4. A.J. Nelson et al., Optics Express, Vol. 17. Iss. 20, 18271-18278 (2009)
5. E. Louis, A.E. Yakshin, T. Tsarfati, and F. Bijkerk, Progress in Surface Science, Vol. 86, Iss. 11, 255-294 (2011)
6. M.K. Tiwari, K.J.S. Sawhney, and G.S. Lodha, Spectrochimica Acta Part B, Vol. 65, 434-440 (2010)
7. A.M. Hawryluk and N.M. Ceglio, Applied Optics, Vol. 32, 7062-7067 (1993)
8. I. A. Makhotkin, E. Zoethout, E. Louis, A.M. Yakunin, S. Müllender, and F. Bijkerk, Optics Express, Vol. 20, 11778–11786 (2012)
9. I.A. Makhotkin, E. Zoethout, R.W.E. van de Kruijs, S.N. Yakunin, E. Louis, A.M. Yakunin, V. Banine, S. Müllender, and F. Bijkerk, Optics Express, Vol. 21, 29894–29904 (2013)
10. D.S. Kuznetsov, A.E. Yakshin, J.M. Sturm, R.W.E. van de Kruijs, E. Louis, and F. Bijkerk, Optics Letters, Vol. 40, 3778–3781 (2015)
11. D.S. Kuznetsov, A.E. Yakshin, J.M. Sturm, R.W.E. van de Kruijs, and F. Bijkerk, AIP Advances, 6 115117 (2016)
12. B. Van Devener, J.P.L. Perez, J. Jankovich, and S.L. Anderson, Energy Fuels, Vol. 23, 6111–6120 (2009)
13. A. Jain, S. Anthonysamy, K. Ananthasivan, and G. Gupta, Thermochimica Acta, Vol. 500, 63–68 (2010)
14. W.G. Shin, S. Calder, O. Ugurlu, and S.L. Girshick, Journal of Nanoparticle Research, Vol. 13, 7187–7191 (2011)
15. D.S. Kuznetsov, A.E. Yakshin, J.M. Sturm, and F. Bijkerk, Journal of Nanoscience and Nanotechnology, Vol. 19, 1-8 (2019)
16. S.L. Nyabero, R.W.E. van de Kruijs, A.E. Yakshin, I.A. Makhotkin, J. Bosgra, and F. Bijkerk, Journal of Micro/Nanolithography, MEMS and MOEMS, Vol. 13, 013014 (2014)
17. W.-B. Zhang, X.-J. Ma, A. Loh, X. Li, F.C. Walsh, and L.-B. Kong, ACS Energy Letters, Vol. 2, 336–341 (2017)
18. B.J. Beaudry and P.E. Palmer, Journal of the Less Common Metals, Vol. 34, Iss. 2, 225-231 (1974)

19. J. Häglund, A. Fernández Guillermet, G. Grimvall, and M. Körling, Physical Review B, Vol. 48, No. 16, 11685 (1993)
20. R.J.M Konings and O. Beneš, Journal of Physical and Chemical Reference Data, Vol. 39, 043102 (2010)
21. P. Ettmayer, J. Waldhart, A. Vendl, and G. Banik, Chemical Monthly 111, Iss. 4, 945–948 (1980)
22. E. Zhao and Z. Wu, Journal of Solid State Chemistry, Vol. 181, Iss. 10, 2814-2827 (2008)
23. M. Ghezali, B. Amrani, Y. Cherchab, and N. Sekkal, Materials Chemistry and Physics, Vol. 112, Iss. 3, 774-778 (2008)
24. M. Kaufholz, B. Krause, S. Kotapati, M. Köhl, M.F. Mantilla, M. Stüber, S. Ulrich, R. Schneider, D. Gerthsen, and T. Baumbach, Journal of Synchrotron Radiation, Vol. 22, Part 1, 76-85 (2015)
25. B. Krause, G. Abadias, A. Michel, P. Wochner, S. Ibrahimkutty, T. Baumbach, Applied Materials and Interfaces, 8, 34888–34895 (2016)
26. B. Krause, S. Darma, M. Kaufholz, H.-H. Gräfe, S. Ulrich, M. Mantilla, R. Weigel, S. Rembold, and T. Baumbach, Journal of Synchrotron Radiation, Vol. 19, 216–222 (2012)
27. E. Haye, F. Capon, S. Barrat, D. Mangin, and J.-F. Pierson, Surface and Coating Technology, Vol. 298, 39–44 (2016)
28. R. Kumar, M.H. Mintz, and J.W. Rabalais, Surface Science, Vol. 147, Iss. 2, 37-47 (1984)
29. M. Sunding, K. Hadidi, S. Diplas, O.M. Løvvik, T. Norby, and A.E. Gunnaes, Journal of Electron Spectroscopy and related Phenimena, Vol. 184, 399-409 (2011)
30. B. Cos, H.-C. Kim. F.S. Aguirre-Tostado, R.M. Wallace, and J. Kim, Microelectronic Engineering, Vol. 86, Iss. 3, 235-239 (2009)
31. B. Paulus, F.-J. Shi, and H. Stoll, Journal of Physics: Condensed Matter, Vol. 9, No. 113, 2745-2758 (1997)
32. P. Schroth, M. Köhl, J.-W. Hornung, E. Dimakis, C. Somaschini, L. Geelhaar, A. Biermanns, S. Bauer, S. Lazarev, U. Pietsch, and T. Baumbach, Physical Review Letters, Vol. 114, 055504 (2015)
33. D. Kester, K. Ailey, R. Davis, and K. More, Journal of Materials Research, Vol. 8, Iss. 6, 1213–1216 (1993)
34. K.-U. Demasius, T. Phung, W. Zhang, B.P. Hughes, S.-H. Yang, A. Kellock, W. Han, A. Pushp, and S.S.P. Parkin, Nature Communications 7, 10644 (2016)
35. E. Chason, Thin Solid Films, Vol. 526, 1-14 (2012)
36. I. Petrov, P.B. Barna, L. Hultman, and J.E. Greene, Journal of Vacuum Science and Technology A 21, S117 (2003)
37. F. Nita, C. Mastail, and G. Abadias, Physical Review B, Vol. 93, 064107 (2016)

Note on Chapter 7

The in situ growth studies of La and LaN, presented in chapter 7, have the status of initial work. Further studies might be beneficial for detailing the knowledge on the contributing physical processes. For example, the contribution of reflected neutrals (neutralized sputter and, in case of LaN, reactive gas species, reflected from the sputter target towards growing film) might be different for La and LaN deposition.

The influence of the order of magnitude slower deposition of LaN compared to La should be studied as well. Generally, a lower material flux results in higher average energy per deposited atom, and therefore higher diffusivity might be expected for LaN vs La. The results presented in chapter 7 might seem to contradict this theoretical expectation. Especially if enhanced diffusivity does take place when LaN deposition rate is reduced by an order of magnitude (down to 0.010 nm s^{-1}), the diffusivity versus La still stays low, being dominated by reduced diffusion in nitride vs metal. Therefore, the results presented in chapter 7 are considered valid. However, it is acknowledged that the studies of separate contributions and various deposition parameters might yield new valuable knowledge.

An alternative explanation on the nitridation of deposited La film (sub-chapter 7.3.4) can be proposed. The reaction might be self-limiting, since a formed monolayer can significantly reduce the rate of further interaction of underlying La with nitrogen species. However, a monolayer is known not to be visible at the used experimental XRD setup. Moreover, from general knowledge on crystallization, it is commonly expected that at least a few monolayers are required to obtain a polycrystalline layer, having a non-ideal (not an ideal single crystal) polycrystalline layer with a different crystalline structure as substrate-layer. This alternative explanation has therefore not been considered in chapter 7.

Summary
Nanoscale multilayer structures are employed in a wide range of analytical and imaging applications. Extreme Ultraviolet (XUV) multilayer coatings are key enablers of optical components in this wavelength range. This thesis addresses multilayers wavelengths above 6.6 nm, which have a perspective for light sources like FELs, diagnostic techniques like XRF, optical elements like beam-splitters and telescopes for space research, as well as for high resolution imaging systems. The focus of this work was on the synthesis of multilayers with high performance (reflectivity and thermal stability), insight into the growth and control of deposition at the atomic scale.

The figure of merit of the understanding of the basic physics processes in nanoscale multilayers, as well as the ability to control these, is usually expressed by its reflectivity. At the start of this thesis project, the highest reflectivity at near normal incidence of 6.7 nm wavelength amounted 57.3%. Nitridation of the La/B multilayers was shown to protect the B-on-La interface from the formation of optically unfavorable lanthanum boride compounds at that interface. Further development in this thesis opened up a way to improved layer control. This is based on the fact that La will not take more N than needed for the formation of a stoichiometric LaN compound. Excessive N_2 during La growth results in the formation of optically unfavorable BN at the LaN-on-B interface. Therefore, the layer growth process was controlled by a special approach, so called partial (delayed) nitridation. The use of sub-nm but closed (~0.3 nm or thicker) interlayers of elemental La deposited on B was shown to minimize the interaction of N with B. This hybrid deposition allowed to synthesize multilayer structures with new record reflectivity: 64.1% at λ≈6.66 nm, AOI=1.5°. Further improvements can be anticipated.

In addition, the thermal stability was studied for the new multilayer structure with partial (delayed) nitridation. The observed changes under elevated temperatures were associated with interdiffusion and formation of compound(s). For both B-on-LaN and LaN-on-La-on-B interfaces no additional compound formation was resolved in the temperature range up to 200°C. The partial (delayed) nitridation LaN-on-La-on-B interface was still not activated for interdiffusion at 200°C, judging by no registered compound formation. This result could be explained by the formation of a LaB_x interlayer. Therefore, novel partial (delayed) nitridation demonstrated a thermal stability similar to previously developed LaN/B multilayers.

Finally, the possibility of fabricating La/B-based multilayers for ~6.7 nm radiation at grazing angles of incidence (GI) was investigated. LaN/B for GI (period 15 nm) showed deterioration accompanied by oxidation of at least two of the topmost LaN layers. A special scheme called La surface nitridation was invented, in which only top part of La layers is nitridized. It was found that the B protective properties depend on the thickness of the underlying LaN layer. The LaN thickness for which no deterioration occurs, was determined to be at least 0.4-1.0 nm. In order to obtain further insight into La and LaN growth, special in situ studies were accomplished at a synchrotron light source. Crystallographic structures of La and LaN during growth were revealed, and initial formation of textures and roughness transitions were observed. Two probable explanations for the LaN degradation were developed. Employing the

special La surface nitridation scheme, a record reflectivity of 74.5% at 6.66 nm at off-normal (77°) incidence was achieved. These multilayers were demonstrated to be stable to storage in atmosphere during at least one year and a half. An absolute drop of reflectivity of about 0.5% was explained by contamination, accumulated by a B top layer.

The results of the research presented in this thesis demonstrate how knowledge on layer growth, combined with a high, atomic scale, degree of control of the deposition can be employed to improve the performance of nanoscale multilayer systems. The experimental and analytical approaches, employed in the study of reflective multilayers for the wavelengths above 6.6 nm, might be adapted for various stacked systems with nm- and sub-nm-thick layers.

Samenvatting

Multilaag structuren op nanoschaal worden gebruikt binnen meerdere analytische en afbeeldende toepassingen. In het bijzonder zijn Extreem Ultraviolet (XUV) multilaag coatings een "key enabler" voor meerdere optische componenten in het XUV golflengtegebied. Dit proefschrift behandeld multilagen die ontwikkeld worden voor ~6.7 nm golflengte, met als perspectief toepassing als optieken voor vrije elektronen lasers, in fluorescentie diagnostiek, als bundelsplitsers, en in telescopen en andere hoge resolutie afbeeldingssystemen. Het doel van het onderzoek was om bij te dragen aan de ontwikkeling van hoge kwaliteit multilagen met hoge reflectiviteit en thermische stabiliteit, met de nadruk op het vergaren van inzicht in de groei en controle van de eigenschappen van dunne lagen op een atomaire schaal.

De reflectiviteit van een multilaag is algemeen erkend als een maat voor het begrip van de fundamentele fysische processen die plaatsvinden, alsmede het vermogen om dit begrip te gebruiken om deze processen te kunnen sturen en een nog hogere reflectiviteit te realiseren. Aan het begin van het hier gepresenteerde onderzoek was de hoogst gerapporteerde reflectiviteit van 6.6 nm multilagen slechts 57.3%. Door middel van nitridatie van de lanthaan/boor multilagen is het gelukt om het boor-op-lanthaan interface te passiveren en de formatie van optisch ongewenste lanthaanborides tegen te gaan. Een verdere ontwikkeling in dit proefschrift was de verbeterde groei van lanthaannitride. Dit was gebaseerd op de ontdekking dat lanthaan een verzadigingsconcentratie van stikstof heeft, gerelateerd aan een stoichiometrische groei van lanthaannitride. Wanneer te veel stikstof aanwezig is tijdens de groei van lanthaan, vormt zich een optisch niet gewenst boornitride aan het lanthaan-op-boor interface. Om vorming van boornitride tegen te gaan is een speciaal groeiproces ontwikkeld, waar het eerste deel (circa 0.3 nm) van de La laag gegroeid wordt zonder stikstof, waardoor de interactie van stikstof met boor tot een minimum gebracht wordt, gevolgd door verdere lanthaannitride groei. Door middel van dit hybride groeiproces zijn uiteindelijk multilagen gerealiseerd met wereldrecord reflectiviteit: 64.1% bij een golflengte van 6.66 nm en hoek van inval van 1.5 graden van de normaal. Verdere verbeteringen zijn nog mogelijk door een verdere optimalisatie van het hier ontwikkelde proces.

Naast het ontwikkelen van hybride gegroeide LaN/B multilagen voor hoge reflectiviteitstoepassingen, is ook de thermische stabiliteit van deze multilagen bestudeerd. De veranderingen die onder verhoogde temperatuur zijn geobserveerd worden toegekend aan interdiffusie en vorming van verbindingen aan de interfaces. Voor zowel B-op-LaN en LaN-op-B interfaces werd geen temperatuur-gedreven bindingen waargenomen voor temperaturen lager dan 200 °C. Hieruit blijkt dat een hybride gegroeide lanthaanlaag zich minstens even goed gedraagt onder thermische belasting als een volledig gepassiveerde LaN laag.

Ten slotte is aandacht besteed aan de ontwikkeling van La/B gebaseerde multilagen voor toepassing als optieken voor ~6.7 nm golflengte bij scherende inval. Hiertoe zijn speciale multilagen gefabriceerd waarbij alleen het bovenste deel van elke La laag is genitrideerd om LaB formatie tegen te gaan. Deze multilagen leden echter aan verval door oxidatie van de bovenste LaN lagen. Het bleek dat de beschermende

eigenschappen van de bovenste boor laag afhangen van de dikte van de daaronder liggende LaN laag. Tot ongeveer 1 nm LaN treedt geen verval op, maar vanaf ongeveer 2 nm treedt wel verval op. Om een beter begrip te krijgen in de groei van La en LaN zijn X-ray metingen gedaan tijdens groei van de laag, gebruikmakend van een hoge-intensiteit synchrotronlichtbron. De kristallijne structuur van La en LaN is bestudeerd en liet de initiële vorming van textuur en daaraan gerelateerde opbouw van ruwheid zien. Hieruit volgden twee mogelijke verklaringen voor de degradatie van LaN. Verder is met behulp van oppervlaktenitridatie een recordreflectiviteit gerealiseerd van 74.5% bij 6.66 nm golflengte en 13 graden scherende inval. Deze multilagen zijn stabiel onder atmosferische opslag voor tenminste anderhalf jaar, waarbij een verlaging van de reflectiviteit van 0.5% in die periode toegeschreven kan worden aan oppervlakteverontreiniging van de boor toplaag.

De resultaten van het onderzoek demonstreren hoe een gedetailleerd begrip van de laaggroei, gecombineerd met een nauwkeurige controle op atomaire schaal van het depositieproces, gebruikt kunnen worden om de prestaties van nanoschaal multilaagsystemen te verbeteren. De experimentele en analytische procedures, zoals ontwikkeld voor het onderzoek aan reflecterende multilagen voor ~6.7 nm golflengte, hebben goede potentie om toegepast te worden in diverse andere multilaagsystemen met nanometer en sub-nanometer dikke lagen en de prestaties van die systemen daarmee te verbeteren.

Valorisation

Control of the quality of nanoscale thin films is crucial for various practical applications. These include Extreme UV telescopes for space research, beam line optics for free electron lasers (FEL), monochromators used in X-ray fluorescence (XRF) and various XUV systems for high resolution imaging schemes. These examples have both an academic (scientific), an industrial (economical), as well as a social impact.

XUV space telescopes allow the study of the sun and other astronomy objects, for instance, to improve weather forecasts and estimate potential climate changes. The multilayer coatings developed in this research provide high reflectivity in the boron spectral window, i.e. above 6.6 nm wavelength. Our approaches in the deposition process also provide control of multilayer growth for development of optics for other bands in space research.

FEL-based short wavelength light sources (like LCLS in Stanford or the XFEL in Hamburg) allow one to probe samples with pulses as short as few fs. Therefore, observations of dynamic behaviour including biomolecular systems (e.g. proteins), chemical reactions [1] and other complex non-crystalline matter is possible by these sources. One of the advantages of a FEL is that the wavelength can be tuned depending on the needs of the particular experiment or application. Moreover, a FEL has the potential to become a relatively compact light source [2]. Multilayer optics are functional here as beam-splitters (to create multiple beams), as monochromators (to select the wavelength of interest) and as focusing mirrors (to obtain a high intensity at the focus or sample probe). Multilayer mirrors provide high reflectance at various angles of incidence and are less sensitive to misalignment than grazing-incidence, single-layer mirrors. The higher reflectivity achieved within the scope of this research opens up many opportunities for FELs and similar X-ray sources.

Using X-ray fluorescence (XRF) spectrometry, the elemental composition of a sample can be determined, regardless the state of the sample (solid, liquid). The special form of total reflection X-ray fluorescence (TXRF) [3] provides the possibility to detect nanoparticles, and heavy ions in organic monolayers or thick Langmuir-Blodgett films [4-8]. The latter are used as anti-reflective coatings, or as biological membranes to investigate the action modes of medical drugs, the permeability of biologically active molecules, and chain reactions in biological systems. Our high reflectivity above 6.6 nm wavelength improves the sensitivity of XRF to boron, an important low-Z element. The approaches employed in this thesis may be applicable for various multilayer stacks in order to improve their reflectivity, and, consequently, the sensitivity of XRF to different other chemical elements.

For those systems used for complex imaging applications, including future generations of photolithography optics, reflectivity is far more important than for systems consisting of a single optical element. This thesis describes the increase of the peak reflectivity up to 64.1% at 6.65 nm and 1.5° off-normal incidence [9]. For a 10 mirror optical system, this provides about a factor of 3 higher optical transmission as compared to the previous single-mirror reflectivity of 57.3% [10].

Since many optical schemes contain elements used at off-normal (grazing) angles, also multilayers for this geometry were developed. Here, 74.5% at 6.66 nm and

77° off-normal was achieved, employing so-called La surface nitridation during deposition [11]. Moreover, the stability under storage in air was verified for one and a half year. Our reflectivity is not far from the theoretical limit of 79.2% [11]. Also studies were done on the influence of the crystalline nature of the La and LaN, as a function of the thickness of the layers and the protective properties of the top, B, layer, including in situ growth studies [12]. Finally, the radiation stability was studied and a relatively stable reflectivity up to 300° C was found. Studies on interdiffusion and compound formation gave indications for further stability improvement [13].

Summarizing, the research described in this PhD thesis resulted in a record high reflectivity of B-containing multilayers, suitable for a wavelength of e.g. above 6.6 nm, a crucial ability which enables various short-wavelength optical applications. These include X-ray fluorescence analysis, the use of Extreme UV space telescopes, FEL beam line optics, and high resolution photolithographic imaging schemes. The understanding of the processes in these nanoscale layers and their application is not limited to the explored wavelength, but can be used to control deposition of different materials in single and multilayer configurations.

References

1. H.-P. Schlenvoigt, K. Haupt, A. Debus, F. Budde, O. Jäckel, S. Pfotenhauer, H. Schwoerer, E. Rohwer, J.G. Gallacher, E. Brunetti, R.P. Shanks, S.M. Wiggins, and D.A. Jaroszynski, Nature Physics 4, 130–133 (2008)
2. K. Nakajima, Nature Physics 4, 92 - 93 (2008)
3. M.K. Tiwaria, K.J.S. Sawhneya, and G.S. Lodhab, Spectrochimica Acta Part B: Atomic Spectroscopy, Volume 65, Issue 6, 434–440 (2010)
4. M.J. Bedzyk, D.H. Bilderback, G.M. Bommarito, M. Caffrey, and J.S. Schildkraut, Science 241 (4874), 1788–1791 (1988)
5. H.D. Abruña, G.M. Bommarito, and D. Acevedo, Science 250 (4977), 69–74 (1990)
6. N.N. Novikova, S.I. Zheludeva, N.D. Stepina, A.L. Tolstikhina, R.V. Gaynutdinov, W. Haase, A.I. Erko, A.A. Knyazev, and Y.G. Galyametdinov, Appl. Phys. A 94, 461–466 (2009)
7. S.I. Zheludeva, M.V. Kovalchuk, N.N. Novikova, A.N. Sosphenov, V.E. Erochin, and L.A. Feigin, J. Phys. D Appl. Phys. 26, A202–A205 (1993)
8. M.K. Tiwari, G.M. Bhalerao, M. Babu, A.K. Sinha, and C. Mukherjee, J. Appl. Phys. 103, 054311–054316 (2008)
9. D.S. Kuznetsov, A.E. Yakshin, J.M. Sturm, R.W.E. van de Kruijs, E. Louis, and F. Bijkerk, Optics Letters 40(16), 3778-3781 (2015)
10. I.A. Makhotkin, E. Zoethout, R.W.E. van de Kruijs, S.N. Yakunin, E. Louis, A.M. Yakunin, V. Banine, S. Muellender, and F. Bijkerk, Opt. Express 21, 29894-29904 (2013)
11. D.S. Kuznetsov, A.E. Yakshin, J.M. Sturm, and F.Bijkerk, accepted for publication in JNN (2018)
12. B. Krause, D.S. Kuznetsov, A.E. Yakshin, S. Ibrahimkutty, T. Baumbach and F. Bijkerk, Journal of Applied Crystallography, Vol. 51, Part 4 (Aug 2018)

13. D.S. Kuznetsov, A.E. Yakshin, J.M. Sturm, and F.Bijkerk, Journal of Applied Physics 122, 125302 (2017)

Acknowledgements
Firstly, I like to acknowledge my former MEPhI University teachers for their dedication and patience while explaining the sciences. All teachers greatly contributed to my education, and I highlight the general physics teacher E.N. Aksenova. Dedicating a lot of extra time on questions from us, students, she also arranged the organization of nice outings of our university group to picnics and sports in nature. I would especially acknowledge the supervisor of my graduation project Yu.A. Voronov, who, in my view, is an admirable example of attitude to his work, doing great effort in everyday education of students.

My brother Alexey Kuznetsov is guilty (many thanks for the guilty ones!) of introducing me to the Industrial Focus XUV Optics Group, where back in 2013 I started my PhD and currently being busy with a PostDoc project.

I am grateful to Prof. Fred Bijkerk for this nice opportunity to conduct this PhD research, for support and attention to the project and the people. No matter how urgent the discussion or question that I had, Fred always tried to dedicate some time for that.

Many thanks to my daily supervisor Andrey Yakshin for devoting a lot of time, fruitful discussions, and critical view. I am grateful for the knowledgeable answers to my work-related questions as well as for discussions and advices on daily-life-issues.

I would like to acknowledge the colleagues at Carl Zeiss SMT GmbH, especially Stephan Müllender and Hartmut Enkisch, for making this project possible, for the attention to our work and the fruitful discussions. I also thank all other industrial partners.

I am grateful for the good luck still to catch a few months of my PhD in the FOM Differ location in Nieuwegein. Erwin, thanks for being always challenging and criticizing, no matter the topic! Bob, Santi, Han, and the other technical specialists, thanks for the technical support and help with the depositions!

Robbert, thanks for long educative talks about ADC, Cu-k, diffraction, etc., and random stuff as well! Many thanks for always being opened for analyzing a scientific question, software or any other challenge and providing your valuable view.

Marko, thank you for numerous XPS experiments, analysis, and interesting scientific discussions.

Eric, thank you for various organizational help as well as actively taking part in planning and some of the scientific discussions.

I would like to thank the team of technical engineers at the University of Twente. You guys keep all that complex equipment running obviously.

An acknowledgement for Andrey Zameshin, it was fun to share a rented apartment and sometimes have a talk during those not so easy years right after relocation abroad. Thanks!

Igor, thank you for nice discussions and advices in my first few months in the Netherlands! Always fun to grab a beer or wine in a random place.

Kostya, thanks for nice talks, advices, being available just to talk on good as well as bad things, being ready to help! Special highlight goes for shashlik-arrangements, tv-evenings back in Hengelo, small trips, and step-by-step unwinding of some complex situations so that they do not seem complex anymore. Great to be around!

Igor, Parikshit, Christiane, thank you for somewhat rare but still very fun celebrations together!

Thanks to all former and current group members for being around and sharing all this time together!

Short CV

Dmitry S. Kuznetsov was born in Moscow, 28 June 1990. He finished the State Gymnasium №1526 in a group focused on the exact sciences with an Honours degree in 2007. Then Dmitry performed his Bachelor and Master studies at the Moscow Engineering Physical Institute (MEPhI) in the department №27 "Nano- and microelectronics". Here the graduation project was done on the topic "Studies of the properties of dielectric films, synthesized by the method of reactive magnetron sputtering". The project took about half a year and was done under supervision of Dr. Yuri A. Voronov, and head of the department Prof.Dr. Vyacheslav S. Pershenkov. After defending his graduation project, Dmitry accepted a PhD position in the Industrial Focus Group XUV Optics at the MESA+ Institute for Nanotechnology, Faculty of Applied Sciences, University of Twente, on research on XUV multilayers for a wavelength of ~6.7 nm, under daily supervision of Dr. Andrey E. Yakshin and supervision of Prof.Dr. Fred Bijkerk. The work within this PhD project resulted in 5 publications in peer-reviewed journals, several conference contributions, one patent, and this thesis. In July 2017 Dmitry continued his research in the XUV Optics group as a PostDoc on the topic of advanced XUV multilayers for the wavelength of 13.5 nm.